

PNNL-33996

MatLib-1.2: Nuclear Material Properties Library

Developed under NQA-1-2017

March 2023

KJ Geelhood, PNNL
CE Goodson, PNNL

WG Luscher, PNNL
J Corson, NRC

L Kyriazidis, NRC
JJ Whitman, NRC



Prepared for the U.S. Nuclear Regulatory Commission
Office of Nuclear Regulatory Research
Under contract DE-AC05-76RL01830
Interagency Agreement 31310019N0001
Task Order Number: 31310019F0047

DISCLAIMER

This report was prepared as an account of work sponsored by an agency of the United States Government. Neither the United States Government nor any agency thereof, nor Battelle Memorial Institute, nor any of their employees, makes **any warranty, express or implied, or assumes any legal liability or responsibility for the accuracy, completeness, or usefulness of any information, apparatus, product, or process disclosed, or represents that its use would not infringe privately owned rights.** Reference herein to any specific commercial product, process, or service by trade name, trademark, manufacturer, or otherwise does not necessarily constitute or imply its endorsement, recommendation, or favoring by the United States Government or any agency thereof, or Battelle Memorial Institute. The views and opinions of authors expressed herein do not necessarily state or reflect those of the United States Government or any agency thereof.

PACIFIC NORTHWEST NATIONAL LABORATORY
operated by
BATTELLE
for the
UNITED STATES DEPARTMENT OF ENERGY
under Contract DE-AC05-76RL01830

Printed in the United States of America

Available to DOE and DOE contractors from
the Office of Scientific and Technical Information,
P.O. Box 62, Oak Ridge, TN 37831-0062

www.osti.gov
ph: (865) 576-8401
fox: (865) 576-5728
email: reports@osti.gov

Available to the public from the National Technical Information Service
5301 Shawnee Rd., Alexandria, VA 22312
ph: (800) 553-NTIS (6847)
or (703) 605-6000
email: info@ntis.gov
Online ordering: <http://www.ntis.gov>

MatLib-1.2: Nuclear Material Properties Library

Developed under NQA-1-2017

March 2023

KJ Geelhood, PNNL
L Kyriazidis, NRC
J Corson, NRC

WG Luscher, PNNL
CE Goodson, PNNL
JJ Whitman, NRC

Prepared for the U.S. Nuclear Regulatory Commission
Office of Nuclear Regulatory Research
Under Contract DE-AC05-76RL01830
Interagency Agreement 31310019N0001
Task Order Number: 31310019F0047

Pacific Northwest National Laboratory
Richland, Washington 99352

Project Summary and Document Characteristics

Project Name	FAST Fuel Performance Code Development and Assessment
Project No.	77701 Task 3130019F0047
Product Management Office No. / Organization	PM053 / Nuclear Science and Legacy Waste

Approvals

Role	Name	Signature	Date
Project Manager	Katie Wagner	Katie A Wagner <small>Digitally signed by Katie A Wagner Date: 2023.03.27 12:45:50 -07'00'</small>	
Lead Software Developer	Ken Geelhood	Kenneth J (Ken) Geelhood <small>Digitally signed by Kenneth J (Ken) Geelhood Date: 2023.03.26 21:02:05 -07'00'</small>	
Code Custodian	David Colameco	David V Colameco <small>Digitally signed by David V Colameco Date: 2023.03.25 20:17:28 -07'00'</small>	

Revision History

Revision	Date	Comments
0	March 2023	Initial Release

Abstract

The U.S. Nuclear Regulatory Commission (NRC) uses the computer code Fuel Analysis under Steady-state and Transients (FAST) to model steady-state and transient fuel behavior to support regulatory decisions. FAST relies on a material properties library (MatLib) that contains the thermal and mechanical properties of the nuclear materials and coolants of interest to support the U.S. commercial nuclear industry. MatLib contains properties for a variety of nuclear fuels, cladding and other structural materials, gases, and coolants.

In this document, material property correlations for the materials contained within MatLib are presented and discussed. When available, comparisons are made between the material property correlations and available data. Additionally, uncertainties are quantified on the material properties, which is then used by the NRC to support uncertainty quantification for best-estimate plus uncertainty safety evaluation reviews.

This document describes MatLib-1.2, which was updated from MatLib-1.1 to include cleanup of the code for streamlined calls to MatLib from the main FAST source code, and to enable easier readability of the code by developers that maintain and enhance the FAST code. The results of MatLib did not change between MatLib-1.1 and MatLib-1.2; however, the source code changes warranted incrementing the minor numbering of the software version number. The changes may result in faster execution times of FAST-1.2 as compared to FAST-1.1.

This document is one of a series of documents on FAST; the other documents detail the models used by FAST as well as its integral assessment to experiments and commercial data.

This page intentionally blank.

Foreword

The U.S. Nuclear Regulatory Commission uses the computer code FAST to model steady-state and transient fuel behavior to support regulatory analyses. To effectively model fuel behavior, material property correlations applicable to a wide range of operating conditions (e.g., temperature and burnup) must be available. In this sense, a “material property” is a physical characteristic of the material whose quantitative value is necessary in the analysis process.

The consolidated resource for “material properties” cited most often in the literature is MATPRO [Siefken et al., 2001]. MATPRO is a compilation of fuel and cladding material property correlations with an extensive history of use with fuel performance and severe accident codes. Since 2001, MATPRO has not been updated despite recent advances in understanding of high burnup material properties and recent evolutions in cladding alloys and fuel types. These updates were documented as part of the FRAPCON [Geelhood et al., 2015b] and FRAPTRAN [Geelhood et al., 2015a] codes in a material property handbook [Luscher et al., 2015]. These codes were the predecessor to FAST [Geelhood et al., 2023a].

The primary purpose of this report is to document the current material property correlations used by FAST. Documentation includes the mathematical formulas, comparisons to available data, range of applicability, and model uncertainty.

Historically, FRAPCON and FRAPTRAN were applicable solely to commercial BWRs and PWRs with oxide fuel (UO_2 and $(\text{U,Pu})\text{O}_2$) and zirconium-alloy cladding (Zircaloy-2, Zircaloy-4, M5^{®1}, ZIRLO^{®2} and Optimized ZIRLO^{™3}). In order to be applicable to future reactors and fuels, currently available material properties for new fuels (uranium metal alloys), claddings (FeCrAl and HT-9), and coolants (liquid sodium) are included in the MatLib library.

Unlike the UO_2 -Zr-alloy system, which has a long irradiation history, the development of advanced fuels and materials is ongoing and irradiation data are sparse. Consequently, the applicable ranges of these advanced fuel systems is smaller and the uncertainty is greater. Nevertheless, these correlations, supporting data, range of applicability, and uncertainties are documented here.

¹ M5[®] is a registered trademark of Framatome.

² ZIRLO[®] is a registered trademark of Westinghouse Electric Company LLC

³ Optimized ZIRLO[™] is a trademark of Westinghouse Electric Company LLC.

This page intentionally blank.

Acronyms and Abbreviations

BWR	boiling water reactor
CRUD	Chalk River Unidentified Deposit
FAST	Fuel Analysis under Steady-state and Transients
LWR	light water reactor
MatLib	Material Properties Library
MOX	mixed oxide
MTU	metric ton of uranium
NFI	Nuclear Fuel Industries
NRC	U.S. Nuclear Regulatory Commission
O/M	oxygen-to-metal
PNNL	Pacific Northwest National Laboratory
PWR	pressurized water reactor
TD	theoretical density
PuO ₂	plutonium oxide

This page intentionally blank.

Contents

Abstract	v
Foreword	vii
Acronyms and Abbreviations	ix
Contents	xi
Figures	xv
Tables	xix
 1.0 Introduction	 1
1.1 Objective of MatLib	2
1.2 Relation to Other Reports	2
 2.0 Fuel Material Properties	 5
2.1 Oxide Fuel Properties (UO ₂ , (U,Pu)O ₂)	5
2.1.1 Thermal Conductivity	5
2.1.2 Specific Heat Capacity and Enthalpy	11
2.1.3 Melting Temperature	15
2.1.4 Thermal Expansion	16
2.1.5 Emissivity	20
2.1.6 Density	22
2.1.7 Densification	23
2.1.8 Swelling	25
2.2 Metallic Fuel U-Pu-Zr Material Properties	29
2.2.1 Thermal Conductivity	29
2.2.2 Specific Heat Capacity	30
2.2.3 Density	32
2.2.4 Melting Temperature	33
2.2.5 Eutectic Temperature	33

2.2.6	Thermal Expansion	33
2.2.7	Emissivity	34
2.2.8	Swelling	35
3.0	Cladding Material Properties	37
3.1	Zirconium-based Alloys	37
3.1.1	Thermal Conductivity	37
3.1.2	Specific Heat	39
3.1.3	Melting Temperature	41
3.1.4	Thermal Expansion	41
3.1.5	Emissivity	45
3.1.6	Density	46
3.1.7	Young's Modulus and Shear Modulus	47
3.1.8	Meyer's Hardness	50
3.1.9	Axial Growth	51
3.1.10	Strain (Creep) Rate	56
3.2	Iron-Chrome-Aluminum (FeCrAl) Alloys	62
3.2.1	Thermal Conductivity	62
3.2.2	Specific Heat	65
3.2.3	Melting Temperature	68
3.2.4	Thermal Expansion	68
3.2.5	Emissivity	71
3.2.6	Density	72
3.2.7	Young's Modulus and Shear Modulus	72
3.2.8	Meyer's Hardness	74
3.2.9	Axial Growth	74
3.2.10	Strain (Creep) Rate	75
3.3	HT-9 Alloy	77

3.3.1	Thermal Conductivity	77
3.3.2	Specific Heat Capacity	79
3.3.3	Melting Temperature	80
3.3.4	Thermal Expansion	81
3.3.5	Emissivity	82
3.3.6	Density	83
3.3.7	Young's Modulus	83
3.3.8	Shear Modulus	84
3.3.9	Meyer's Hardness	85
3.3.10	Strain (Creep) Rate	85
3.3.11	Yield Stress	87
4.0	Gas Material Properties	89
4.1	Thermal Conductivity	89
4.1.1	Model Description	89
4.1.2	Comparisons to Data	91
4.1.3	Applicability and Uncertainty	98
5.0	Oxide/CRUD Material Properties	99
5.1	Zirconium Dioxide (ZrO_2)	99
5.1.1	Thermal Conductivity	99
5.1.2	Specific Heat Capacity	100
5.1.3	Melting Temperature	101
5.1.4	Density	101
5.2	CRUD	101
5.2.1	Thermal Conductivity	102
5.2.2	Specific Heat Capacity	102
5.2.3	Density	102

- 6.0 Fluid Material Properties 103
 - 6.1 Water 103
 - 6.2 Sodium 104
 - 6.2.1 Thermal Conductivity 104
 - 6.2.2 Viscosity 104
 - 6.2.3 Density 105
 - 6.2.4 Specific Heat Capacity 106
 - 6.2.5 Enthalpy 107
 - 6.2.6 Melting Temperature 108
 - 6.2.7 Vapor Pressure 108
- 7.0 References 111

Figures

2-1	Model-to-data Comparison for Unirradiated UO_2 Thermal Conductivity Correlation . . .	8
2-2	Model-to-data Comparison for Irradiated UO_2 Thermal Conductivity Correlation . . .	8
2-3	Model-to-Data Comparison for Unirradiated $\text{UO}_2\text{-Gd}_2\text{O}_3$ Thermal Conductivity Correlation	9
2-4	Model-to-Data Comparison for Irradiated $\text{UO}_2\text{-Gd}_2\text{O}_3$ Thermal Conductivity Correlation	9
2-5	Model-to-Data Comparison for MOX Thermal Conductivity Correlation	10
2-6	Model-to-Data Comparison for UO_2 Specific Heat Capacity Correlation	13
2-7	Model-to-Data Comparison for MOX Specific Heat Capacity Correlation	14
2-8	Model-to-Data Comparison for UO_2 , PuO_2 , MOX, and $\text{UO}_2\text{-Gd}_2\text{O}_3$ Melting Temperature Correlation	16
2-9	Model-to-Data Comparison for UO_2 Correlation	18
2-10	Model-to-Data Comparison for PuO_2 Correlation	19
2-11	Model-to-Data Comparison for Emissivity of Oxide Fuel	21
2-12	Model-to-Data Comparison for Densification of Oxide Fuel	25
2-13	Model-to-Data Comparison for Solid Swelling Correlation	27
2-14	Model-to-Data Comparison for Solid Swelling Rate Correlation	28
3-1	Model-to-Data Comparison for Zirconium-based Alloy Cladding Thermal Conductivity Correlation	38
3-2	Model-to-Data Comparison for Zirconium-based Alloy Cladding Specific Heat Correlation	40
3-3	Model-to-Data Comparison for for Zirconium-based Alloy Cladding Circumferential Thermal Expansion Correlation	43
3-4	Model-to-Data Comparison for for Zirconium-based Alloy Cladding Axial Thermal Expansion Correlation	44
3-5	Model-to-Data Comparison for Zirconium-based Alloy Emissivity Correlation	46
3-6	Model-to-Data Comparison for Zirconium Alloy Cladding Young's Modulus	49
3-7	Model-to-Data Comparison for Zirconium-based Alloy Cladding Meyer's Hardness Correlation	51
3-8	Model-to-Data Comparison for Zircaloy-2 Axial Irradiation Growth Correlation	53

3-9	Model-to-Data Comparison for Zircaloy-4 Axial Irradiation Growth Correlation	54
3-10	Model-to-Data Comparison for ZIRLO Axial Irradiation Growth Correlation	55
3-11	Model-to-Data Comparison for M5 Axial Irradiation Growth Correlation	55
3-12	Model-to-data Comparison for RXA Ziracloy Strain Correlation	60
3-13	Model-to-data Comparison for SRA Ziracloy Strain Correlation	61
3-14	Model-to-Data Comparison for Kanthal APMT FeCrAl Alloy Thermal Conductivity Correlation	63
3-15	Model-to-Data Comparison for C35M FeCrAl Alloy Thermal Conductivity Correlation	64
3-16	Model-to-Data Comparison for C36M FeCrAl Alloy Thermal Conductivity Correlation	64
3-17	Model-to-Data Comparison for Kanthal APMT FeCrAl Alloy Specific Heat Correlation	66
3-18	Model-to-Data Comparison for C35M FeCrAl Alloy Specific Heat Correlation	67
3-19	Model-to-Data Comparison for C36M FeCrAl Alloy Specific Heat Correlation	67
3-20	Model-to-Data Comparison for Kanthal APMT FeCrAl Alloy Thermal Expansion Coefficient	70
3-21	Model-to-Data Comparison for C35M FeCrAl Alloy Thermal Expansion Coefficient Correlation	70
3-22	Model-to-Data Comparison for C36M FeCrAl Alloy Thermal Expansion Coefficient Correlation	71
3-23	Model-to-Data Comparison for FeCrAl Alloys Elastic Modulus Correlation	74
3-24	Model-to-Model Comparison for HT-9 Alloy Thermal Conductivity Correlations	78
3-25	HT-9 Alloy Specific Heat Capacity Correlation	80
3-26	Model-to-Model Comparison for HT-9 Alloy Thermal Expansion Correlations	82
4-1	Model-to-Data Comparison for Helium Thermal Conductivity Correlation	92
4-2	Model-to-Data Comparison for Argon Thermal Conductivity Correlation	93
4-3	Model-to-Data Comparison for Krypton Thermal Conductivity Correlation	94
4-4	Model-to-Data Comparison for Xenon Thermal Conductivity Correlation	95
4-5	Model-to-Data Comparison for Hydrogen Thermal Conductivity Correlation	95
4-6	Model-to-Data Comparison for Nitrogen Thermal Conductivity Correlation	96
4-7	Model-to-Data Comparison for Steam Thermal Conductivity Correlation	97

4-8	Model-to-Data Comparison for Gas Mixture Thermal Conductivity Correlation	97
5-1	Model-to-Data Comparison for ZrO ₂ Thermal Conductivity Correlation	100

This page intentionally blank.

Tables

1-1	Roadmap to documentation of models and properties used in NRC's fuel performance code FAST	3
2-1	Constants Used in UO_2 , Gd_2O_3 , and PuO_2 Heat Capacity and Enthalpy Correlations	12
2-2	Constants Used in UO_2 , $\text{UO}_2\text{-Gd}_2\text{O}_3$, and PuO_2 Solid-Phase Thermal Expansion Correlations	17
2-3	Phase Transition Temperatures Used in the Specific Heat Capacity Correlations for U-Pu-Zr Metallic Fuel	31
2-4	Constants Used in the Thermal Expansion Correlations for U-Pu-Zr Metallic Fuel . .	34
3-1	Example Heat Treatments and Cold Worked Conditions for Different Zirconium-Based Alloys	37
3-2	Interpolated Values for the Zirconium-Based Alloys Specific Heat Capacity Correlation	39
3-3	Interpolated Values for the Zirconium-Based Alloys Thermal Expansion Correlation .	42
3-4	Cladding Cold Work Dependent Parameters for the Thermal and Irradiation Strain Rate Correlations	58
3-5	Nominal Composition of Various FeCrAl Alloys in Matlib	62
3-6	Constants Used in the FeCrAl Thermal Conductivity Correlation	63
3-7	Constants Used in the FeCrAl Specific Heat Correlation	66
3-8	Constants Used in the FeCrAl Thermal Expansion Correlation	69
3-9	Densities of Various FeCrAl Alloys	72
3-10	Constants Used in the FeCrAl Thermal Strain Rate Correlation	76
3-11	Constants Used in the HT-9 Specific Heat Capacity Correlation	79
3-12	Constants Used in the HT-9 Thermal Expansion Correlation	81
3-13	Constants Used in the HT-9 Thermal Strain Rate Correlation	86
3-14	Constants Used in the HT-9 Yield Stress Correlation	88
4-1	Constants Used in the Gas Thermal Conductivity Correlation	90

This page intentionally blank.

1.0 Introduction

The U.S. Nuclear Regulatory Commission (NRC) uses the computer code FAST to model steady-state and transient fuel behavior to support regulatory analyses. To effectively model fuel behavior, material property correlations must be used for a wide range of operating conditions (e.g., temperature and burnup). In this sense, a “material property” is a physical characteristic of the material whose quantitative value is necessary in the analysis process. Further, the property may be used to compare the benefits of one material with those of another. Generally speaking, the material properties of interest in thermal-mechanical regulatory analysis of nuclear fuel behavior as performed by FAST are mechanical properties such as elastic modulus, yield stress, and creep rate and thermal properties such as thermal conductivity and specific heat.

In this report, the thermal and mechanical properties are included. Other characteristics of the material (e.g., fission gas release) are considered “models” rather than properties and are discussed elsewhere [Geelhood et al., 2023a]. The primary purpose of this report is to document the current material property correlations used in FAST. Material property correlations for oxide fuels, including uranium dioxide (UO₂) and mixed oxide (MOX) fuels are described in Section 2.1. Throughout this document, the term MOX is used to describe fuels that are blends of uranium and plutonium oxides, (U,Pu)O₂. The properties for UO₂ with other additives (e.g., gadolinia) are also discussed. Material properties for metallic fuel U-Pu-Zr are discussed in Section 2.2. Material property correlations for cladding materials of zirconium-based alloys, iron-based alloys, and HT-9 are described in Section 3.0. Material property correlations for gases used as fill gas are described in Section 4.0. Properties for oxides and CRUD are described in Section 5.0. Coolant properties for sodium are described in Section 6.0.

In addition to describing the material property correlations used in the subroutines of FAST, this report also shows comparison to experimental data for each material property correlation. Because these correlations are semi-empirical or empirical, the applicability of the correlations is limited to the range of available data. Therefore, based on the data comparison, a range of applicability will be identified and model uncertainty will be given. Model uncertainty is given in terms of either an absolute standard error or a relative standard error. The standard errors are calculated according to the following equations.

$$\sigma_{abs} = \sqrt{\frac{\sum_{i=1}^n (x_i - x_{model})^2}{n - 1}} \quad (1-1)$$

$$\sigma_{rel} = \sqrt{\frac{\sum_{i=1}^n [(x_i - x_{model}) / x_{model}]^2}{n - 1}} \quad (1-2)$$

Where,

σ_{abs} = absolute standard error (same units as x)

σ_{rel} = relative standard error (fraction)

n = number of data measurement

x_i = value of data point i (various units)

x_{model} = model prediction at conditions of data point i (various units)

A determination of which σ is used is made based on examining the trend of measured and predicted values as a function of the independent variable of interest such as temperature or burnup. In some cases where data are sparse or it is not possible to calculate this standard error, engineering judgement is used to estimate a standard error.

1.1 Objective of MatLib

The ability to accurately calculate the performance of light water reactor (LWR) fuel rods under long-term burnup conditions is a major objective of the reactor safety research program being conducted by the NRC. To achieve this objective, the NRC has sponsored an extensive program of analytical computer code development, as well as both in-pile and out-of-pile experiments to benchmark and assess the analytical code capabilities. Historically, the computer code developed to calculate the long-term burnup response of a single fuel rod was FRAPCON. Recently the transient temperature solution and various other transient models from FRAPTRAN have been added to FRAPCON and the resulting code, which is the next evolution of FRAPCON, is FAST. This report describes the material properties used in FAST-1.2.

1.2 Relation to Other Reports

The full documentation of the steady-state and transient fuel performance codes is described in three documents. The basic fuel, cladding, and gas material properties used in FAST-1.2 are described in the material properties handbook (this report). The FAST-1.2 code structure and behavioral models are described in the FAST-1.2 code description document [Geelhood et al., 2023a]. The integral assessment of FAST-1.2 against steady-state and transient test data is given in the FAST-1.2 integral assessment document [Geelhood et al., 2023b]. Table 1-1 shows where each specific material property and model used in the NRC fuel performance code is documented.

Table 1-1. Roadmap to documentation of models and properties used in NRC's fuel performance code FAST

Model/Property	FAST-1.2^(a)
Fuel thermal conductivity	MatLib Document
Fuel thermal expansion	MatLib Document
Fuel melting temperature	MatLib Document
Fuel specific heat	MatLib Document
Fuel enthalpy	MatLib Document
Fuel emissivity	MatLib Document
Fuel densification	MatLib Document
Fuel swelling – solid	MatLib Document
Fuel swelling – gaseous	MatLib Document
Fission gas release	FAST-1.2 Code Description
Fuel relocation	FAST-1.2 Code Description
Fuel grain growth	FAST-1.2 Code Description
High burnup rim model	FAST-1.2 Code Description
Nitrogen release	FAST-1.2 Code Description
Helium release	FAST-1.2 Code Description
Radial power profile	FAST-1.2 Code Description
Stored energy	FAST-1.2 Code Description
Decay heat model	FAST-1.2 Code Description
Fuel and cladding temperature solution	FAST-1.2 Code Description
Cladding thermal conductivity	MatLib Document
Cladding thermal expansion	MatLib Document
Cladding Young's modulus	MatLib Document
Cladding creep model	MatLib Document
Cladding specific heat	MatLib Document
Cladding emissivity	MatLib Document
Cladding axial growth	MatLib Document
Cladding Meyer hardness	MatLib Document
Cladding annealing	FAST-1.2 Code Description
Cladding yield stress, ultimate stress, and plastic deformation	FAST-1.2 Code Description
Cladding failure criteria	FAST-1.2 Code Description
Cladding waterside corrosion	FAST-1.2 Code Description
Cladding hydrogen pickup	FAST-1.2 Code Description
Cladding high temperature oxidation	FAST-1.2 Code Description
Cladding ballooning model	FAST-1.2 Code Description

Table 1-1. Roadmap to documentation of models and properties used in NRC's fuel performance code FAST (continued)

Model/Property	FAST-1.2 ^(a)
Cladding mechanical deformation	FAST-1.2 Code Description
Oxide thermal conductivity	MatLib Document
Crud thermal conductivity	MatLib Document
Gas conductivity	MatLib Document
Gap conductance	FAST-1.2 Code Description
Plenum gas temperature	FAST-1.2 Code Description
Rod internal pressure	FAST-1.2 Code Description
Coolant temperature and heat transfer coefficients	FAST-1.2 Code Description
Not Developed at PNNL	
Water-cooled, water-moderated energy reactor fuel and cladding models	NUREG/IA-0164
Cladding finite element analysis model	VTT-R-11337-06

^(a) MatLib Document (this document) [Geelhood et al., 2023c]

FAST-1.2 Code Description [Geelhood et al., 2023a]

NUREG/IA-0164 [Shestopalov et al., 1999]

VTT-R-11337-06 [Knuutila, 2006]

2.0 Fuel Material Properties

2.1 Oxide Fuel Properties (UO₂, (U,Pu)O₂)

Material property correlations for UO₂ and (U,Pu)O₂ are described in the following sections. When indicated, some of the correlations also account for the addition of Gadolinia (Gd₂O₃) in the UO₂ fuel pellet.

2.1.1 Thermal Conductivity

The thermal conductivity of oxide nuclear fuel is modeled in MatLib as a function of five parameters:

1. Temperature
2. Composition
3. Burnup
4. Density
5. Oxygen-to-metal (O/M) ratio

2.1.1.1 Model Description

UO₂ and UO₂-Gd₂O₃

The thermal conductivity of 95% theoretical density (TD) UO₂ and UO₂-Gd₂O₃ is based on the model proposed by Nuclear Fuel Industries (NFI) [Ohira and Itagaki, 1997] and was modified to alter the temperature-dependent portion of the burnup and include a dependency on gadolinia content [Lanning et al., 2005]:

$$k_{95} = \left(\frac{1}{A + \alpha_{gad} + BT + f(Bu) + (1 - 0.9e^{-0.04Bu})g(Bu)h(T)} \right) + \frac{C}{T^2} \exp\left(-\frac{D}{T}\right) \quad (2-1)$$

$$h(T) = \frac{1}{1 + 396 \exp(-Q/T)} \quad (2-2)$$

Where,

k_{95} = Thermal conductivity of 95% TD fuel, W/m-K

T = Temperature, K

Bu = Burnup, GWd/MTU

$f(Bu)$ = Effect of fission products in crystal matrix (solution) = $0.00187Bu$

$g(Bu)$ = Effect of irradiation defects = $0.038Bu^{0.28}$

$h(T)$ = Temperature dependence of annealing on irradiation defects (Equation 2-2)

Q = Temperature-dependent parameter ("Q/R") = 6380 K

$A = 0.0452 \text{ m-K/W}$

$B = 2.46 \times 10^{-4} \text{ m-K/W/K}$

$C = 3.5 \times 10^9 \text{ W-K/m}$

$D = 16361 \text{ K}$

α = Constant = 1.1599

gad = Weight fraction of gadolinia, unitless

MOX

The thermal conductivity of 95% theoretical density MOX is based on the model proposed by Nuclear Fuel Industries (NFI) [Ohira and Itagaki, 1997] and was modified to alter the temperature-dependent portion of the burnup and include a dependency on gadolinia content [Lanning et al., 2005] and plutonia content [Duriez et al., 2000]:

$$k_{95} = \left(\frac{1}{A(x) + \alpha gad + B(x)T + f(Bu) + (1 - 0.9e^{-0.04Bu})g(Bu)h(T)} + \frac{C_{mod}}{T^2} \exp\left(-\frac{D}{T}\right) \right) \quad (2-3)$$

Where,

k_{95} = Thermal conductivity of 95% TD fuel, W/m-K

T = Temperature, K

Bu = Burnup, GWd/tHM

$f(Bu)$ = Effect of fission products in crystal matrix (solution) = $0.00187Bu$

$g(Bu)$ = Effect of irradiation defects = $0.038Bu^{0.28}$

$h(T)$ = Temperature dependence of annealing on irradiation defects (Equation 2-2)

Q = Temperature dependent parameter ("Q/R") = 6380 K

$x = 2.00$ —O/M ratio

$$A(x) = 2.85x + 0.035 \text{ m-K/W}$$

$$B(x) = (2.86 - 7.15x) \times 10^{-4}, \text{ m/W}$$

$$C_{mod} = 1.5 \times 10^9 \text{ W-K/m}$$

$$D = 13520 \text{ K}$$

$$\alpha = \text{Constant} = 1.1599$$

gad = Weight fraction of gadolinia, unitless

Density Adjustment

All of the above models are adjusted for the fuel density (in fraction of TD) using the Lucuta recommendation for spherical-shaped pores [Lucuta et al., 1996], as shown in Equation 2-4.

$$k_d = 1.0789k_{95} \frac{d}{1 + 0.5(1 - d)} \quad (2-4)$$

Where,

k_d = Thermal conductivity adjusted for fuel density, W/m-K

k_{95} = Thermal conductivity of 95% TD fuel, W/m-K

d = Fraction of fuel TD, including as-fabricated and densification changes, unitless

2.1.1.2 Comparison to Data

Thermal conductivity data have been collected for UO_2 from unirradiated samples [Ronchi et al., 1999] [Lucuta et al., 1996] [Christensen et al., 1964] [Godfrey et al., 1964] [Bates et al., 1967] [Gibby, 1971] [Weilbacher, 1972] [Goldsmith and Douglas, 1973] [Hobson et al., 1974] and irradiated [Ronchi et al., 2004] [Carrol et al., 1994]. A comparison between these data for UO_2 is presented in Figure 2-1 for unirradiated data and in Figure 2-2 for irradiated data. This comparison demonstrates good agreement between the correlation and the database within range 300 K to 2800 K and 0 to 90 GWd/MTU.

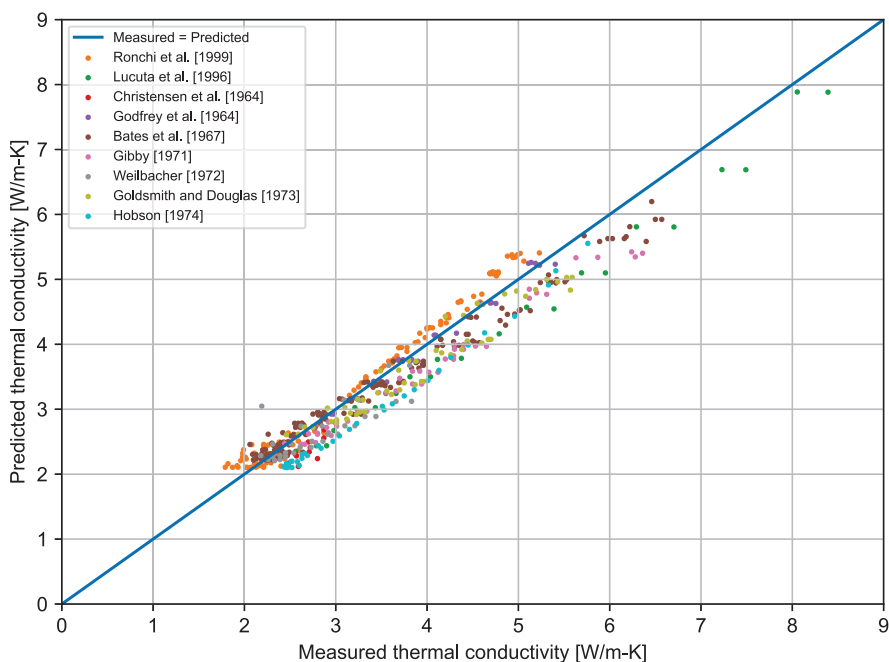


Figure 2-1. Model-to-data Comparison for Unirradiated UO_2 Thermal Conductivity Correlation

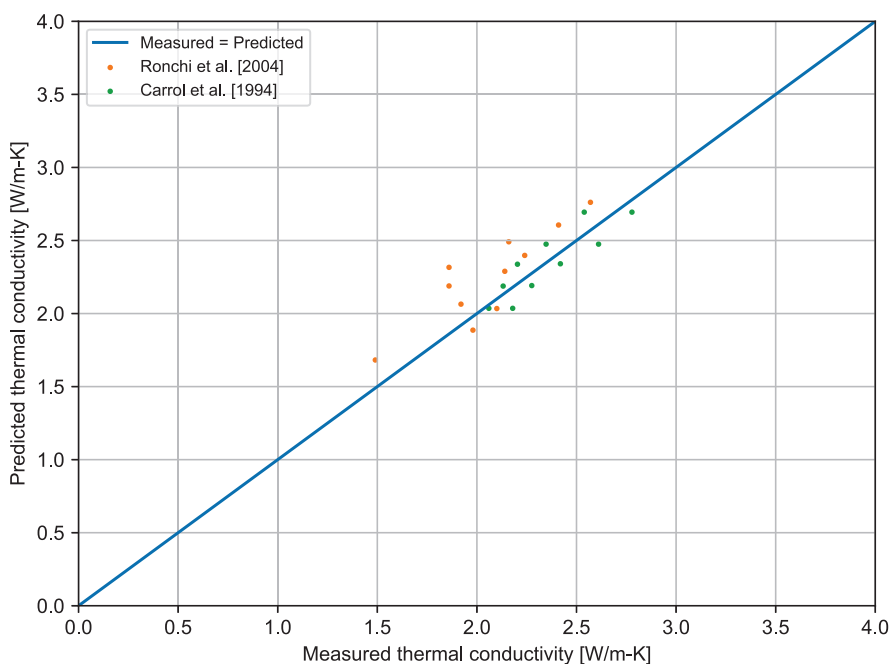


Figure 2-2. Model-to-data Comparison for Irradiated UO_2 Thermal Conductivity Correlation

Thermal conductivity data have been collected for $\text{UO}_2\text{-Gd}_2\text{O}_3$ from unirradiated [Minato et al., 2001] [Newman, 1982] [Amaya and Hirai, 1997] [Hirai and Ishimoto, 1991] and irradiated [Minato et al., 2001] [Amaya and Hirai, 1997] samples. A comparison between these data for $\text{UO}_2\text{-Gd}_2\text{O}_3$ is

presented in Figure 2-3 for unirradiated data and in Figure 2-4 for irradiated data. This comparison demonstrates good agreement between the correlation and the database within range 300 K to 2800 K and 0 to 50 GWd/MTU.

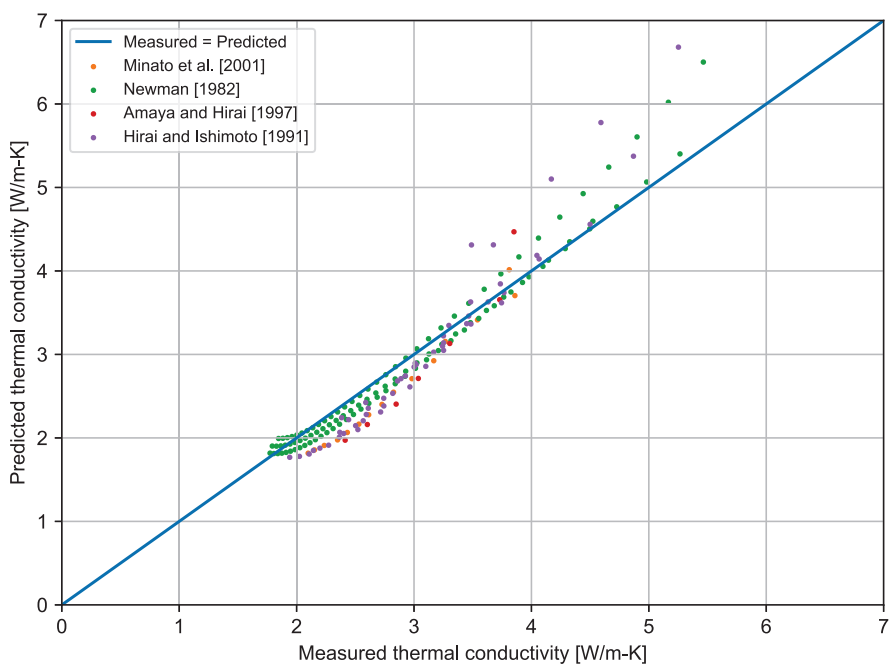


Figure 2-3. Model-to-Data Comparison for Unirradiated $\text{UO}_2\text{-Gd}_2\text{O}_3$ Thermal Conductivity Correlation

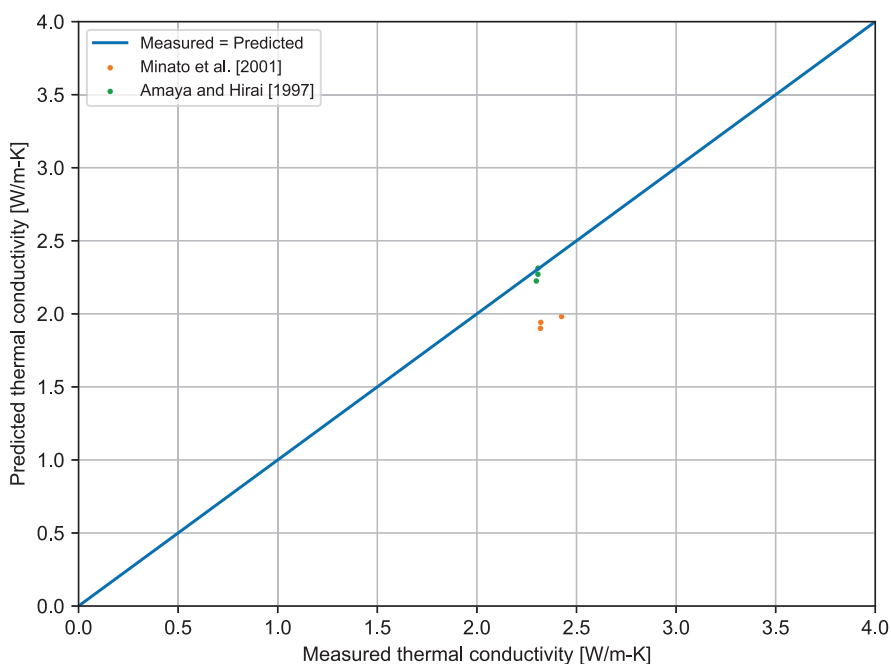


Figure 2-4. Model-to-Data Comparison for Irradiated $\text{UO}_2\text{-Gd}_2\text{O}_3$ Thermal Conductivity Correlation

Thermal conductivity data have been collected for MOX from unirradiated samples [Duriez et al., 2000] [Philipponneau, 1992]. A comparison between these data for MOX is presented in Figure 2-5. This comparison demonstrates good agreement between the correlation and the database within range 660 K to 2800 K and O/M ratio of 1.95 to 2.0.

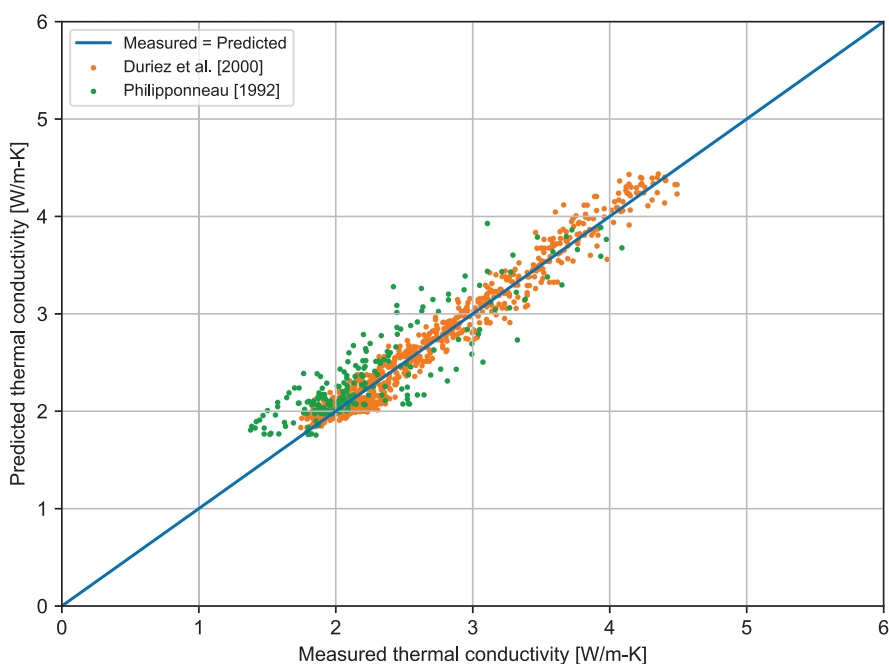


Figure 2-5. Model-to-Data Comparison for MOX Thermal Conductivity Correlation

2.1.1.3 Applicability and Uncertainty

UO₂ and UO₂-Gd₂O₃ Applicability

The thermal conductivity model (Equation 2-1) is applicable to the range of available data:

- Fuel types: UO₂ and UO₂-Gd₂O₃
- Gadolinia content: 0 to 10 wt%
- Temperature: 300 to 2800 K
- Rod-average burnup: 0 to 90 GWd/MTU for UO₂; 0 to 50 GWd/MTU for UO₂-Gd₂O₃
- As-fabricated density: 90 to 98.6 %TD

Engineering judgment should be used if analysis outside of these ranges is needed.

MOX Applicability

The thermal conductivity model (Equation 2-3) is applicable to the range of available data:

- Fuel type: MOX
- Temperature: 660 to 2800 K

- Rod-average burnup: 0 to 90 GWd/MTU (assumed to be the same as for UO₂)
- As-fabricated density: 90 to 98.6 %TD (assumed to be the same as for UO₂)
- O/M ratio: 1.95 to 2.00

Engineering judgment should be used if analysis outside of these ranges is needed.

Uncertainty

The uncertainty of the correlation is given below for each fuel type as a relative standard error.

- UO₂: $\sigma = 8.3\%$
- UO₂-Gd₂O₃: $\sigma = 8.8\%$
- MOX: $\sigma = 7.8\%$

2.1.2 Specific Heat Capacity and Enthalpy

The specific heat capacity and enthalpy of oxide fuel are modeled as functions of four parameters:

1. Temperature
2. Composition
3. Molten fraction
4. O/M ratio

2.1.2.1 Model Description

The specific heat capacity and enthalpy of UO₂, Gd₂O₃, and PuO₂ are given by:

$$C_p = \frac{K_1 \theta^2 \exp\left(\frac{\theta}{T}\right)}{T^2 \left(\exp\left(\frac{\theta}{T}\right) - 1\right)^2} + K_2 T + \frac{Y K_3 E_D}{2RT^2} \exp\left(\frac{-E_D}{RT}\right) \quad (2-5)$$

$$H = \frac{K_1 \theta}{\exp\left(\frac{\theta}{T}\right) - 1} + \frac{K_2 T^2}{2} + \frac{Y}{2} K_3 \exp\left(\frac{-E_D}{RT}\right) \quad (2-6)$$

Where,

C_p = Specific heat capacity, J/kg-K

H = Enthalpy, J/kg

T = Temperature, K

Y = O/M ratio

R = Universal gas constant = 8.3143 J/mol-K

K_1, K_2, K_3 = Constants (Table 2-1)

θ = Einstein temperature, K (Table 2-1)

E_D = Activation energy for Frenkel defects, J/mol (Table 2-1)

Table 2-1. Constants Used in UO_2 , Gd_2O_3 , and PuO_2 Heat Capacity and Enthalpy Correlations

Constant	$\text{UO}_2^{(a)}$	$\text{PuO}_2^{(b)}$	Gd_2O_3	Units
K_1	2.967×10^2	3.474×10^2	3.1586×10^2	J/kg-K
K_2	2.43×10^{-2}	3.95×10^{-4}	4.044×10^{-2}	J/kg-K ²
K_3	8.745×10^7	3.860×10^7	0.0	J/kg
θ	5.35285×10^2	5.710×10^2	3.480×10^2	K
E_D	1.577×10^5	1.967×10^5	0.0	J/mol

^(a) [Kerrisk and Clifton, 1972]

^(b) [Kruger and Savage, 1968]

For a mixture of UO_2 , Gd_2O_3 , and PuO_2 , the specific heat capacity of the solid is determined by combining the contribution from each constituent in proportion to its weight fraction.

The specific heat capacity of UO_2 in the liquid state (Equation 2-7) was determined by [Leibowitz et al., 1971] and assumed to be valid for PuO_2 in the liquid state.

$$C_p(\text{liquid}) = 503 \text{ J/kg-K} \quad (2-7)$$

When the material is partially molten, the heat capacity is determined similarly with a weighted sum of the solid and molten fractions.

2.1.2.2 Comparison Data

Specific heat data have been collected for UO_2 from unirradiated samples [Grønvold et al., 1970] [Hein et al., 1968] [Leibowitz et al., 1969]. A comparison between these data for UO_2 is presented in Figure 2-6. This comparison demonstrates good agreement between the correlation and the database up to about 2800 K. Beyond this temperature, the data begins to fall lower than the model. This is attributed to partial melting due to a non-uniform temperature distribution within the sample.

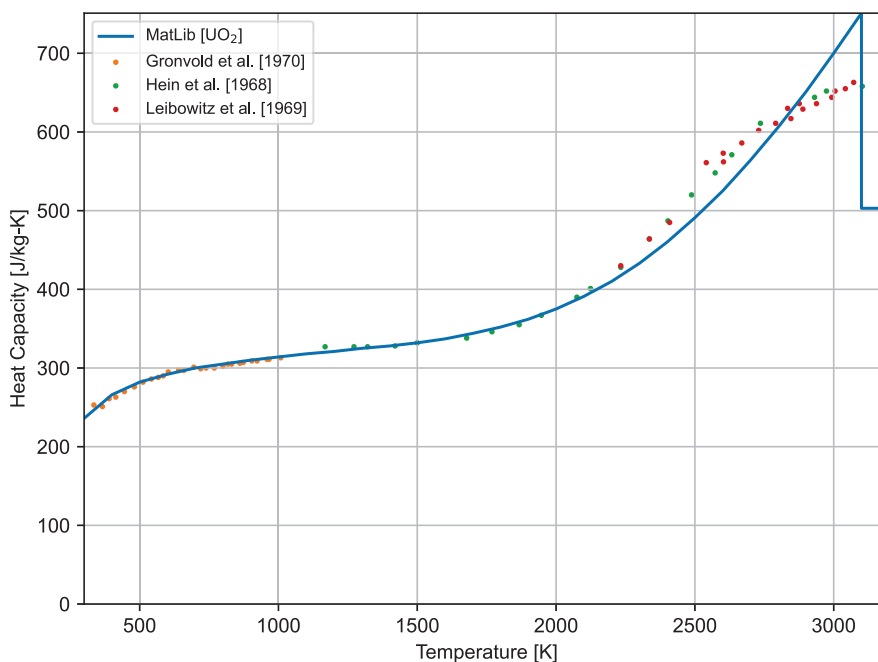


Figure 2-6. Model-to-Data Comparison for UO_2 Specific Heat Capacity Correlation

Specific heat capacity data have been collected for $(\text{U}_{0.8}\text{Pu}_{0.2})\text{O}_2$ from unirradiated samples [Gibby et al., 1974] [Leibowitz et al., 1972] [Affortit and Marcon, 1970]. A comparison between these data for UO_2 is presented in Figure 2-7. This comparison demonstrates good agreement with two of the data sets between the correlation and the database up to about the melting point of about 3000 K. The third data set is overpredicted above 2300 K. Since the Affortit results are known to be generally low in comparison to results from other investigators, the correlation is considered to be in good agreement with the experimental data.

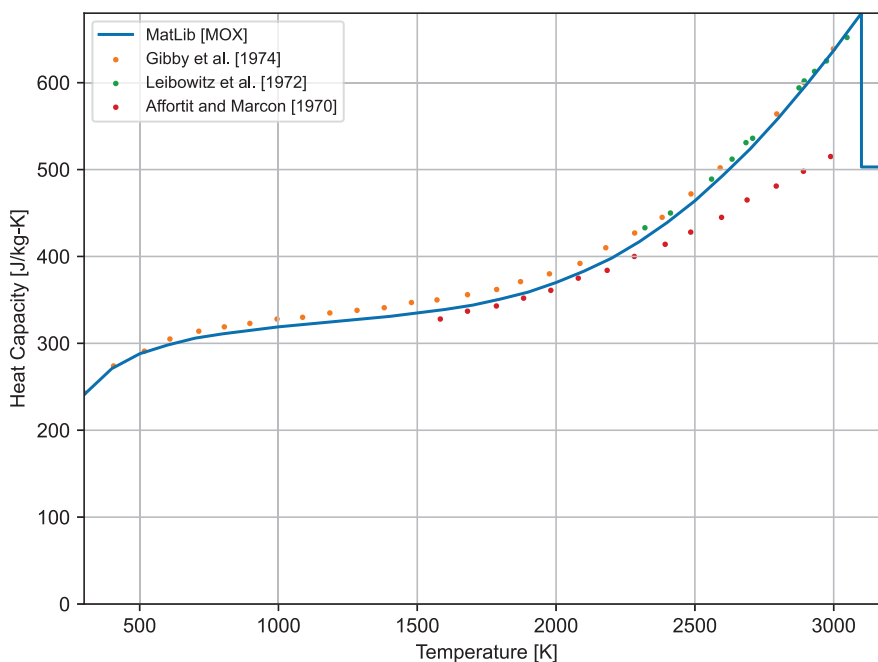


Figure 2-7. Model-to-Data Comparison for MOX Specific Heat Capacity Correlation

2.1.2.3 Applicability and Uncertainty

The fuel specific heat capacity (Equation 2-5) and enthalpy (Equation 2-6) models are applicable to the range of available data:

- Fuel types: UO_2 , $\text{UO}_2\text{-Gd}_2\text{O}_3$, MOXrowc
- Gadolinia content: 0 to 10 wt%
- Temperature: 300 K to the applicable melting temperature (see Section 2.1.3)
- Rod-average burnup: No burnup dependence observed
- As-fabricated density: No density dependence observed

Engineering judgment should be used if analysis outside of these ranges is needed.

The uncertainty of the correlation is given below for each fuel type as an absolute standard error. The uncertainty of the pooled data appears to be relatively constant with temperature. Therefore, an absolute error is given.

- UO_2 and $\text{UO}_2\text{-Gd}_2\text{O}_3$: $\sigma = 26 \text{ J/kg-K}$
- MOX : $\sigma = 28 \text{ J/kg-K}$

The standard error of the $\text{UO}_2\text{-Gd}_2\text{O}_3$ is assumed to be the same as that of UO_2 based on the small fraction of Gd_2O_3 in UO_2 . When excluding the [Affortit and Marcon, 1970] data from the MOX comparison, the standard error is 9.6 J/kg-K.

2.1.3 Melting Temperature

The melting temperature of oxide nuclear fuel is modeled in MatLib as a function of two parameters:

1. Composition
2. Burnup

2.1.3.1 Model Description

The melting temperature of UO_2 , Gd_2O_3 , and PuO_2 is given by:

$$T_{melt} = 3113.15 - 0.5Bu - 4.8X_{\text{Gd}_2\text{O}_3} - 5.41395X_{\text{PuO}_2} + 7.468390 \times 10^{-3}X_{\text{PuO}_2}^2 \quad (2-8)$$

Where,

T_{melt} = Melting temperature, K

X_{PuO_2} = PuO_2 content, wt%

$X_{\text{Gd}_2\text{O}_3}$ = Gd_2O_3 content, wt%

Bu = Burnup, GWd/MTU

2.1.3.2 Comparison to Data

Melting temperature data have been collected for UO_2 , PuO_2 , MOX, and $\text{UO}_2\text{-Gd}_2\text{O}_3$ from unirradiated and irradiated samples [Popov et al., 2000] [Yamada et al., 1999]. A comparison between these data for UO_2 , PuO_2 , MOX and $\text{UO}_2\text{-Gd}_2\text{O}_3$ is presented in Figure 2-8. This comparison demonstrates good agreement between the correlation and the database within range of 0 to 100 GWd/MTU for UO_2 , PuO_2 , MOX and $\text{UO}_2\text{-Gd}_2\text{O}_3$ up to 30% Gd_2O_3 .

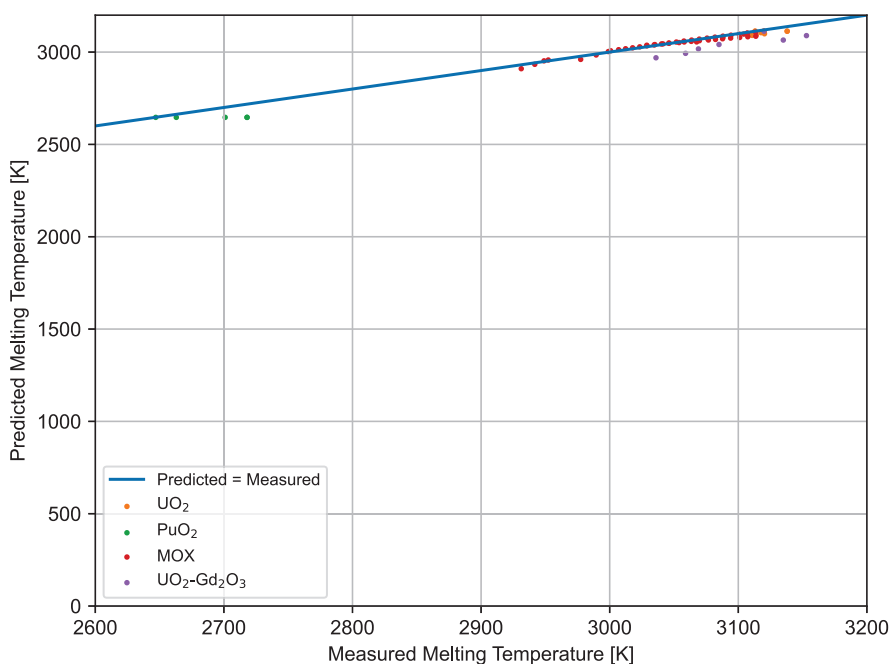


Figure 2-8. Model-to-Data Comparison for UO_2 , PuO_2 , MOX, and $\text{UO}_2\text{-Gd}_2\text{O}_3$ Melting Temperature Correlation

2.1.3.3 Applicability and Uncertainty

The fuel melting temperature model is applicable to the range of available data:

- Fuel types: UO_2 , PuO_2 , MOX, and $\text{UO}_2\text{-Gd}_2\text{O}_3$
- Gadolinia content: 0 to 30 wt%
- Rod-average burnup: 0 to 100 GWd/MTU
- As-fabricated density: No density dependence observed

Engineering judgment should be used if analysis outside of these ranges is needed.

The uncertainty of the correlation is given below for all four fuel types as an absolute standard error.

- UO_2 , PuO_2 , MOX, and $\text{UO}_2\text{-Gd}_2\text{O}_3$: $\sigma = 25 \text{ K}$

2.1.4 Thermal Expansion

The thermal expansion of oxide nuclear fuel is modeled in MatLib as a function of three parameters:

1. Temperature
2. Composition
3. Molten fraction

2.1.4.1 Model Description

The thermal expansion of UO_2 , $\text{UO}_2\text{-Gd}_2\text{O}_3$, and PuO_2 is given by:

$$\Delta L/L = K_1 T - K_2 + K_3 \exp\left(-\frac{E_D}{kT}\right) \quad (2-9)$$

Where,

$\Delta L/L$ = Linear strain caused by thermal expansion (equal to zero at 300 K), unitless

T = Temperature, K

K_1, K_2, K_3 = Constants (Table 2-2)

E_D = Energy of formation of a defect, J (Table 2-2)

k = Boltzmann's constant = 1.38×10^{-23} J/K

Table 2-2. Constants Used in UO_2 , $\text{UO}_2\text{-Gd}_2\text{O}_3$, and PuO_2 Solid-Phase Thermal Expansion Correlations

Constant	UO ₂ and UO ₂ -Gd ₂ O ₃		Units
	UO ₂ -Gd ₂ O ₃	PuO ₂	
K_1	9.80×10^{-6}	9.0×10^{-6}	1/K
K_2	2.61×10^{-3}	2.7×10^{-3}	unitless
K_3	3.16×10^{-1}	7.0×10^{-2}	unitless
E_D	1.32×10^{-19}	7.0×10^{-20}	J

For mixed UO_2 and PuO_2 , the thermal expansion of the solid is found by combining the contribution from each constituent in proportion to its weight fraction.

The fuel thermal expansion model includes terms for partially molten and completely molten fuel. However, these correlations are not well validated and their use is subject to greater uncertainty.

During melting, an expansion equal to a linear strain of 0.043 occurs. If the fuel is partially molten, the strain due to thermal expansion is given by Equation 2-10:

$$\Delta L/L_0 = \Delta L/L_0(T_m) + 0.043f_{molten} \quad (2-10)$$

Where,

$\Delta L/L_0(T_m)$ = Thermal expansion strain of solid fuel from equations with $T = T_m$

T_m = Melting temperature, K

f_{molten} = Fraction of the fuel which is molten, unitless

The correlation used to describe the expansion of entirely molten fuel is given by Equation 2-11:

$$\Delta L/L_0 = \Delta L/L_0(T_m) + 0.043 + 3.6 \times 10^{-5}(T - (T_m + \Delta T_m)) \quad (2-11)$$

The solid-to-liquid phase transition is isothermal only for pure UO_2 or pure PuO_2 . For MOX, the transition occurs over a finite temperature range, denoted in Equation 2-11 by ΔT_m .

2.1.4.2 Comparisons to Data

Thermal expansion data have been collected for UO_2 from unirradiated samples [Baldock et al., 1966] [Grønvold, 1955] [Burdick and Parker, 1956] [Hagman et al., 1981] [Martin, 1988]. A comparison between these data for UO_2 is presented in Figure 2-9. This comparison demonstrates good agreement between the correlation and the database from room temperature to the melting temperature (~ 3000 K).

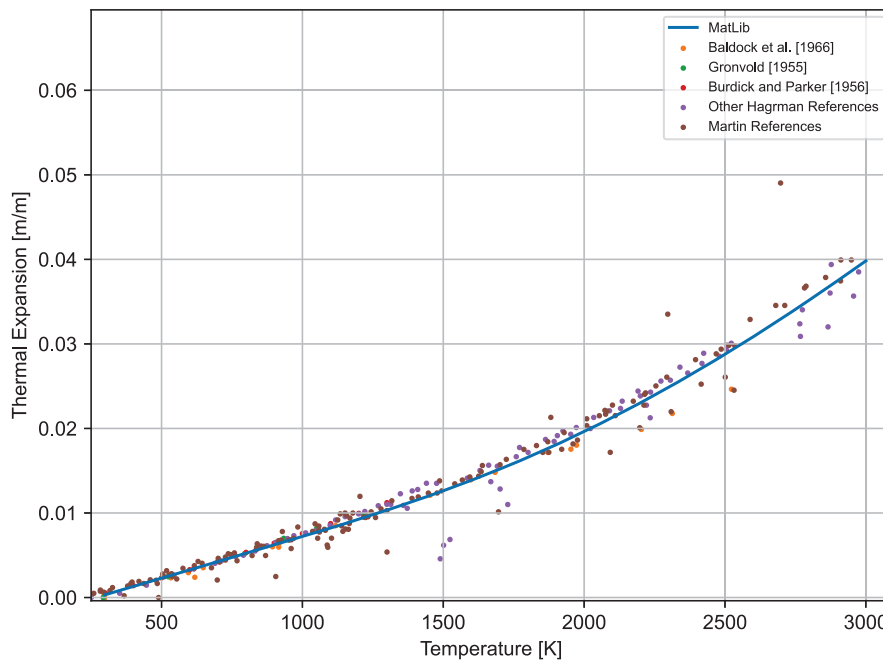


Figure 2-9. Model-to-Data Comparison for UO_2 Correlation

Thermal expansion data have been collected for PuO_2 from unirradiated samples [Brett and Russel, 1960] [Tokar and Nutt, 1972]. A comparison between these data for PuO_2 is presented in Figure 2-10. This comparison demonstrates good agreement between the correlation and the database from room temperature to the melting temperature (~ 3000 K).

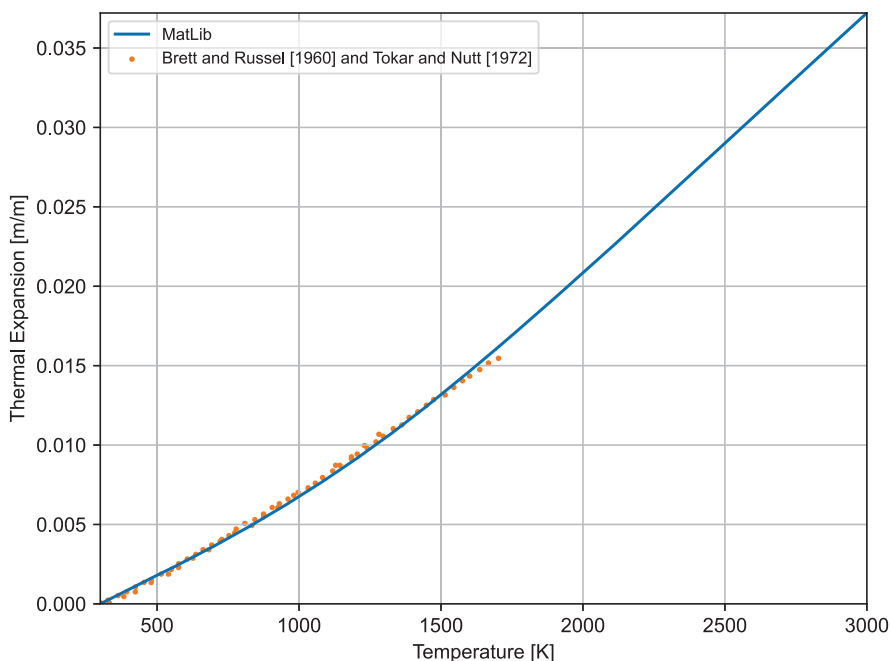


Figure 2-10. Model-to-Data Comparison for PuO_2 Correlation

2.1.4.3 Applicability and Uncertainty

The fuel thermal expansion model is applicable to the range of available data:

- Fuel types: UO_2 , $\text{UO}_2\text{-Gd}_2\text{O}_3$, MOX
- Gadolinia content: 0 to 10 wt%
- Temperature: 300 K to the applicable melting temperature (see Section 2.1.3)
- Rod-average burnup: No burnup dependence observed
- As-fabricated density: No density dependence observed

Engineering judgment should be used if analysis outside of these ranges is needed.

The uncertainty of the correlation is given below for each fuel type as a relative standard error. The uncertainty of the pooled data was found to be temperature dependent, increasing approximately linearly with temperature. Therefore, a relative error is given rather than an absolute error.

- UO_2 and $\text{UO}_2\text{-Gd}_2\text{O}_3$: $\sigma = 10.3\%$
- PuO_2 : $\sigma = 3.5\%$

The relative standard error for UO_2 was calculated by excluding data with very small measured thermal expansion to avoid artificially increasing the relative standard error. In addition, two data with very large deviation were identified as outliers and removed in this calculation.

2.1.5 Emissivity

The emissivity of oxide nuclear fuel is modeled in MatLib as a function of one parameter:

1. Temperature

2.1.5.1 Model Description

The emissivity of UO_2 , MOX and $\text{UO}_2\text{-Gd}_2\text{O}_3$ is given by:

$$\epsilon = 0.78557 + 1.5263 \times 10^{-5}T \quad (2-12)$$

Where,

ϵ = Total hemispherical emissivity, unitless

T = Temperature, K

2.1.5.2 Comparison to Data

Emissivity data have been collected for UO_2 from unirradiated samples [[Held and Wilder, 1969](#)] [[Cabannes et al., 1967](#)]. A comparison between these data for UO_2 is presented in Figure 2-11. This comparison demonstrates reasonable agreement between the correlation and the database within the range of 300 to 2500 K.

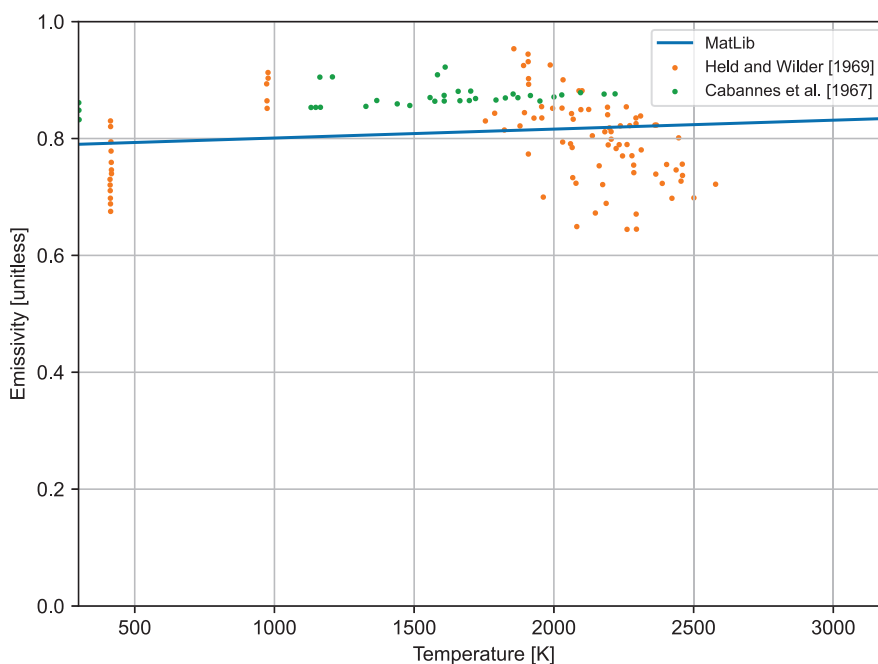


Figure 2-11. Model-to-Data Comparison for Emissivity of Oxide Fuel

2.1.5.3 Applicability and Uncertainty

The emissivity model is applicable to the range of available data:

- Fuel types: UO_2 , MOX and $\text{UO}_2\text{-Gd}_2\text{O}_3$
- Gadolinia content: 0 to 10 wt%
- Temperature: 300 to 2500 K
- Rod-average burnup: No burnup dependence observed
- As-fabricated density: No density dependence observed

Engineering judgment should be used if analysis outside of these ranges is needed.

The uncertainty of the correlation is given below for each fuel type as an absolute standard error.

- UO_2 , MOX, $\text{UO}_2\text{-Gd}_2\text{O}_3$: $\sigma = 0.072$, unitless

The surfaces of UO_2 , MOX and $\text{UO}_2\text{-Gd}_2\text{O}_3$ are optically very similar. Therefore, it is assumed the uncertainty of the correlation will be applicable to all the variants.

2.1.6 Density

The theoretical density of oxide nuclear fuel is modeled in MatLib as a function of one parameter:

1. Composition

2.1.6.1 Model Description

- The theoretical density of pure UO_2 is taken as 10960 kg/m^3
- The theoretical density of pure PuO_2 is taken as 11460 kg/m^3

The addition of gadolinia reduces the theoretical density of UO_2 by Equation 2-13.

$$\rho_{TD} = \rho_{\text{UO}_2} - 3860 f_{\text{Gd}_2\text{O}_3} \quad (2-13)$$

Where,

ρ_{TD} = Theoretical density of $\text{UO}_2/\text{Gd}_2\text{O}_3$ mixture, kg/m^3

ρ_{UO_2} = Theoretical density of UO_2 , kg/m^3

$f_{\text{Gd}_2\text{O}_3}$ = Weight fraction of Gd_2O_3 , unitless

The theoretical density of MOX is determined based on the weight fraction of UO_2 and PuO_2 by Equation 2-14.

$$\rho_{TD} = \rho_{\text{UO}_2} (1 - f_{\text{PuO}_2}) + \rho_{\text{PuO}_2} (f_{\text{PuO}_2}) \quad (2-14)$$

Where,

ρ_{TD} = Theoretical density of UO_2/PuO_2 mixture, kg/m^3

ρ_{UO_2} = Theoretical density of UO_2 , kg/m^3

ρ_{PuO_2} = Theoretical density of PuO_2 , kg/m^3

f_{PuO_2} = Weight fraction of PuO_2 , unitless

2.1.6.2 Applicability and Uncertainty

The theoretical density model is applicable to the range of available data:

- Fuel types: UO_2 , PuO_2 , MOX, and $\text{UO}_2\text{-Gd}_2\text{O}_3$
- Gadolinia content: 0 to 100 wt%
- Temperature: Room temperature
- Rod-average burnup: No burnup dependence observed
- As-fabricated density: Not applicable

Engineering judgment should be used if analysis outside of these ranges is needed.

No uncertainty is given on the theoretical density. Uncertainty in the density of pellets is addressed through the input of fraction of theoretical density.

2.1.7 Densification

The densification of oxide nuclear fuel is modeled in MatLib as a function of two parameters:

1. Maximum expected in-reactor densification
2. Burnup

The maximum expected in-reactor densification is calculated using one of two methods:

- The re-sintering method uses the density change observed during re-sintering tests (1973 K for 24 hours based on Regulatory Guide 1.126 [NRC, 1978]) in a laboratory furnace and is the preferred input for the calculation.
- If a re-sintering density change is not input, the sintering temperature based method uses the initial unirradiated density of the fuel and the fuel fabrication sintering temperature and burnup for density calculations.

2.1.7.1 Model Description

The densification of UO_2 , MOX and $\text{UO}_2\text{-Gd}_2\text{O}_3$ is given by [Rolstad et al., 1974]:

$$\frac{\Delta L}{L} = \left(\frac{\Delta L}{L} \right)_m + \exp[-3(Bu + B)] + 2 \exp[-35(Bu + B)] \quad (2-15)$$

$$\left(\frac{\Delta L}{L}\right)_m = \begin{cases} \frac{100\rho_{sint}}{(3\rho_{start})}, & \text{for } \rho_{sint} > 0 \text{ kg/m}^3 \\ \begin{cases} \frac{-22.2(100 - \rho_{TD})}{(T_{sint} - 1453.15)}, & \text{for } T < 1000 \text{ K} \\ \frac{-66.6(100 - \rho_{TD})}{(T_{sint} - 1453.15)}, & \text{for } T \geq 1000 \text{ K} \end{cases} & \text{for } \rho_{sint} = 0 \text{ kg/m}^3 \end{cases} \quad (2-16)$$

Where,

$\frac{\Delta L}{L}$ = Dimension change, %

$\left(\frac{\Delta L}{L}\right)_m$ = Maximum dimension change due to irradiation, % (Equation 2-16)

Bu = Burnup MWd/kgU

B = A constant determined by the code to fit the boundary condition; $\frac{\Delta L}{L} = 0$ when $Bu = 0$, unitless

ρ_{sint} = Resintered fuel density change, kg/m³

T = Fuel temperature, K

ρ_{start} = Starting (as-fabricated) density, kg/m³

ρ_{TD} = Initial density, percent theoretical

T_{sint} = Sintering temperature, K (default is 1873.15 K)

2.1.7.2 Comparison to Data

Densification data have been collected for UO₂ and MOX pellets from irradiated samples [Banks, 1974] [Freshley et al., 1979] [Freshley et al., 1976]. A comparison between these data is presented in Figure 2-12. This comparison demonstrates that basing densification on the sintering temperature provides a large degree of uncertainty.

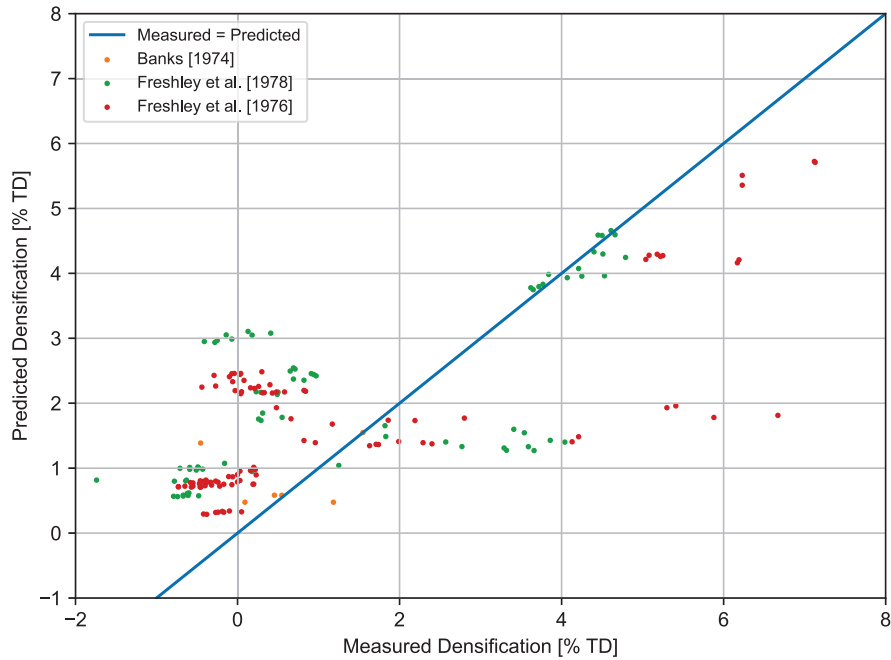


Figure 2-12. Model-to-Data Comparison for Density of Oxide Fuel

2.1.7.3 Applicability and Uncertainty

The density correlation used in MatLib is applicable to the range of available data (i.e., fuels with pore size distributions similar to those included in the [Freshley et al., 1976] study). Engineering judgment should be used if analysis outside of these ranges is needed. Due to the scatter in the experimental data, it is difficult to establish a meaningful measure of uncertainty.

2.1.8 Swelling

The swelling in the oxide fuels is modeled in MatLib as two different phenomena; solid swelling and gaseous swelling. Solid swelling proceeds at a constant rate with increasing burnup and with no temperature dependence. Gaseous swelling only occurs at high burnup (>40 GWd/MTU) and occurs over a specific temperature range (1233 to 2105 K)

2.1.8.1 Model Description

Solid Swelling

The solid swelling of UO_2 and MOX is given by:

$$\frac{\Delta V}{V} = \begin{cases} 0, & \text{for } Bu \leq 6 \text{ GWd/MTU} \\ 0.00062 (Bu - 6), & \text{for } 6 < Bu \leq 80 \text{ GWd/MTU} \\ 0.00062 (80 - 6) + 0.00086 (Bu - 80), & \text{for } Bu > 80 \text{ GWd/MTU} \end{cases} \quad (2-17)$$

Where,

$\Delta V/V$ = Fractional volume change due to solid fission products, m^3/m^3

Bu = Pellet-average burnup, GWd/MTU

The solid swelling of $\text{UO}_2\text{-Gd}_2\text{O}_3$ is given by:

$$\frac{\Delta V}{V} = 0.0005Bu \quad (2-18)$$

Where,

$\Delta V/V$ = Fractional volume change due to solid fission products m^3/m^3

Bu = Pellet-average burnup GWd/MTU

Gaseous Swelling

The gaseous swelling of UO_2 , $\text{UO}_2\text{-Gd}_2\text{O}_3$, and MOX is given by:

- $Bu < 40$ GWd/MTU

$$\frac{\Delta L}{L} = 0 \quad (2-19)$$

- $40 < Bu < 50$ GWd/MTU

$$\frac{\Delta L}{L} = \begin{cases} 0, & \text{for } T < 1233 \text{ K} \\ \frac{Bu - 40}{Bu - 40} (-4.37 \times 10^{-2} + 4.55 \times 10^{-5}T), & \text{for } 1233 \leq T < 1643 \text{ K} \\ \frac{Bu - 40}{10} (7.40 \times 10^{-2} - 4.05 \times 10^{-5}T), & \text{for } 1643 \leq T < 2105 \text{ K} \\ 0, & \text{for } T > 2105 \text{ K} \end{cases} \quad (2-20)$$

- $Bu \geq 50$ GWd/MTU

$$\frac{\Delta L}{L} = \begin{cases} 0, & \text{for } T < 1233 \text{ K} \\ -4.37 \times 10^{-2} + 4.55 \times 10^{-5}T, & \text{for } 1233 \leq T < 1643 \text{ K} \\ 7.40 \times 10^{-2} - 4.05 \times 10^{-5}T, & \text{for } 1643 \leq T < 2105 \text{ K} \\ 0, & \text{for } T > 2105 \text{ K} \end{cases} \quad (2-21)$$

Where,

$\Delta L/L$ = Fractional volume change due to solid fission products, m^3/m^3

Bu = Pellet-average burnup, GWd/MTU

T = Pellet ring temperature, K

2.1.8.2 Comparison to Data

Solid swelling increase data have been collected for UO_2 from irradiated samples [Garde, 1986] [Newman, 1986] [Smith et al., 1994] [Dideon and Bain, 1983] [Turnbull, 2001] [Colombier et al., 2010]. A comparison between these data for UO_2 is presented in Figure 2-13. This comparison demonstrates reasonable comparison between the correlation and the database.

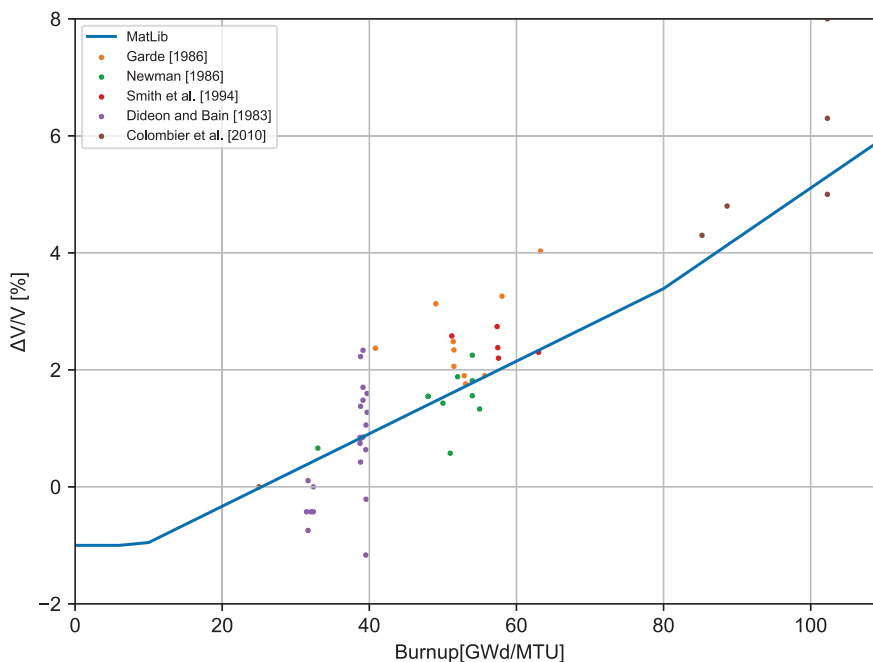


Figure 2-13. Model-to-Data Comparison for Solid Swelling Correlation

Solid swelling rate data have been collected for UO_2 from irradiated Halden tests [Colombier et al., 2010] [Petiprez, 2002] [Matsson and Turnbull, 1998] [Turnbull, 2001]. A comparison between these data for UO_2 is presented in Figure 2-14. This comparison demonstrates reasonable comparison between the correlation and the database.

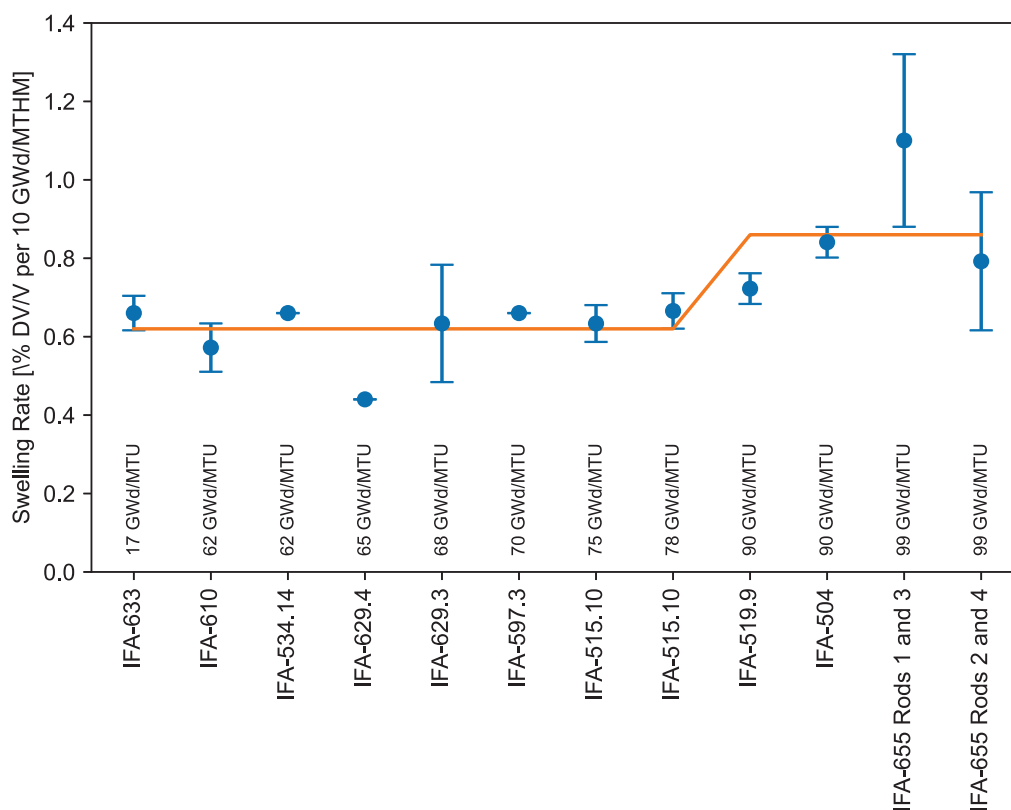


Figure 2-14. Model-to-Data Comparison for Solid Swelling Rate Correlation

2.1.8.3 Applicability and Uncertainty

The swelling model is applicable to the range of available data:

- Fuel types: UO_2 , PuO_2 , MOX and $\text{UO}_2\text{-Gd}_2\text{O}_3$
- Gadolinia content: 0 to 10 wt%
- Temperature: Entire temperature range
- Rod-average burnup: 0 to 100 GWd/MTU
- As-fabricated density: 90 to 98 %TD

Engineering judgment should be used if analysis outside of these ranges is needed.

The uncertainty of the correlation is given below for each fuel type as an absolute standard error.

- UO_2 , MOX: $\sigma = 0.00008 \Delta V/V$ per 1 GWd/MTU, $Bu < 80$ GWd/MTU

- UO_2 , MOX: $\sigma = 0.00016 \Delta V/V$ per 1 GWd/MTU, $Bu < 80$ GWd/MTU
- $\text{UO}_2\text{-Gd}_2\text{O}_3$: $\sigma = 0.00008 \Delta V/V$ per 1 GWd/MTU

2.2 Metallic Fuel U-Pu-Zr Material Properties

Material property correlations for metallic fuels are described in the following sections. Metallic fuel is limited to both U-Zr and U-Pu-Zr. U-Zr and U-Pu-Zr are relatively new fuel types for use in new fast reactor designs.

2.2.1 Thermal Conductivity

The thermal conductivity of metallic fuel is modeled in MatLib as a function of four parameters:

1. Temperature
2. Pu content
3. Zr content
4. Porosity

2.2.1.1 Model Description

The thermal conductivity of metallic fuel containing U-Pu-Zr is given by Equation 2-22 [Baker and Wilson, 1992]:

$$k = \frac{D_1}{100} \left(AT + \frac{BT^2}{2} + \frac{CT^3}{3} \right) \quad (2-22)$$

Where,

$$D_1 = \frac{1 - P}{1 + 2P} \quad (2-23a)$$

$$A = 17.5 \left(\frac{1 - 2.23\chi_{\text{Zr}}}{1 + 1.61\chi_{\text{Zr}}} - 2.62\chi_{\text{Pu}} \right) \quad (2-23b)$$

$$B = 1.54 \times 10^{-2} \left(\frac{1 + 0.061\chi_{\text{Zr}}}{1 + 1.61\chi_{\text{Zr}}} + 0.90\chi_{\text{Pu}} \right) \quad (2-23c)$$

$$C = 9.38 \times 10^{-6} (1 - 2.70\chi_{\text{Pu}}) \quad (2-23d)$$

and,

k = Thermal conductivity, W/m-K

P = Fraction of porosity in the fuel, unitless

T = Temperature, K

χ_x = Weight fraction of species x in the fuel mixture, unitless

2.2.1.2 Applicability and Uncertainty

The thermal conductivity model is applicable to the range of available data:

- Fuel types: U-Zr and U-Pu-Zr
- Temperature: 273 to 1000 K
- Rod-average burnup: 0 GWd/MTU

Engineering judgment should be used if analysis outside of these ranges is needed.

2.2.2 Specific Heat Capacity

The specific heat capacity of U-Pu-Zr metallic fuel is modeled as a function of two parameters:

1. Temperature
2. Composition

2.2.2.1 Model Description

The model for specific heat in MatLib is based on published experimental data produced from measuring calculated specific heats from incremental enthalpies in a drop calorimeter to about 1200 °C [Savage, 1968]. Equations 2-24, 2-25, and 2-26 present the specific heat correlations for U-Pu-Zr fuel, dependent on the phase.

$$C_p^{\alpha+\delta} = A_0 + \frac{A_1}{MW}T \quad (2-24)$$

Where,

$C_p^{\alpha+\delta}$ = Heat capacity of U-Pu-Zr fuel, J/kg-K

A_0 = Constant = 26.58

A_1 = Constant = 0.027

MW = Molecular weight of the metallic fuel mixture

T = Temperature, °C

$$C_p^\gamma = A_0 + \frac{A_1}{MW}T \quad (2-25)$$

Where,

C_p^γ = Specific heat capacity of metallic fuel (U-Pu-Zr / U-Zr), J/kg-K

A_0 = Constant = 15.84

A_1 = Constant = 0.026

MW = Molecular weight of the metallic fuel mixture

T = Temperature, °C

$$C_p^{\beta+\gamma} = \frac{C_p^\gamma - C_p^{\alpha+\delta}}{T_2 - T_1}(T - T_1) + C_p^{\alpha+\delta} \quad (2-26)$$

Where,

$C_p^{\beta+\gamma}$ = Specific heat capacity of metallic fuel in the $\beta + \gamma$ phase, J/kg-K

C_p^γ = Specific heat capacity of metallic fuel in the γ phase, J/kg-K

$C_p^{\alpha+\delta}$ = Specific heat capacity of metallic fuel in the $\alpha + \delta$ phase, J/kg-K

T = Temperature, °C

T_1 = Transition temperature between $\alpha + \delta$ and $\beta + \gamma$ phases, K (Table 2-3)

T_2 = Transition temperature between $\beta + \gamma$ and γ phases, L (Table 2-3)

The transition temperature between phases assumes there is no dependence on Zr content and that the behavior is linear between 0 and 19 wt% Pu.

Table 2-3. Phase Transition Temperatures Used in the Specific Heat Capacity Correlations for U-Pu-Zr Metallic Fuel

Pu Content (wt%)	T_1 (K)	T_2 (K)
0	935.15	965.15
19	868.15	923.15

2.2.2.2 Applicability and Uncertainty

The specific correlations derived from the published data [Savage, 1968] are applicable for:

- Fuel types: U-Pu-Zr
- Phases: $\alpha + \gamma$, $\beta + \gamma$, and γ

Metallic fuel outside the bounds of the correlations will be executed and the user will be prompted with an error message.

2.2.3 Density

The theoretical density of metallic fuel is modeled in MatLib as a function of one parameter:

1. Composition

2.2.3.1 Model Description

The density of metallic fuel is a function of the weight fractions and densities of uranium and zirconium:

$$\rho_{TD} = \frac{1}{\frac{(1 - W_{Zr})}{\rho_U} + \frac{W_{Zr}}{\rho_{Zr}}} \quad (2-27)$$

Where,

ρ_{TD} = Theoretical density of U-Pu-Zr metallic fuel, kg/m³

W_x = Weight fraction of species x , unitless

ρ_{Zr} = Theoretical density of Zr = 6500 kg/m³

ρ_U = Theoretical density of U = 19000 kg/m³

2.2.3.2 Comparison to Data

No comparisons to data are provided as these are theoretical quantities.

2.2.3.3 Applicability and Uncertainty

No uncertainty is given on the theoretical density. Uncertainty in the density of the pellets is addressed through the input of fraction of theoretical density.

2.2.4 Melting Temperature

The melting temperature of metallic fuel in MatLib is a function of one parameter:

1. Composition

2.2.4.1 Model Description

The melting temperature is a function of the weight fractions of Pu and Zr [Baker and Wilson, 1992]:

$$T_{melt} = 1132(1 - 0.77W_{Pu})(1 - 0.94W_{Zr}) + 273.15 \quad (2-28)$$

Where,

T_{melt} = Melting temperature of metallic fuel, K

W_x = Weight fraction of species x , unitless

2.2.5 Eutectic Temperature

The eutectic temperature is the temperature at the onset of liquid-phase attack between the metallic fuel and cladding. It is assumed constant [Baker and Wilson, 1992].

$$T_{eutectic} = 973 \text{ K} \quad (2-29)$$

2.2.6 Thermal Expansion

The thermal expansion of metallic fuel is modeled in MatLib as a function of one parameter:

1. Temperature

2.2.6.1 Model Description

The thermal expansion of U-Pu-Zr and U-Zr is given by:

$$\frac{\Delta L}{L} = A + BT \quad (2-30)$$

Where,

$\left(\frac{\Delta L}{L}\right)$ = Linear strain caused by thermal expansion, unitless

T = Temperature, K

A, B = Constants (see Table 2-4)

Table 2-4. Constants Used in the Thermal Expansion Correlations for U-Pu-Zr Metallic Fuel

Temperature (K)	A (unitless)	B (K ⁻¹)
$T < 868$ K	-5.2448×10^{-3}	1.76×10^{-5}
$868 \text{ K} \leq T < 938$ K	-5.4462×10^{-2}	7.43×10^{-5}
$T \geq 938$ K	-3.6538×10^{-3}	2.01×10^{-5}

2.2.6.2 Applicability and Uncertainty

The thermal expansion model is applicable to the range of available data:

- Temperature: 293 to 1073 K

Engineering judgment should be used if analysis outside of these ranges is needed.

2.2.7 Emissivity

The emissivity unitless of metallic fuel in MatLib is treated as a constant value [Baker and Wilson, 1992]:

$$\epsilon = 0.80 \quad (2-31)$$

Where,

ϵ = Emissivity, unitless

2.2.7.1 Applicability and Uncertainty

The thermal expansion model is applicable to the range of available data:

- Temperature: 293 to 1073 K

Engineering judgment should be used if analysis outside of these ranges is needed.

2.2.8 Swelling

The swelling in metallic fuels is modeled in MatLib as two different phenomena: pre-contact and post-contact. Post-contact swelling is much slower than pre-contact swelling due to the formation and accumulation of solid fission products. Swelling is a function of one parameter:

1. Burnup

2.2.8.1 Model Description

The swelling rate is assumed constant for each region; a no contact region and a post contact region:

$$\frac{\Delta V}{V} = \begin{cases} 0.05Bu, & \text{for Pre-Contact} \\ 0.009Bu, & \text{for Post-Contact} \end{cases} \quad (2-32)$$

Where,

$$\left(\frac{\Delta V}{V} \right) = \text{Fuel volumetric swelling, unitless}$$

Bu = Burnup, at% (Note: 1 GWd/MTM = 0.1066 at%)

3.0 Cladding Material Properties

3.1 Zirconium-based Alloys

Material property correlations for Zirconium-based claddings are described in the following subsections. Unless otherwise specified, the correlations below are applicable to Zircaloy-2, Zircaloy-4, ZIRLO, Optimized ZIRLO, and M5. Various heat treatments can be accommodated by specifying the cold worked condition of the alloy. Examples of cold worked conditions for the different alloys are provided in Table 3-1.

Table 3-1. Example Heat Treatments and Cold Worked Conditions for Different Zirconium-Based Alloys

Alloy	Heat Treatment	Cold Worked Conditions
Zircaloy-2	RXA ^(a)	0%
Zircaloy-4	CWRSA ^(b)	50%
ZIRLO	CWRSA	50%
Opt. ZIRLO	pRXA ^(c)	<50%
M5	RXA	0%

^(a) Recrystallized Annealed

^(b) Cold Worked, Stress Relief Annealed

^(c) Partially Recrystallized Annealed

3.1.1 Thermal Conductivity

The thermal conductivity of zirconium-based alloy cladding is modeled in MatLib as a function of one parameter:

1. Temperature

3.1.1.1 Model Description

The thermal conductivity of Zircaloy-4, Zircaloy-2, ZIRLO, Optimized ZIRLO, and M5 is given by:

$$k = 7.511 + 2.088 \times 10^{-2}T - 1.45 \times 10^{-5}T^2 + 7.668 \times 10^{-9}T^3 \quad (3-1)$$

Where,

k = Cladding thermal conductivity, W/m-K

T = Temperature, K

For temperatures greater than or equal to 2098 K, the thermal conductivity is given by:

$$k = 36 \text{ W/m-K} \quad (3-2)$$

3.1.1.2 Comparison to Data

Thermal conductivity data have been collected for Zircaloy-2 and Zircaloy-4 from unirradiated and irradiated samples [Anderson et al., 1962] [Chirigos et al., 1961] [Feith, 1966] [Lucks and Deem, 1958] [Powers, 1961] [Scott, 1965] [Krett and Cleveland, 1997] [Gilchrist, 1976] [Bunnell et al., 1983] [Murabayashi et al., 1975] [Peggs et al., 1976] [Maglić et al., 1994]. A comparison between these data is presented in Figure 3-1. This comparison demonstrates a good agreement between the correlation and the database within a range of 285 to 1770 K.

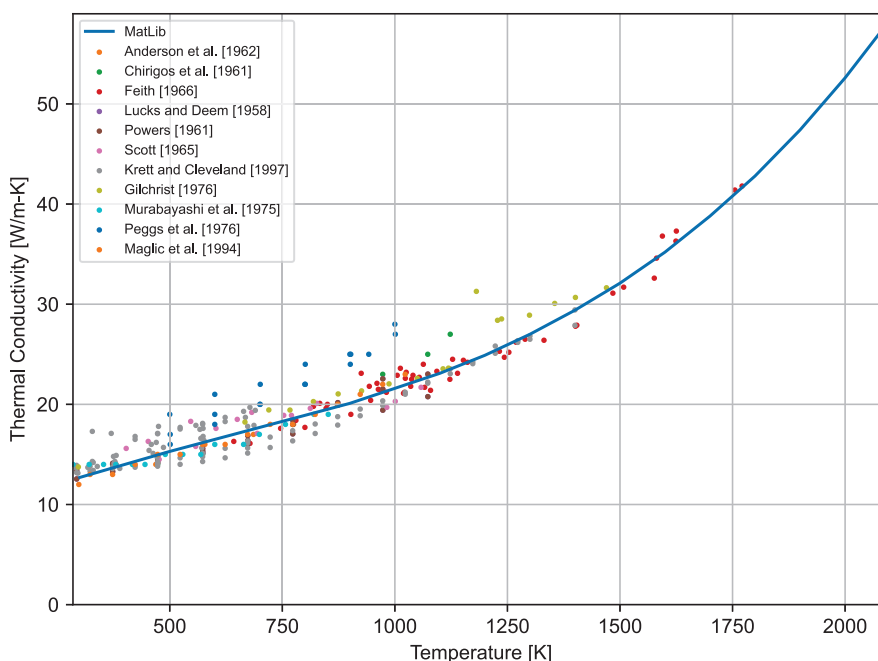


Figure 3-1. Model-to-Data Comparison for Zirconium-based Alloy Cladding Thermal Conductivity Correlation

3.1.1.3 Applicability and Uncertainty

The thermal conductivity model is applicable to the range of available data:

- Cladding types: Zircaloy-4, Zircaloy-2, M5, ZIRLO, and Optimized ZIRLO
- Temperature: 285 to 1770 K
- Rod-average burnup: No burnup dependence observed

Engineering judgment should be used if analysis outside of these ranges is needed.

The uncertainty of the correlation is given below and is applicable for each cladding type. No variation in thermal conductivity uncertainty is observed with increasing temperature, so an absolute uncertainty is used.

- Zircaloy-4, Zircaloy-2, M5, ZIRLO, and Optimized ZIRLO : $\sigma = 1.9 \text{ W/m-K}$

3.1.2 Specific Heat

The specific heat of zirconium-based alloy cladding is modeled in MatLib as a function of one parameter:

1. Temperature

3.1.2.1 Model Description

The specific heat of Zircaloy-4, Zircaloy-2, M5, ZIRLO, and Optimized ZIRLO is given by a lookup table. Specific values at a given temperature can be found by linear interpolation between these temperatures:

Table 3-2. Interpolated Values for the Zirconium-Based Alloys Specific Heat Capacity Correlation

Temperature (K)	Specific Heat Capacity (J/kg-K)
<290	279
290	279
300	281
400	302
640	331
1090	375
1093	502
1113	590
1133	615
1153	719
1173	816
1193	770
1213	619
1233	469
1248	356
>1248	356

3.1.2.2 Comparison to Data

Specific heat data have been collected for Zircaloy-2 and Zircaloy-4 from unirradiated samples [Deem and Eldridge, 1967] [Brooks and Stansbury, 1966]. A comparison between these data is presented in Figure 3-2. This comparison demonstrates good agreement between the correlation and the database within the range 348 to 1300 K.

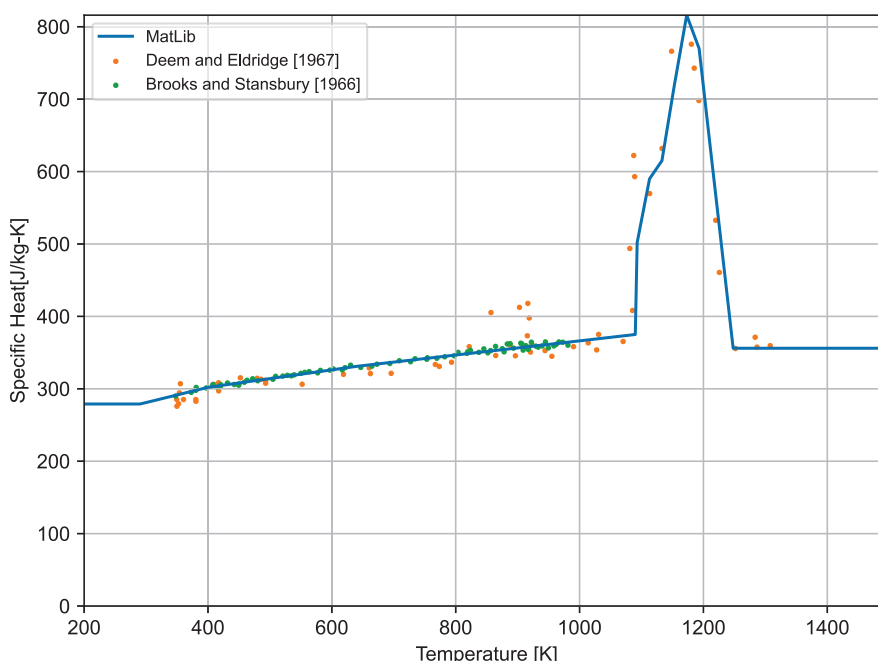


Figure 3-2. Model-to-Data Comparison for Zirconium-based Alloy Cladding Specific Heat Correlation

3.1.2.3 Applicability and Uncertainty

The specific heat model is applicable to the range of available data:

- Cladding types: Zircaloy-4, Zircaloy-2, M5, ZIRLO, and Optimized ZIRLO
- Temperature: 285 to 1300 K
- Rod-average burnup: No burnup dependence observed

Engineering judgment should be used if analysis outside of these ranges is needed.

The uncertainty of the correlation is given below and is applicable for each cladding type. No variation in thermal conductivity uncertainty is observed with increasing temperature, so an absolute uncertainty is used.

For Zircaloy-4, Zircaloy-2, M5, ZIRLO, and Optimized ZIRLO:

$$\sigma \text{ (J/kg - k)} = \begin{cases} 10, & \text{for temperatures less than 1090 K} \\ 25, & \text{for temperatures between 1090 K and 1248 K} \\ 100, & \text{for temperatures greater than 1248 K} \end{cases}$$

3.1.3 Melting Temperature

The melting temperature of zirconium-based alloy cladding is modeled in MatLib as a constant value.

3.1.3.1 Model Description

The melting temperature of Zircaloy-4, Zircaloy-2, M5, ZIRLO, and Optimized ZIRLO is given by a constant value:

$$T_{melt} = 2123.15 \text{ K} \quad (3-3)$$

Where,

T_{melt} = Melting temperature, K

3.1.3.2 Comparison to Data

No Comparison to Data are provided as this is a theoretical quantity.

3.1.3.3 Applicability and Uncertainty

The melting temperature model is applicable to the range of available data:

- Cladding types: Zircaloy-4, Zircaloy-2, M5, ZIRLO and Optimized ZIRLO
- Rod-average burnup: No burnup dependence observed

Engineering judgment should be used if analysis outside of these ranges is needed.

No uncertainty is given on the melting temperature. Greater uncertainty exists on the prediction of cladding temperature.

3.1.4 Thermal Expansion

The thermal expansion of zirconium-based alloy cladding is modeled in MatLib as a function of one parameter:

1. Temperature

3.1.4.1 Model Description

Rolled and drawn zirconium-based alloy products are known to have anisotropy in the thermal expansion. Correlations for thermal expansion in the axial and circumferential directions are provided

in MatLib. The thermal expansion of Zircaloy-4, Zircaloy-2, M5, ZIRLO and Optimized ZIRLO is given by:

$$\varepsilon_{axial} = \begin{cases} -2.5060 \times 10^{-5} + 4.4410 \times 10^{-6} (T - 273.15) & \text{for } 280 < T \leq 1073.15 \text{ K} \\ -8.300 \times 10^{-3} + 9.70 \times 10^{-6} (T - 273.15) & \text{for } T \geq 1273.15 \text{ K} \end{cases} \quad (3-4)$$

$$\varepsilon_{diametral} = \begin{cases} -2.3730 \times 10^{-4} + 6.7210 \times 10^{-6} (T - 273.15) & \text{for } 280 < T \leq 1073.15 \text{ K} \\ -6.800 \times 10^{-3} + 9.70 \times 10^{-6} (T - 273.15) & \text{for } T \geq 1273.15 \text{ K} \end{cases} \quad (3-5)$$

Where,

ε_{axial} = Axial thermal expansion, m/m

$\varepsilon_{diametral}$ = Circumferential thermal expansion, m/m

T = Temperature, K

For $1073.15 \text{ K} \leq T \leq 1273.15 \text{ K}$ the thermal expansion is given by a lookup table. Specific values at a given temperature can found by linear interpolation between these temperatures:

Table 3-3. Interpolated Values for the Zirconium-Based Alloys Thermal Expansion Correlation

Temperature (K)	ε_{axial} (m/m)	$\varepsilon_{diametral}$ (m/m)
1073.15	0.00352774	0.00513950
1083.15	0.00353000	0.00522000
1093.15	0.00350000	0.00525000
1103.15	0.00346000	0.00528000
1113.15	0.00341000	0.00528000
1123.15	0.00333000	0.00524000
1133.15	0.00321000	0.00522000
1143.15	0.00307000	0.00515000
1153.15	0.00280000	0.00508000
1163.15	0.00250000	0.00490000
1173.15	0.00200000	0.00470000
1183.15	0.00150000	0.00445000
1193.15	0.00130000	0.00410000
1203.15	0.00116000	0.00350000
1213.15	0.00113000	0.00313000
1223.15	0.00110000	0.00297000

Table 3-3. Interpolated Values for the Zirconium-Based Alloys Thermal Expansion Correlation (continued)

Temperature (K)	ε_{axial} (m/m)	$\varepsilon_{diametral}$ (m/m)
1233.15	0.00111000	0.00292000
1243.15	0.00113000	0.00287000
1253.15	0.00120000	0.00286000
1263.15	0.00130000	0.00288000
1273.15	0.00140000	0.00290000

3.1.4.2 Comparison to Data

Circumferential thermal expansion data have been collected for Zircaloy-2 and Zircaloy-4 from unirradiated samples [Bunnell et al., 1977] [Kearns, 1965] [Scott, 1965] [Mehan and Wiesinger, 1961]. A comparison between these data for circumferential thermal expansion is presented in Figure 3-3. This comparison demonstrates good agreement between the correlation and the database between 300 and 1080 K.

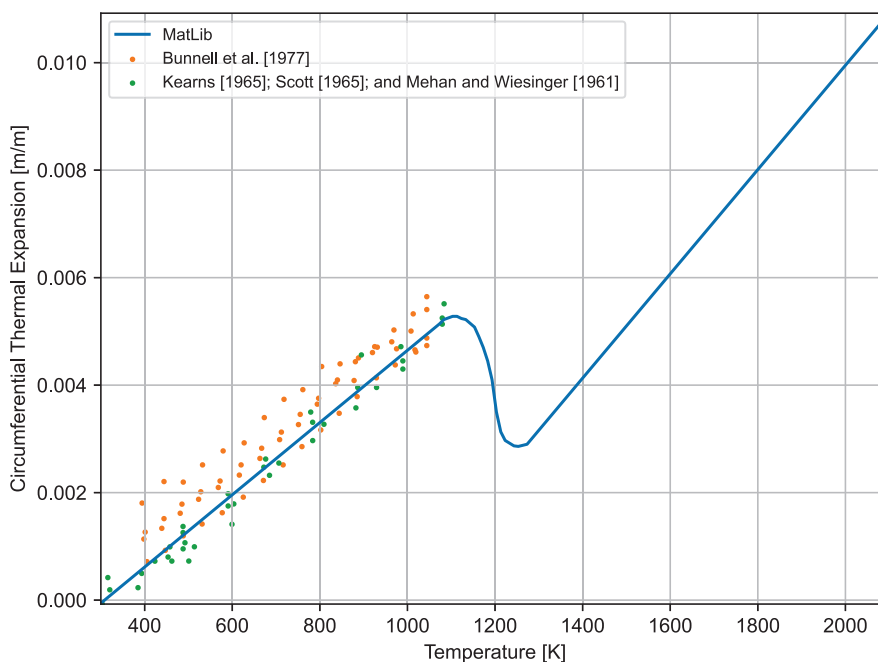


Figure 3-3. Model-to-Data Comparison for Zirconium-based Alloy Cladding Circumferential Thermal Expansion Correlation

Axial thermal expansion data have been collected for Zircaloy-2 and Zircaloy-4 from unirradiated samples [Bunnell et al., 1977] [Kearns, 1965] [Scott, 1965] [Mehan and Wiesinger, 1961]. A comparison between these data for circumferential thermal expansion is presented in Figure 3-4. This

comparison demonstrates good agreement between the correlation and the database between 300 and 1273 K.

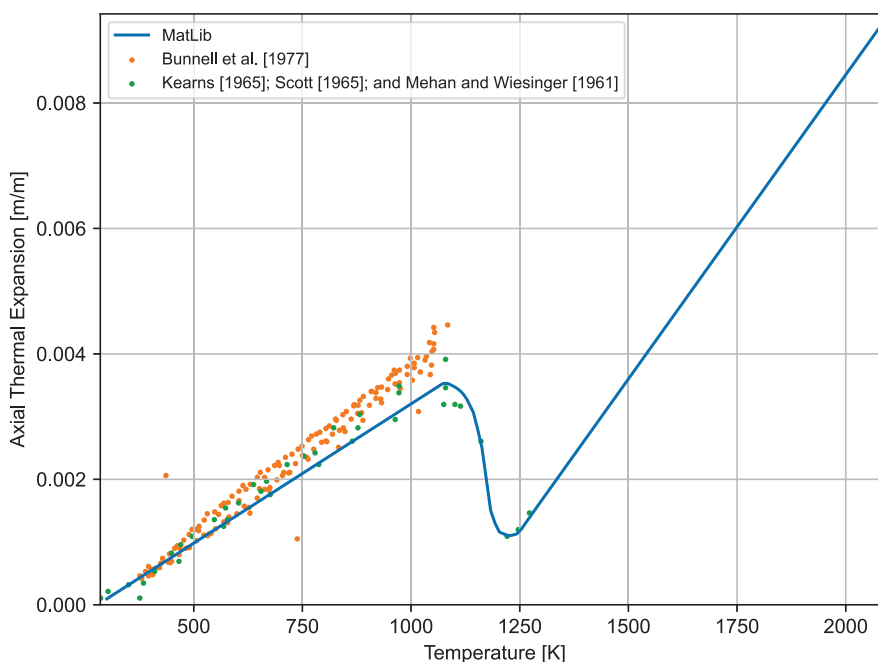


Figure 3-4. Model-to-Data Comparison for Zirconium-based Alloy Cladding Axial Thermal Expansion Correlation

3.1.4.3 Applicability and Uncertainty

The thermal expansion model is applicable to the range of available data:

- Cladding types: Zircaloy-4, Zircaloy-2, M5, ZIRLO and Optimized ZIRLO
- Temperature: 300 to 1080 K for circumferential expansion; 300 to 1273 K for axial expansion
- Rod-average burnup: No burnup dependence observed

Engineering judgment should be used if analysis outside of these ranges is needed.

The uncertainty of the correlation is given below and is applicable for each cladding type. No variation in thermal conductivity uncertainty is observed with increasing temperature, so an absolute uncertainty is used.

For Zircaloy-4, Zircaloy-2, M5, ZIRLO and Optimized ZIRLO:

- Circumferential thermal expansion: $\sigma = 4.6 \times 10^{-4}$ m/m
- Axial thermal expansion: $\sigma = 4.8 \times 10^{-5}$ m/m

3.1.5 Emissivity

The emissivity of zirconium-based alloy cladding is modeled in MatLib as a function of two parameters:

1. Temperature
2. Cladding inner surface oxide thickness

3.1.5.1 Model Description

The emissivity of Zircaloy-4, Zircaloy-2, M5, ZIRLO and Optimized ZIRLO is given by:

$$\epsilon_1 = \begin{cases} 0.325 + 0.1246 \times 10^6 t_{oxide}, & \text{for } t_{oxide} < 3.88 \times 10^{-6} \\ 0.808642 - 50.0 t_{oxide}, & \text{for } t_{oxide} \geq 3.88 \times 10^{-6} \end{cases} \quad (3-6)$$

When the cladding temperature is greater than 1500 K, emissivity is given by:

$$\epsilon_2 = MAX \left[0.325, \exp \left(\frac{1500 - T}{300} \right) \epsilon_1 \right] \quad (3-7)$$

Where,

ϵ_1, ϵ_2 = Cladding emissivity, unitless

T = Temperature, K

t_{oxide} = Inner surface oxide thickness, m

3.1.5.2 Comparison to Data

Emissivity data have been collected for Zircaloy-2 and Zircaloy-4 from irradiated samples [Murphy and Havelock, 1976] [Juenke and Sjudahl, 1968] [Burgoyne and Garlick, 1976]. A comparison between these data for is presented in Figure 3-5. This comparison demonstrates good agreement between the correlation and the database up to 1575 K and 120 μm oxide thickness.

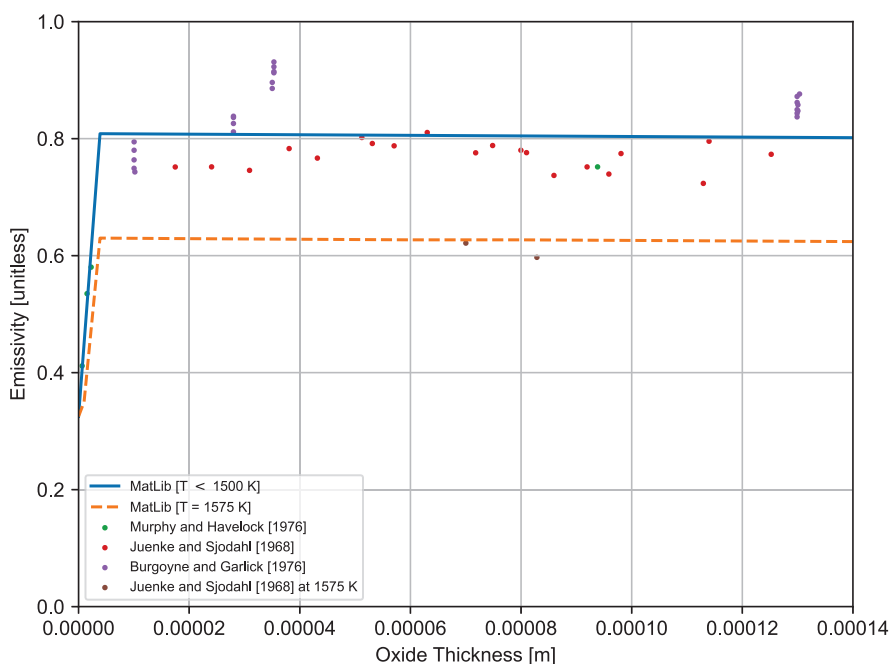


Figure 3-5. Model-to-Data Comparison for Zirconium-based Alloy Emissivity Correlation

3.1.5.3 Applicability and Uncertainty

The emissivity model is applicable to the range of available data:

- Cladding types: Zircaloy-4, Zircaloy-2, M5, ZIRLO and Optimized ZIRLO
- Temperature: 285 to 1575 K
- Oxide Thickness: 0 to 120 μm
- Rod-average burnup: No burnup dependence observed

Engineering judgment should be used if analysis outside of these ranges is needed.

The uncertainty of the correlation is given below and is applicable for each cladding type. No variation in emissivity uncertainty is observed with increasing oxide thickness, so an absolute uncertainty is used.

- Zircaloy-4, Zircaloy-2, M5, ZIRLO and Optimized ZIRLO : $\sigma = 0.054$ (unitless)

3.1.6 Density

The density of Zircaloy-4, Zircaloy-2, M5, ZIRLO and Optimized ZIRLO is modeled in MatLib as a constant value:

$$\rho = 6520 \text{ kg/m}^3 \quad (3-8)$$

Where,

ρ = Density of zirconium-based alloy cladding, kg/m³

3.1.6.1 Comparison to Data

No comparisons to data are provided as this is a theoretical quantity.

3.1.6.2 Applicability and Uncertainty

The density model is applicable to the following:

- Cladding types: Zircaloy-4, Zircaloy-2, M5, ZIRLO and Optimized ZIRLO
- Rod-average burnup: No burnup dependence observed

No uncertainty is given on the density.

3.1.7 Young's Modulus and Shear Modulus

Young's modulus and the shear modulus of zirconium-based alloy cladding are modeled in MatLib as a function of three parameters:

1. Temperature
2. Cladding cold work
3. Fast neutron fluence

3.1.7.1 Model Description

Young's Modulus

The Young's modulus of Zircaloy-4, Zircaloy-2, M5, ZIRLO and Optimized ZIRLO is given by:

$$E = \begin{cases} \frac{1.088 \times 10^{11} - 5.475 \times 10^7 T + c_1 \Delta Oxygen + c_3 CW}{c_2}, & \text{for } T < 1090 \text{ K} \\ 9.21 \times 10^{10} - 4.05 \times 10^7 T, & \text{for } T > 1255 \text{ K} \end{cases} \quad (3-9)$$

For temperatures between 1090 and 1255 K a linear interpolation between the predictions at 1090 K and 1255 K is used.

Where,

E = Young's modulus, Pa

T = Temperature, K

$\Delta Oxygen$ = Input average oxygen concentration excluding oxide layer (hardwired to 0.0012 in MatLib), kg-oxygen/kg-Zircaloy

CW = Input effective cold work (ratio of areas), unitless

$$c_1 = 6.61 \times 10^{11} + 5.912 \times 10^8 T$$

$$c_2 = 0.88 + 0.12 \exp\left(-\frac{\Phi}{1 \times 10^{25}}\right)$$

$$c_3 = -2.6 \times 10^{10}$$

Φ = Fast neutron (>1.0 MeV) fluence n/m²

Shear Modulus

The shear modulus of Zircaloy-4, Zircaloy-2, M5, ZIRLO and Optimized ZIRLO is given by:

$$G = \begin{cases} \frac{4.04 \times 10^{10} - 2.168 \times 10^7 T + c_1 \Delta Oxygen + c_3}{c_2}, & \text{for } T < 1090 \text{ K} \\ 3.49 \times 10^{10} - 1.66 \times 10^7 T, & \text{for } T > 1255 \text{ K} \end{cases} \quad (3-10)$$

For temperatures between 1090 and 1255 K a linear interpolation between the predictions at 1090 K and 1255 K is used.

Where,

G = Shear modulus, Pa

T = Temperature, K

$\Delta Oxygen$ = Input average oxygen concentration excluding oxide layer (hardwired to 0.0012 in MatLib), kg-oxygen/kg-Zircaloy

CW = Input effective cold work (ratio of areas), unitless

$$c_1 = 7.07 \times 10^{11} - 2.315 \times 10^8 T$$

$$c_2 = 0.88 + 0.12 \exp\left(-\frac{\Phi}{1 \times 10^{25}}\right)$$

$$c_3 = -0.867 \times 10^{10}$$

Φ = Fast neutron (>1.0 MeV) fluence, n/m²

3.1.7.2 Comparison to Data

Young's modulus data have been collected for zirconium, Zircaloy-2, and Zircaloy-4 from unirradiated samples [Armstrong and Brown, 1964] [Padel and Groff, 1976] [Busby, 1966] [Spasic et al., 1968] [Mehan, 1958] [Northwood et al., 1975] [Bolmaro and Povolo, 1988]. This comparison demonstrates a good agreement between the correlation and the database within a range of 293 and 1474 K.

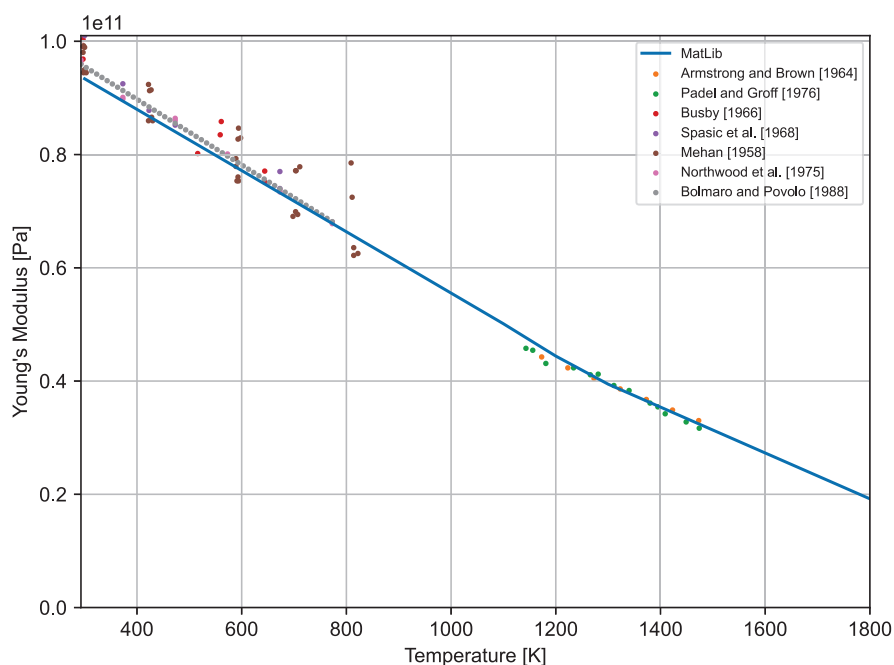


Figure 3-6. Model-to-Data Comparison for Zirconium Alloy Cladding Young's Modulus

Since there is limited data available from shear modulus measurements no model-to-data comparison is shown here.

3.1.7.3 Applicability and Uncertainty

The Young's modulus and shear modulus models are applicable to the range of available data:

- Cladding types: Zircaloy-2, Zircaloy-4, M5, ZIRLO and Optimized ZIRLO
- Temperature: 293 to 1474 K
- Fast neutron flux: 1.5×10^{26} n/m²

Engineering judgment should be used if analysis outside of these ranges is needed.

The uncertainty of the correlation is given below as an absolute uncertainty and is applicable for each cladding type.

For Zircaloy-2, Zircaloy-4, M5, ZIRLO and Optimized ZIRLO:

- Young's modulus: $\sigma = 3.1 \times 10^9$ Pa
- Shear modulus: $\sigma = 6.2 \times 10^9$ Pa (assumed to be twice that of the calculated Young's modulus)

3.1.8 Meyer's Hardness

The Meyer's hardness of zirconium-based alloy cladding is modeled in MatLib as a function of one parameter:

1. Temperature

3.1.8.1 Model Description

The Meyer's hardness of Zircaloy-2, Zircaloy-4, M5, ZIRLO and Optimized ZIRLO is given by:

$$MH = \begin{cases} \exp(26.034 - 2.6394 \times 10^{-2}T \\ \quad + 4.3502 \times 10^{-5}T^2 - 2.5621 \times 10^{-8}T^3) & \text{for } T \leq 1235 \text{ K} \\ 1.0 \times 10^5 & \text{for } T > 1235 \text{ K} \end{cases} \quad (3-11)$$

Where,

MH = Cladding Meyer hardness, Pa

T = Temperature, K

3.1.8.2 Comparison to Data

Meyer's hardness data have been collected for Zircaloy-2 and Zircaloy-4 from unirradiated samples [Peggs and Godin, 1975]. A comparison between these data is presented in Figure 3-7. This comparison demonstrates a good agreement between the correlation and the database within a range of 350 and 875 K.

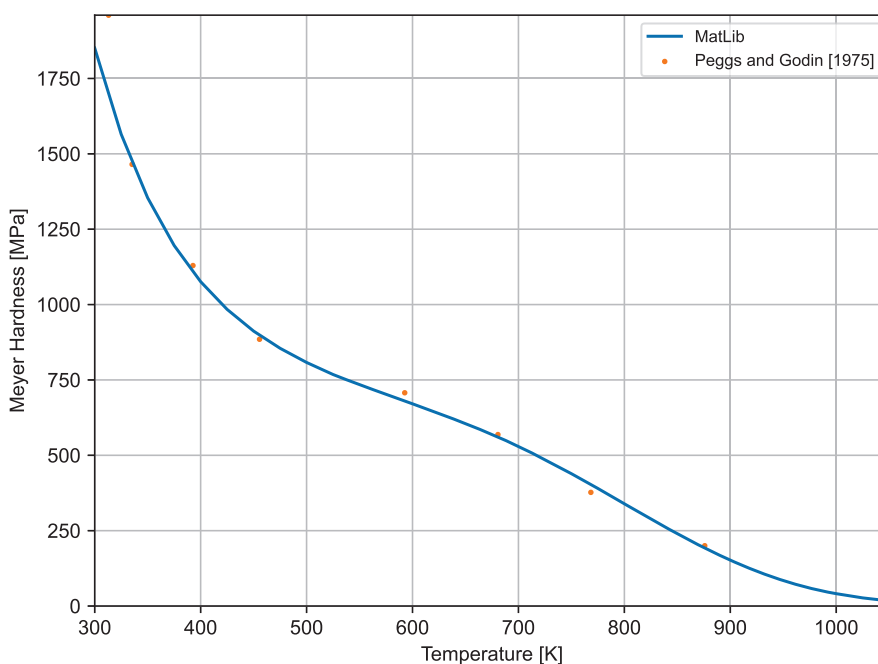


Figure 3-7. Model-to-Data Comparison for Zirconium-based Alloy Cladding Meyer's Hardness Correlation

3.1.8.3 Applicability and Uncertainty

The Meyer's hardness model is applicable to the range of available data:

- Cladding types: Zircaloy-2, Zircaloy-4, M5, ZIRLO, and Optimized ZIRLO; Kanthal APMT, C35M, and C36M (see Section 3.2.8); and HT9 (see Section 3.3.9)
- Temperature: 350 to 875 K
- Rod-average burnup: No burnup dependence observed

Engineering judgment should be used if analysis outside of these ranges is needed.

An estimate of the uncertainty in this correlation has not been established due to the limited data. In FAST this material property is used to determine the fuel-cladding contact conductance and any uncertainty in this value will be reflected in uncertainty in the prediction of the gap conductance.

3.1.9 Axial Growth

The axial irradiation growth of zirconium-based alloy cladding is modeled in MatLib as a function of one parameter:

1. Fast neutron fluence

Different correlations are given for each specific cladding alloy. It should be noted that these correlations are only valid for fuel rod cladding axial irradiation growth and may not represent guide tube growth as these components are under significantly different stress states.

3.1.9.1 Model Description

The axial irradiation growth of Zircaloy-2 is given by:

$$\frac{\Delta L}{L} = 1.09 \times 10^{-21} \Phi^{0.845} \quad (3-12)$$

The axial irradiation growth of Zircaloy-4 is given by:

$$\frac{\Delta L}{L} = 2.18 \times 10^{-21} \Phi^{0.845} \quad (3-13)$$

The axial irradiation growth of ZIRLO and Optimized ZIRLO is given by:

$$\frac{\Delta L}{L} = 9.7893 \times 10^{-25} \Phi^{0.98239} \quad (3-14)$$

The axial irradiation growth of M5 is given by:

$$\frac{\Delta L}{L} = 7.013 \times 10^{-21} \Phi^{0.81787} \quad (3-15)$$

Where,

$$\frac{\Delta L}{L} = \text{Axial growth increment, m/m}$$

$$\Phi = \text{Fast neutron (>1.0 MeV) fluence, n/cm}^2$$

3.1.9.2 Comparison to Data

Axial irradiation growth data have been collected for Zircaloy-2 irradiated samples [Harbottle, 1970] [Gilbon et al., 2000]. A comparison between these data is presented in Figure 3-8. This comparison demonstrates a good agreement between the correlation and the database up to a fast neutron fluence of 1.0×10^{22} n/cm². The [Gilbon et al., 2000] data is from a fast reactor and may not be representative to the behavior in a LWR.

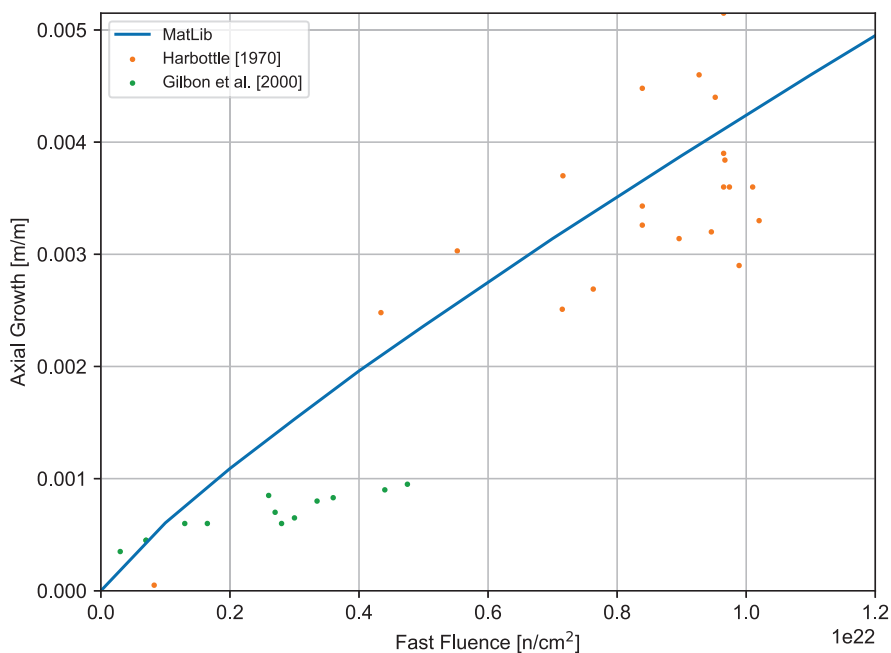


Figure 3-8. Model-to-Data Comparison for Zircaloy-2 Axial Irradiation Growth Correlation

Axial irradiation growth data have been collected for Zircaloy-4 irradiated samples [Newman, 1986] [Franklin et al., 1983] [Gilbon et al., 2000]. A comparison between these data is presented in Figure 3-9. This comparison demonstrates a good agreement between the correlation and the database up to a fast neutron fluence of $8.5 \times 10^{21} \text{ n/cm}^2$. The [Gilbon et al., 2000] data is from a fast reactor and may not be representative to the behavior in a LWR.

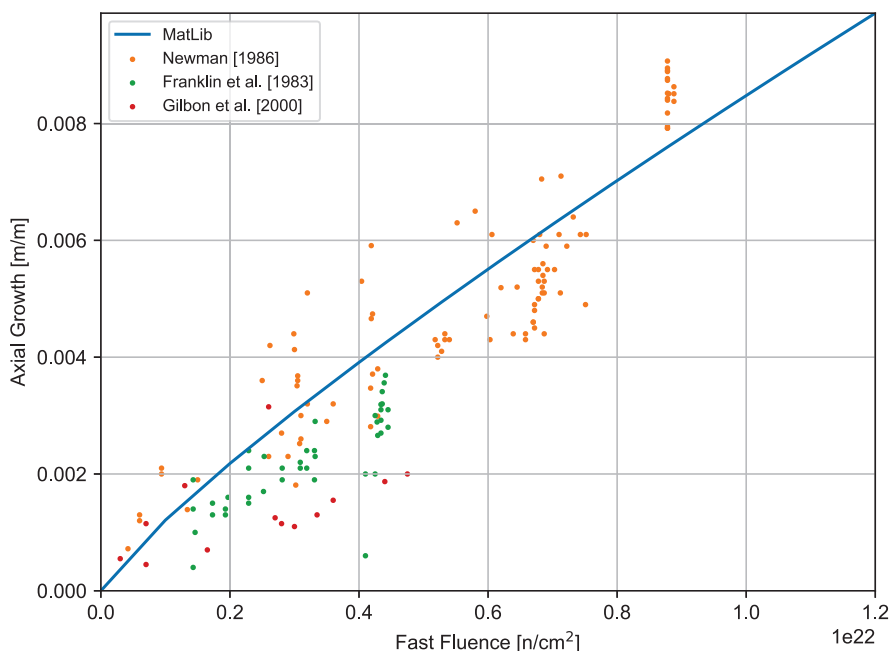


Figure 3-9. Model-to-Data Comparison for Zircaloy-4 Axial Irradiation Growth Correlation

Axial irradiation growth data have been collected for ZIRLO irradiated samples [Irisa and Alonso, 2000] [Sabot et al., 1994]. A comparison between these data is presented in Figure 3-10. This comparison demonstrates a good agreement between the correlation and the database up to a fast neutron fluence of 8.5×10^{21} n/cm². Proprietary data indicates that the axial growth of Optimized ZIRLO is similar or slightly lower than for ZIRLO. For this reason, the ZIRLO correlation is applied for Optimized ZIRLO.

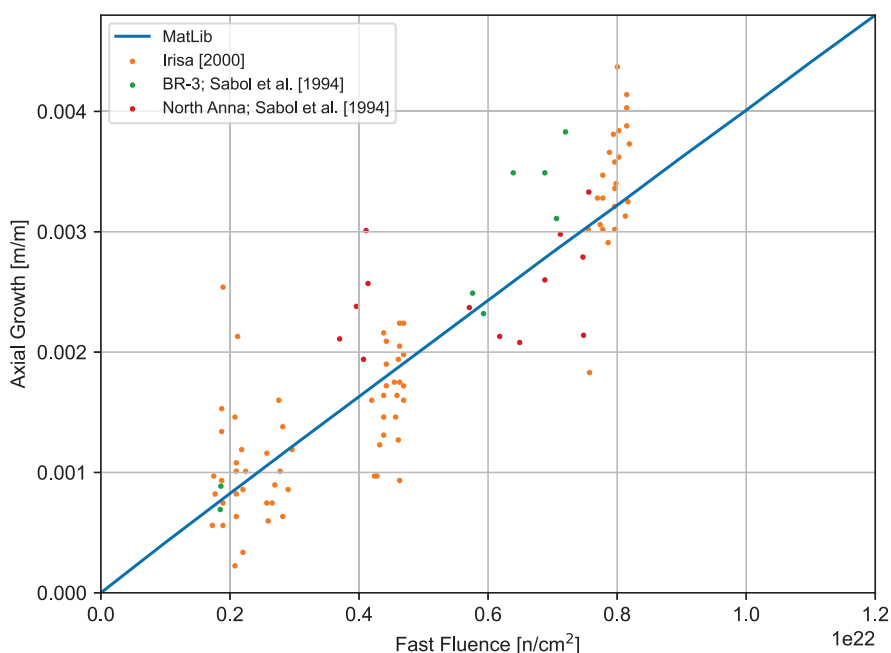


Figure 3-10. Model-to-Data Comparison for ZIRLO Axial Irradiation Growth Correlation

Axial irradiation growth have been collected for M5 irradiated samples [Gilbon et al., 2000]. A comparison between these data is presented in Figure 3-11. This comparison demonstrates a good agreement between the correlation and the database up to a fast neutron fluence of 1×10^{22} n/cm².

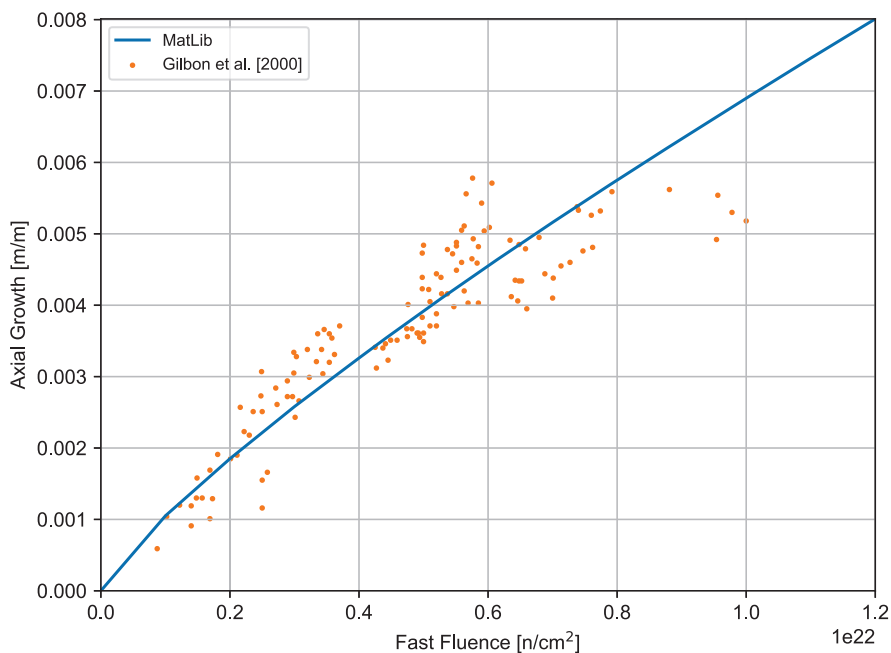


Figure 3-11. Model-to-Data Comparison for M5 Axial Irradiation Growth Correlation

3.1.9.3 Applicability and Uncertainty

The axial irradiation growth correlation is applicable to the range of available data:

- Cladding types: Zircaloy-4, Zircaloy-2, M5, ZIRLO and Optimized ZIRLO
- Temperature: 530 to 620 K
- Fast Neutron Fluence: 0 to 1×10^{22} n/cm² for Zircaloy-2 and M5; 0 to 8.5×10^{21} n/cm² for Zircaloy-4, ZIRLO and Optimized ZIRLO

Engineering judgment should be used if analysis outside of these ranges is needed.

The uncertainty of the correlation is given below and is applicable for each cladding type. A relative uncertainty was used for all the cladding types except ZIRLO and Optimized ZIRLO. For ZIRLO the scatter in the data did not change with fast neutron fluence.

- Zircaloy-2: $\sigma = 20.9\%$
- Zircaloy-4: $\sigma = 22.3\%$
- ZIRLO and Optimized ZIRLO: $\sigma = 0.0005$ m/m
- M5: $\sigma = 18.6\%$

3.1.10 Strain (Creep) Rate

The strain of zirconium-based alloy cladding is modeled in MatLib as a function of six parameters:

1. Temperature
2. Effective stress
3. Fast neutron flux
4. Fast neutron fluence
5. Cladding cold work
6. Time

Different correlations are given for each specific cladding alloy. The RXA correlation is used for Zircaloy-2 and M5. The SRA correlation is used for Zircaloy-4. An adjustment to the SRA correlation is used for ZIRLO. An adjustment to the RXA correlation is used for Optimized ZIRLO.

3.1.10.1 Model Description

The thermal strain rate of zirconium-based alloy cladding is given by:

$$\dot{\epsilon}_{th} = A \frac{E}{T} \left(\sinh \frac{a_i \sigma_{eff}}{E} \right)^n \exp \left(-\frac{Q}{RT} \right) \quad (3-16)$$

Where,

$$E = 1.148 \times 10^5 - 59.9T \quad (3-17a)$$

$$a_i = 650 \left[1 - 0.56 \left(1 - \exp \left(-1.4 \times 10^{-27} \Phi^{1.3} \right) \right) \right] \quad (3-17b)$$

$\dot{\epsilon}_{th}$ = Thermal strain rate, in/in-hr

A = Constant (see Table 3-4)

E = Young's Modulus, MPa

T = Temperature, K

a_i = Fluence term (parameters changed from original Limbäck equation [Limbäck and Andersson, 1996])

σ_{eff} = Effective stress, MPa (see Equation 3-26)

n = Stress exponent (see Table 3-4)

Q = Activation energy = 201000 J/mol

R = Universal gas constant = 8.314 J/mol-K

The irradiation strain rate of zirconium-based alloy cladding is given by:

$$\dot{\epsilon}_{irr} = c_0 \phi^{c_1} \sigma_{eff}^{c_2} f(T) \quad (3-18)$$

Where,

$\dot{\epsilon}_{irr}$ = Irradiation strain rate, in/in-hr

c_0 = Constant (see Table 3-4)

ϕ = Fast neutron (>1.0 MeV) flux, n/m²-s

c_1 = Flux exponent = 0.85, unitless

σ_{eff} = Effective stress MPa (see Equation 3-26)

c_2 = Stress exponent = 1.0, unitless

$f(T)$ = Temperature term

T = Temperature, K

A number of variables for the thermal and irradiation strain rates are dependent on the cladding cold work (refer to Table 3-1):

Table 3-4. Cladding Cold Work Dependent Parameters for the Thermal and Irradiation Strain Rate Correlations

Parameter	SRA Cladding	RXA Cladding	Units
A	1.08×10^9	5.47×10^8	K/MPa-hr
n	2.0	3.5	unitless
c_0	4.0985×10^{-24}	1.87473×10^{-24}	$(\text{n/m}^2\text{-s})^{-c_1} \text{MPa}^{-c_2}$
$f(T)$ for $T \leq 570 \text{ K}$	0.7283	0.7994	unitless
$f(T)$ for $570 \text{ K} < T < 625 \text{ K}$	$-7.0237 + 0.0136T$	$-3.18562 + 0.006699132T$	unitless
$f(T)$ for $T \geq 625 \text{ K}$	1.4763	1.1840	unitless

The thermal and irradiation creep rates may be added together as shown below and used to calculate the saturated primary hoop strain, ε_p^s .

$$\varepsilon_p^s = 0.0216 \dot{\varepsilon}_{th+irr}^{0.109} \left(2 - \tanh \left(3.55 \times 10^4 \cdot \dot{\varepsilon}_{th+irr} \right) \right)^{-2.05} \quad (3-19)$$

$$\dot{\varepsilon}_{th+irr} = \dot{\varepsilon}_{th} + \dot{\varepsilon}_{irr} \quad (3-20)$$

The total strain, ε_H , can then be calculated as a function of time, t hours.

$$\varepsilon_H = \varepsilon_p^s \left(1 - \exp \left(-52 \sqrt{t \dot{\varepsilon}_{th+irr}} \right) \right) + \dot{\varepsilon}_{th+irr} t \quad (3-21)$$

However, in FAST the strain rate is used, which is obtained by taking the derivative of the equation above. This derivative is presented in the equation below which relates the total creep strain rate to the saturated primary hoop strain, the combined thermal and irradiation strain rates, and time, t hours.

$$\dot{\varepsilon}_H = \frac{26 \varepsilon_p^s \sqrt{\dot{\varepsilon}_{th+irr}}}{\sqrt{t}} \exp \left(-52 \sqrt{t \dot{\varepsilon}_{th+irr}} \right) + \dot{\varepsilon}_{th+irr} \quad (3-22)$$

The effective stress in the cladding is found using the principle stresses at the mid-wall radius using the thick wall formula. The principle stresses can be determined with:

$$\sigma_r = \frac{P_i r_i^2 - P_o r_o^2 + \frac{r_i^2 r_o^2 (P_o - P_i)}{r^2}}{r_o^2 - r_i^2} \quad (3-23)$$

$$\sigma_t = \frac{P_i r_i^2 - P_o r_o^2 - \frac{r_i^2 r_o^2 (P_o - P_i)}{r^2}}{r_o^2 - r_i^2} \quad (3-24)$$

$$\sigma_l = \frac{P_i r_i^2 - P_o r_o^2}{r_o^2 - r_i^2} \quad (3-25)$$

Where,

σ_r = Radial stress, MPa

σ_t = Tangential stress, MPa

σ_l = Longitudinal stress, MPa

P_i = Inner pressure, MPa

P_o = Outer pressure, MPa

r_i = Inner radius, cm

r_o = Outer radius, cm

r = Radius within tube, cm

The effective stress (σ_{eff} MPa) can then be calculated by:

$$\sigma_{eff} = \sqrt{0.5 \left((\sigma_l - \sigma_t)^2 + (\sigma_t - \sigma_r)^2 + (\sigma_r - \sigma_l)^2 \right)} \quad (3-26)$$

It has been found that the Zircaloy RXA model adequately describes the creep behavior of M5 [Gilbon et al., 2000]. The Zircaloy SRA model is used for ZIRLO and Optimized ZIRLO with a reduction factor of 0.8 on $\dot{\epsilon}_H$. The reduction factor is the result of studies that have shown that ZIRLO exhibits about 80% of SRA Zircaloy-4 creepdown [Sabol et al., 1994].

3.1.10.2 Comparison to Data

Irradiation strain data have been collected for RXA Zircaloy samples [Franklin et al., 1983] [Soniak et al., 2002] [Gilbon et al., 2000] [Sontheimer and Nissen, 1994]. A comparison between these data is presented in Figure 3-12. This comparison demonstrates a good agreement between the correlation and the database.

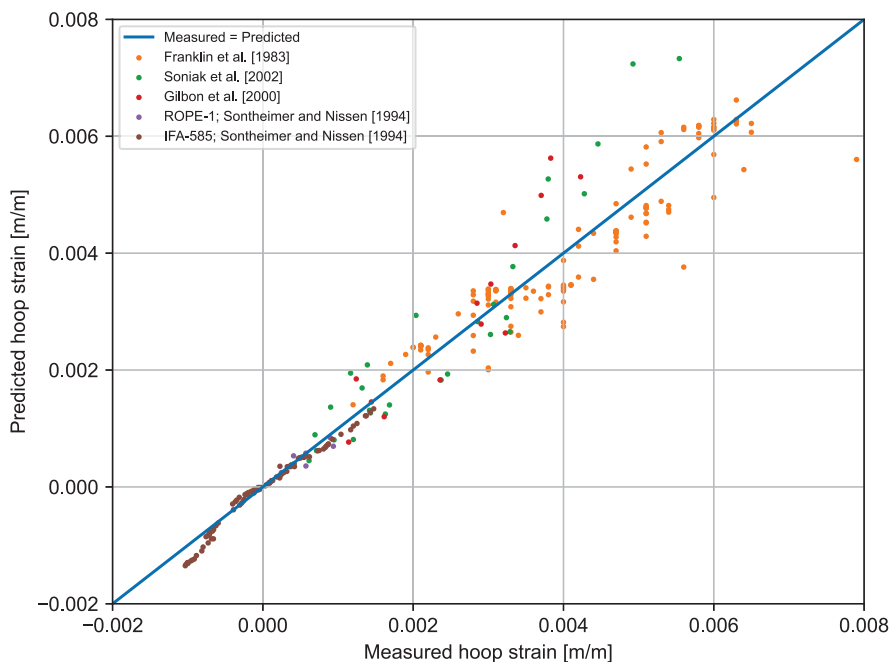


Figure 3-12. Model-to-data Comparison for RXA Zircaloy Strain Correlation

Irradiation strain data have been collected for SRA Zircaloy samples [Franklin et al., 1983] [Soniak et al., 2002] [Gilbon et al., 2000]. A comparison between these data is presented in Figure 3-13. This comparison demonstrates a good agreement between the correlation and the database.

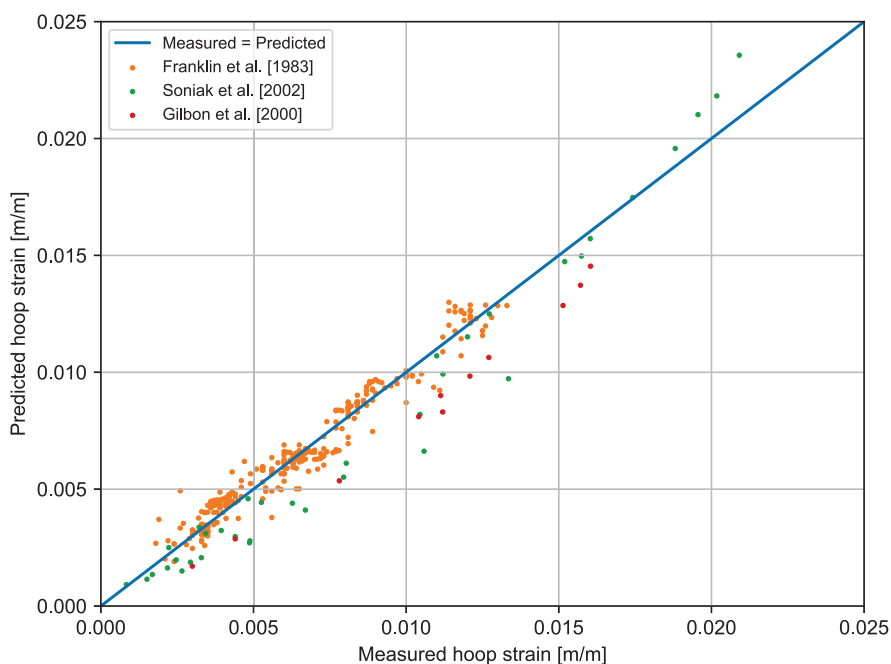


Figure 3-13. Model-to-data Comparison for SRA Zircaloy Strain Correlation

3.1.10.3 Applicability and Uncertainty

The strain correlations for zirconium-based alloy claddings are applicable to the range of available data:

- Cladding types: Zircaloy-4, Zircaloy-2, M5, ZIRLO and Optimized ZIRLO
- Temperature: 570 to 625 K
- Effective stress: 40 to 130 MPa
- Fast Neutron Flux: 1×10^{17} to 2×10^{18} n/cm²-s

Engineering judgment should be used if analysis outside of these ranges is needed.

The uncertainty of the correlation is given below and is applicable for each cladding type:

- Zircaloy-2 and M5: $\sigma = 21.6\%$
- Zircaloy-4, ZIRLO, and Optimized ZIRLO: $\sigma = 14.5\%$

3.2 Iron-Chrome-Aluminum (FeCrAl) Alloys

Material property correlations for FeCrAl alloy based claddings are described in the following subsections. Unless otherwise specified, the correlations below are applicable to Kanthal APMT, C35M, and C36M. The various alloys of FeCrAl have various compositions. Kanthal APMT has 21 wt% Cr and 5 wt% Al; C35M has 13 wt% Cr and 5 wt% Al; and C36M has 13 wt% Cr and 6 wt% Al. Table 3-5 summarizes the nominal composition of the various FeCrAl alloys included in MatLib [Field et al., 2015] [Field, 2018].

Table 3-5. Nominal Composition of Various FeCrAl Alloys in Matlib

Alloy	Nominal Composition (wt%)
Kanthal APMT	Fe-21Cr-5Al-3Mo
C35M	Fe-13Cr-5Al-2Mo-0.2Si-0.05Y
C36M	Fe-13Cr-6Al-2Mo-0.2Si-0.05Y

3.2.1 Thermal Conductivity

The thermal conductivity of FeCrAl-alloy cladding is modeled in MatLib as a function of one parameter:

1. Temperature

3.2.1.1 Model Description

The thermal conductivity of Kanthal APMT, C35M, and C36M is given by:

$$k = A_0 + A_1T + A_2T^2 \quad (3-27)$$

Where,

k = Thermal conductivity, W/m-K

T = Temperature, K

A_x = Fitting constants (see Table 3-6)

Values for the fitting constants for each alloy used to calculate the thermal conductivity are provided in Table 3-6 [Field, 2018].

Table 3-6. Constants Used in the FeCrAl Thermal Conductivity Correlation

Alloy	A_0	$A_1 (1 \times 10^{-2})$	$A_2 (1 \times 10^{-7})$
Kanthal APMT	6.569	1.5628	-7.223
C35M	8.502	1.537	-19.86
C36M	8.187	1.368	-9.184

3.2.1.2 Comparison to Data

Thermal conductivity data have been collected for FeCrAl samples [Field, 2018]. A comparison between these data is presented in Figures 3-14, 3-15, and 3-16 for Kanthal APMT, C35M, and C36M, respectively.

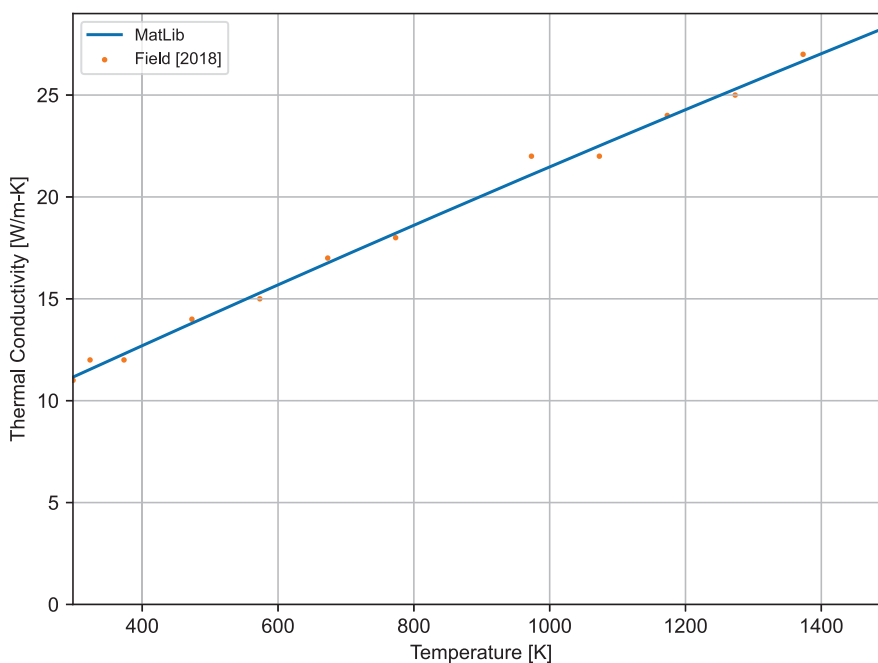


Figure 3-14. Model-to-Data Comparison for Kanthal APMT FeCrAl Alloy Thermal Conductivity Correlation

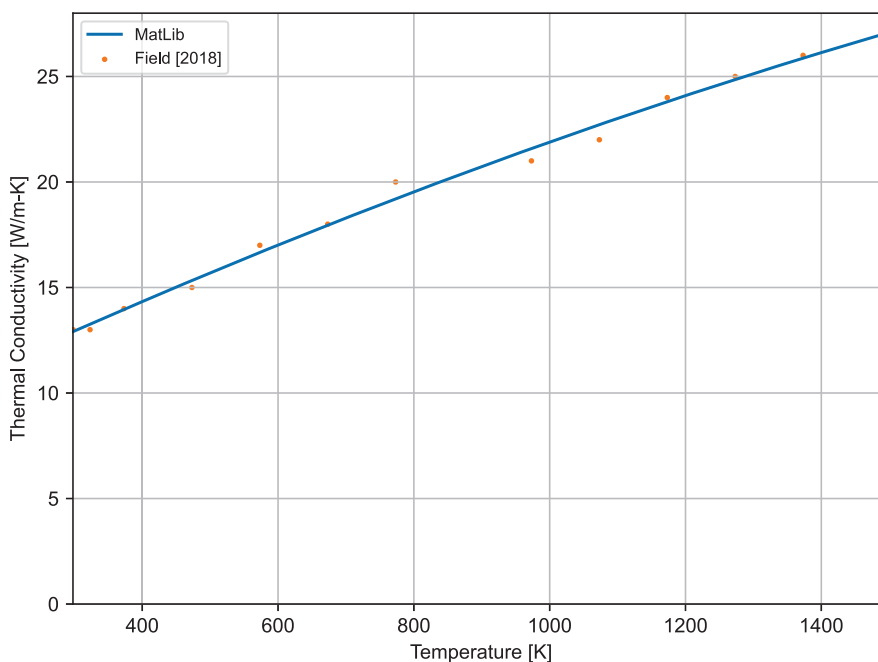


Figure 3-15. Model-to-Data Comparison for C35M FeCrAl Alloy Thermal Conductivity Correlation

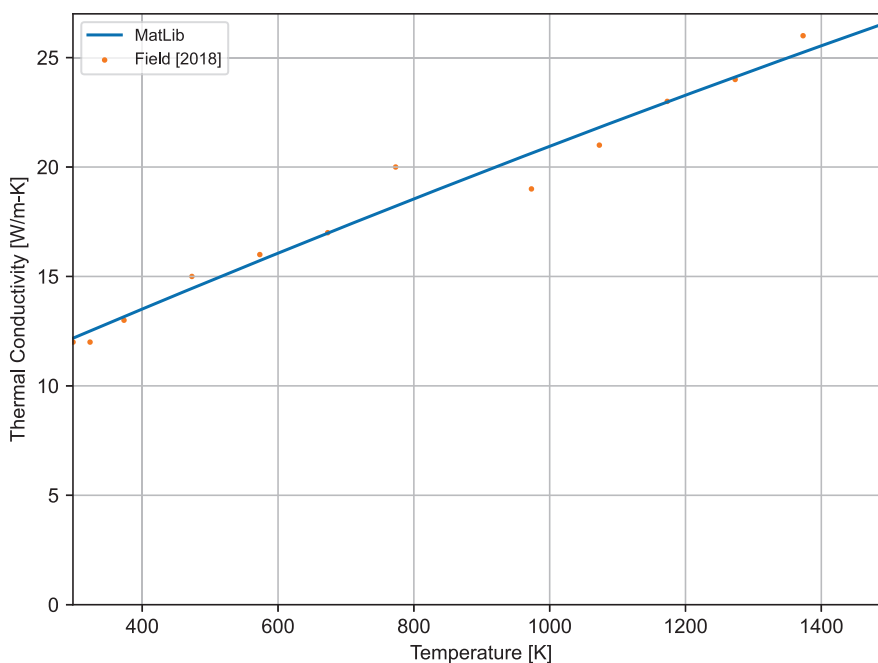


Figure 3-16. Model-to-Data Comparison for C36M FeCrAl Alloy Thermal Conductivity Correlation

3.2.1.3 Applicability and Uncertainty

The thermal conductivity correlation for FeCrAl is applicable to the range of available data:

- Cladding types: Kanthal APMT, C35M, C36M
- Temperature: 300 to 1400 K
- Burnup: unirradiated

Engineering judgment should be used if analysis outside of these ranges is needed.

The data used to generate the 2nd order polynomial reports a 7% uncertainty due to the assumed experimental variability in the heat capacity, thermal diffusivity, and density of the FeCrAl alloys [Field, 2018].

3.2.2 Specific Heat

The specific heat of FeCrAl alloys is modeled in MatLib as a function of one parameter:

1. Temperature

In addition, the specific heat takes into account the alloy-dependent Curie temperature.

3.2.2.1 Model Description

The specific heat model in MatLib is a two-expression correlation based on the cladding temperature. In Equation 3-28, the two expressions used to calculate the specific heat of non-irradiated FeCrAl alloys are presented. The correlations were developed at ORNL [Field, 2018] and are summarized below.

$$c_p = \begin{cases} aT + bT^2 + cT^3, & \text{for } T \leq T_c \\ aT + bT^2 + cT^3 + DT^{-1} + E \ln \left(\frac{|T - T_c|}{T_c} \right), & \text{for } T > T_c \end{cases} \quad (3-28)$$

Where,

c_p = Specific heat capacity, J/kg-K

T = Temperature, K

a , b , c , D , and E = Fitting constants (see Table 3-7)

T_c = Curie temperature, K (see Table 3-7)

The Curie temperature describes the material's magnetic properties at a specific temperature. Above the Curie temperature, materials lose their permanent magnetic property, which is replaced by induced magnetism.

Table 3-7 provides the coefficients used to determine the specific heat for the various FeCrAl alloys used in MatLib [Field, 2018].

Table 3-7. Constants Used in the FeCrAl Specific Heat Correlation

Alloy	Valid Temperature Range (K)	a	b (1×10^{-3})	c (1×10^{-6})	D (1×10^3)	E	T_c (K)
Kanthal APMT	$300 < T \leq T_c$	2.54	-4.311	2.982	—	—	852
Kanthal APMT	$T_c < T < T_m$	1.840	-1.843	0.643	-5.712	-50.38	852
C35M	$300 < T \leq T_c$	2.450	-4.002	2.720	—	—	870
C35M	$T_c < T < T_m$	1.946	-2.002	0.698	-1.652	-53.93	870
C36M	$300 < T \leq T_c$	2.995	-5.953	4.516	—	—	771
C36M	$T_c < T < T_m$	1.456	-1.296	0.438	26.45	-46.89	771

3.2.2.2 Comparison to Data

Figures 3-17, 3-18, and 3-19 show the model-to-data comparisons for the specific heat capacity correlation at constant pressure used in MatLib for Kanthal APMT, C35M, and C36M, respectively, using experimentally measured data from non-radiated FeCrAl alloys [Field, 2018]. The large peaks seen in the figures represent the second order phase transition from the material's ferromagnetic to paramagnetic state.

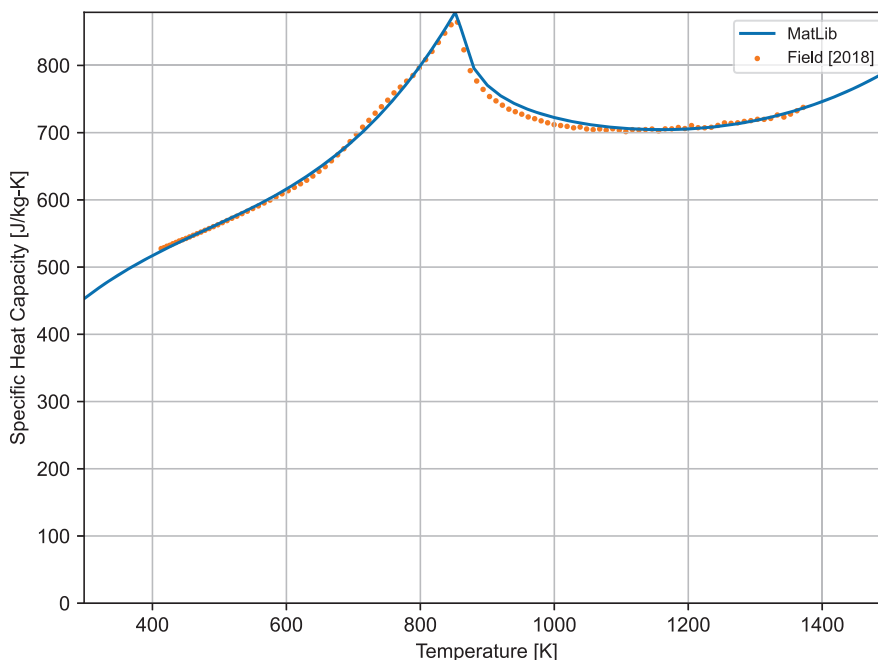


Figure 3-17. Model-to-Data Comparison for Kanthal APMT FeCrAl Alloy Specific Heat Correlation

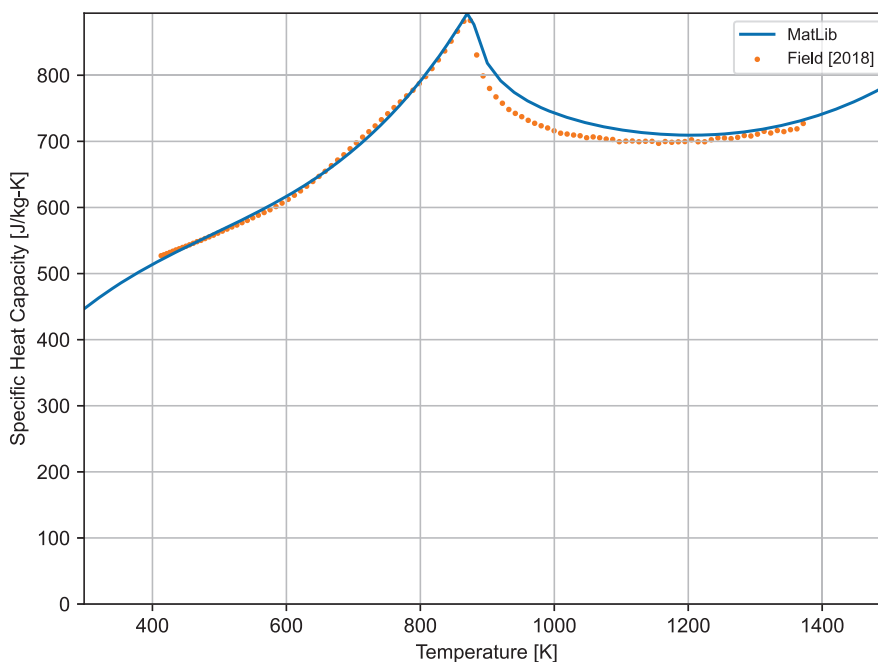


Figure 3-18. Model-to-Data Comparison for C35M FeCrAl Alloy Specific Heat Correlation

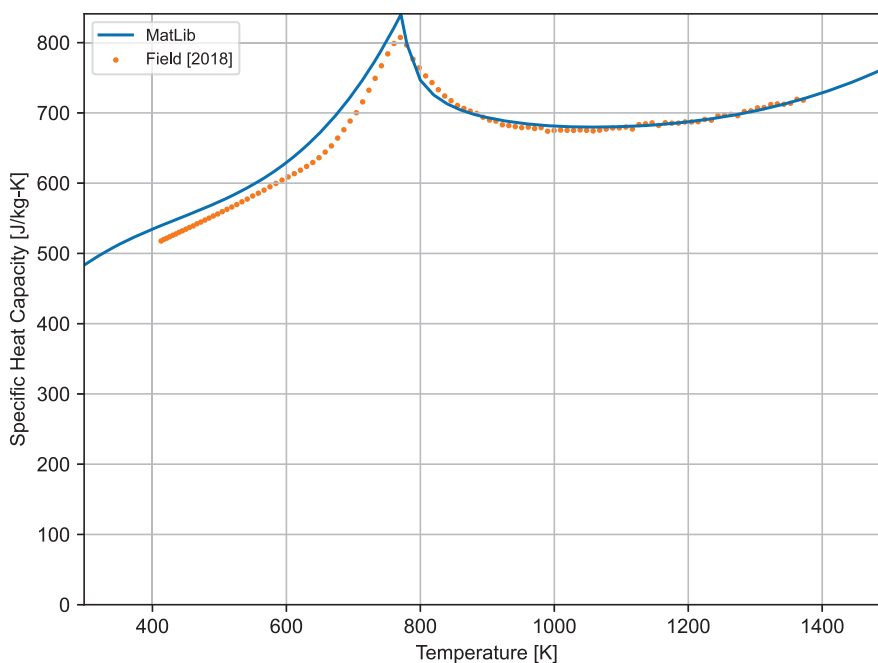


Figure 3-19. Model-to-Data Comparison for C36M FeCrAl Alloy Specific Heat Correlation

3.2.2.3 Applicability and Uncertainty

The specific heat capacity correlation is applicable to the range of available data:

- Cladding types: Kanthal APMT, C35M, C36M
- Temperature: 300 to 1400 K
- Burnup: unirradiated

Engineering judgment should be used if analysis outside of these ranges is needed.

No uncertainty for the specific heat capacity is reported.

3.2.3 Melting Temperature

The melting temperature of the various alloys of FeCrAl is modeled in MatLib as a constant value [Kanthal, 2018]:

$$T_m = 1773.15 \text{ K} \quad (3-29)$$

Where,

T_m = Melting temperature K

3.2.3.1 Applicability and Uncertainty

The melting temperature model is applicable over the following ranges:

- Cladding types: Kanthal APMT, C35M, C36M
- Rod-average Burnup: No burnup dependence observed

No uncertainty is given.

3.2.4 Thermal Expansion

The thermal expansion coefficient of FeCrAl alloys is modeled in MatLib as a function of one parameter:

1. Temperature

The thermal expansion coefficient is assumed to be isotropic.

3.2.4.1 Model Description

The thermal expansion coefficient correlation in MatLib is based on experimentally measured data at ORNL [Field, 2018]. The measured expansion data was fitted against a third order polynomial (Equation 3-30), where alloy-dependent fitting constants are used to represent the various types of FeCrAl alloys.

$$\alpha = A_0 + A_1T + A_2T^2 + A_3T^3 \quad (3-30)$$

Where,

α = Thermal expansion coefficient, K^{-1}

A_x = Fitting constants

T = Temperature, K

Table 3-8 provides the values of the fitting coefficients used to determine the thermal expansion coefficient for the various types of FeCrAl alloys [Field, 2018].

Table 3-8. Constants Used in the FeCrAl Thermal Expansion Correlation

Alloy	A_0	$A_1 (1 \times 10^{-3})$	$A_2 (1 \times 10^{-7})$	$A_3 (1 \times 10^{-10})$
Kanthal APMT	10.27	1.937	9.558	1.771
C35M	9.810	4.530	-17.46	9.095
C36M	10.56	2.535	2.719	3.079

3.2.4.2 Comparison to Data

Thermal expansion data have been collected for FeCrAl samples [Field, 2018]. A model-to-data comparison is presented in Figures 3-20, 3-21, and 3-22 for Kanthal APMT, C35M, and C36M, respectively.

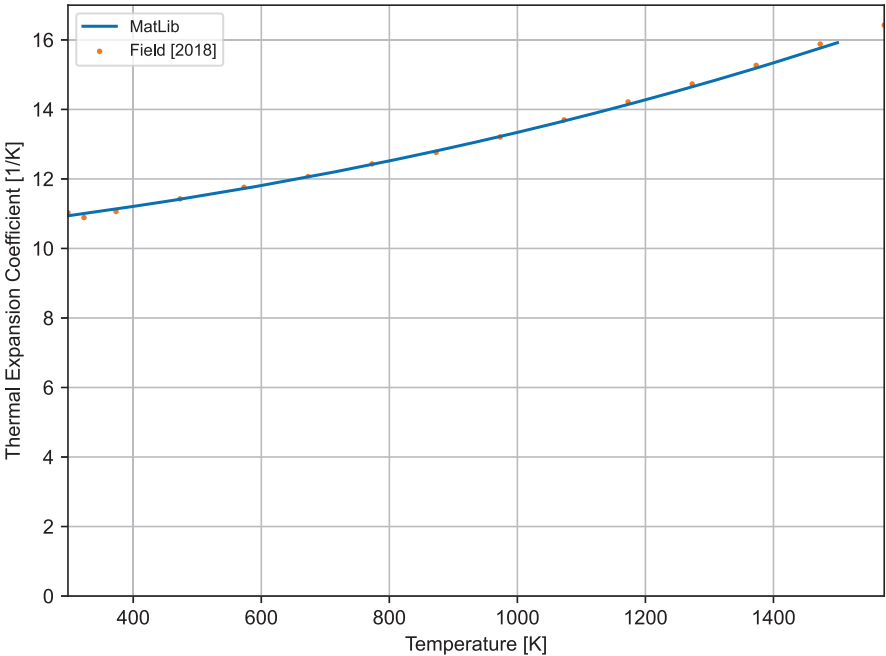


Figure 3-20. Model-to-Data Comparison for Kanthal APMT FeCrAl Alloy Thermal Expansion Coefficient

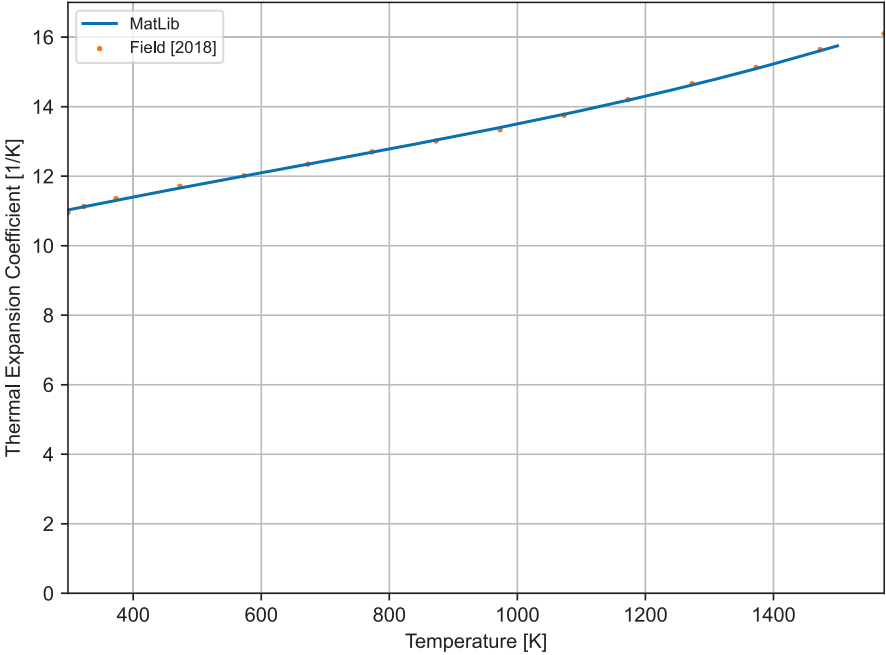


Figure 3-21. Model-to-Data Comparison for C35M FeCrAl Alloy Thermal Expansion Coefficient Correlation

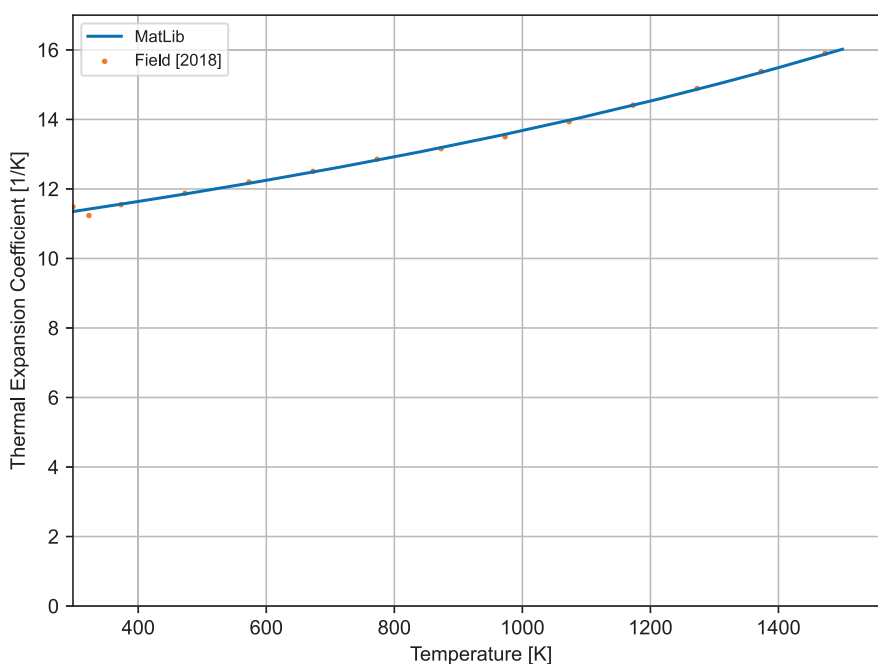


Figure 3-22. Model-to-Data Comparison for C36M FeCrAl Alloy Thermal Expansion Coefficient Correlation

3.2.4.3 Applicability and Uncertainty

The correlation is applicable to the range of available data:

- Cladding types: Kanthal APMT, C35M, C36M
- Temperature: 300 to 1500 K
- Burnup: unirradiated

Engineering judgment should be used if analysis outside of these ranges is needed.

No uncertainty for the thermal expansion coefficient is reported.

3.2.5 Emissivity

The emissivity of the various alloys of FeCrAl is modeled in MatLib as a constant value [Kanthal, 2018]:

$$\epsilon = 0.7 \quad (3-31)$$

Where,

ϵ = Emissivity, unitless

3.2.5.1 Applicability and Uncertainty

The emissivity model is applicable over the following ranges:

- Cladding types: Kanthal APMT, C35M, C36M
- Temperature: No temperature dependence observed
- Rod-average Burnup: No burnup dependence observed

No uncertainty is given on the emissivity.

3.2.6 Density

The densities for the various FeCrAl alloys in MatLib are modeled as constant values per Table 3-9.

Table 3-9. Densities of Various FeCrAl Alloys

Alloy	Density (kg/m ³)
Kanthal APMT	7250
C35M	7180
C36M	7180

3.2.6.1 Applicability and Uncertainty

The density model is applicable over the following ranges:

- Cladding types: Kanthal APMT, C35M, C36M
- Temperature: No temperature dependence observed
- Rod-average Burnup: No burnup dependence observed

No uncertainty is given.

3.2.7 Young's Modulus and Shear Modulus

Young's modulus (or elastic modulus) and shear modulus for FeCrAl-based cladding are modeled within MatLib as a function of one parameter:

1. Temperature

3.2.7.1 Model Description

The Young's modulus and shear modulus are related by Poisson's ratio according to:

$$G = \frac{E}{2(1 + \nu)} \quad (3-32)$$

Where,

G = Shear modulus, Pa

E = Young's modulus, Pa (Equation 3-33)

ν = Poisson's ratio, unitless (Equation 3-34)

Young's Modulus

The Young's modulus of FeCrAl alloys is given by [Field, 2018]:

$$E = 199 - 3.85 \times 10^{-2}T - 5.46 \times 10^{-5}T^2 \quad (3-33)$$

Where,

E = Young's modulus, Pa

T = Temperature, °C

Poisson's Ratio

Poisson's ratio for FeCrAl alloys is given by [Field, 2018]:

$$\nu = 4.46 \times 10^{-5}T + 0.27 \quad (3-34)$$

Where,

ν = Poisson's ratio, unitless

T = Temperature, °C

3.2.7.2 Comparison to Data

Young's modulus data have been collected for C35M and C36M [Field, 2018] and Kanthal APMT [Kanthal, 2018]. A model-to-data comparison is presented in Figure 3-23.

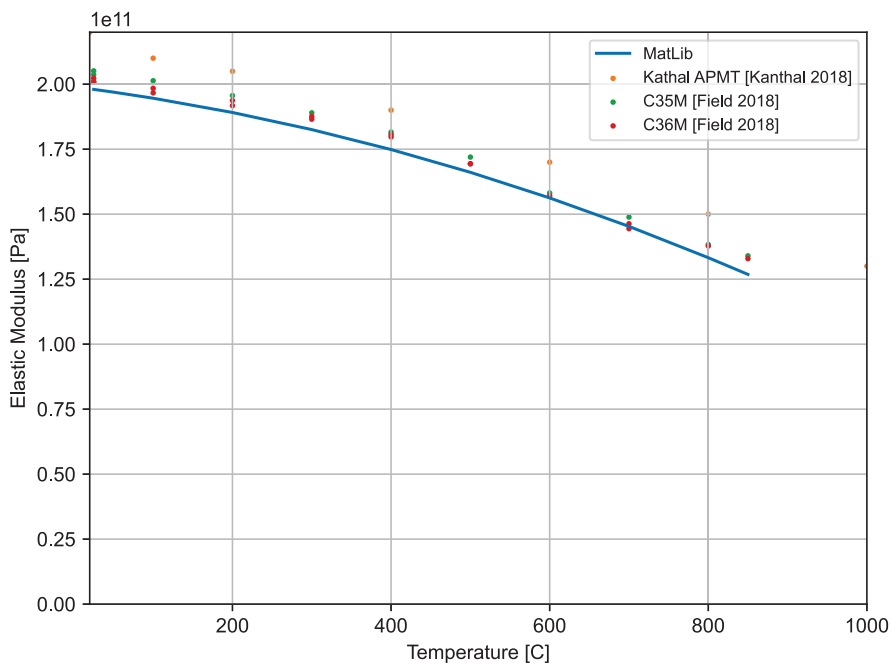


Figure 3-23. Model-to-Data Comparison for FeCrAl Alloys Elastic Modulus Correlation

3.2.7.3 Applicability and Uncertainty

The Young's modulus and shear modulus models are applicable to the range of available data:

- Cladding types: Kanthal APMT, C35M, C36M
- Temperature: 25 to 800 °C
- Rod-average Burnup: No burnup dependence observed

No uncertainty is given.

3.2.8 Meyer's Hardness

The Meyer's hardness model for FeCrAl alloys utilizes the same Meyer's hardness model for zirconium-based alloy (see Section 3.1.8).

3.2.9 Axial Growth

The axial irradiation growth of FeCrAl alloy cladding is modeled in MatLib as a function of one parameter:

1. Fast neutron fluence

3.2.9.1 Model Description

The axial irradiation growth of FeCrAl alloy is given by:

$$\frac{\Delta L}{L} = \frac{0.5\Phi_{dpa}}{3} \quad (3-35)$$

Where,

$$\frac{\Delta L}{L} = \text{Axial growth increment, m/m}$$

$$\Phi_{dpa} = \text{Fast neutron fluence per displacement per atom} = \frac{0.9\Phi}{1 \times 10^{25}}, \text{ dpa}$$

$$\Phi = \text{Fast neutron (>1.0 MeV) fluence, n/m}^2$$

3.2.9.2 Comparison to Data

No comparisons to measured data is provided in this document because of the limited availability of experimentally measured axial growth data.

3.2.9.3 Applicability and Uncertainty

No uncertainty is given.

3.2.10 Strain (Creep) Rate

The strain of FeCrAl alloy cladding is modeled in MatLib as a function of four parameters:

1. Temperature
2. Effective stress
3. Fast neutron fluence
4. Fast neutron flux

The strain rate is assumed isotropic.

3.2.10.1 Model Description

The thermal strain rate of FeCrAl alloy cladding is given by [Field, 2018]:

$$\dot{\epsilon}_{th} = A_0 \sigma^n \exp\left(\frac{-Q}{RT}\right) \quad (3-36)$$

Where,

$\dot{\epsilon}_{th}$ = Thermal strain rate, s^{-1}

A_0 = Constant $MPa^{-n}s^{-1}$ (Table 3-10)

σ = Effective stress, Pa

n = Creep exponent (Table 3-10)

Q = Activation energy, J/mol (Table 3-10)

R = Universal gas constant = 8.314 J/K–mol

T = Temperature, K

Table 3-10. Constants Used in the FeCrAl Thermal Strain Rate Correlation

Alloy	A_0 ($MPa^{-n}s^{-1}$)	n	Q (J/mol)
Kanthal APMT	2.9×10^{-6}	4.5	1.43×10^5
C35M and C35M for $T < 873.15$ K	2.9×10^{-3}	5.5	2.47×10^5
C35M and C35M for $T \geq 873.15$ K	5.96×10^6	5.5	3.92×10^5

The irradiation strain rate of FeCrAl alloy cladding is given by:

$$\dot{\epsilon}_{irr} = \frac{C_{irr}\sigma\phi}{\Phi_{dpa}} \quad (3-37)$$

Where,

$\dot{\epsilon}_{irr}$ = Irradiation strain rate, s^{-1}

C_{irr} = Coefficient of irradiation strain = 5×10^{-12} dpa/Pa

Φ_{dpa} = Fast neutron fluence per displacement per atom = $\frac{0.9\Phi}{1 \times 10^{25}}$ dpa

Φ = Fast neutron (>1.0 MeV) fluence, n/m^2

σ = Effective stress, Pa

ϕ = Fast neutron flux, n/m^2-s

The total strain rate is the sum of the thermal and irradiation strain rates:

$$\dot{\epsilon}_s = \dot{\epsilon}_{th} + \dot{\epsilon}_{irr} \quad (3-38)$$

3.2.10.2 Comparison to Data

Compiled thermal strain data for FeCrAl alloys is tabulated in Reference [Field, 2018]. This compiled list of data presents the strain rate versus applied stresses for various FeCrAl alloys.

It has been noted that Kanthal APMT exhibit excellent strain strength properties when compared to wrought FeCrAl alloys; the MatLib model may over predict strain rates for Kanthal APMT.

3.2.10.3 Applicability and Uncertainty

The strain rate model is applicable over the following ranges:

- Cladding types: Kanthal APMT, C35M, C36M
- Temperature: No range specified
- Effective stress: No range specified

No uncertainty on the strain rate is given.

3.3 HT-9 Alloy

The following section describes the material property correlations used to model HT-9 alloy cladding properties in MatLib. HT-9 cladding is a ferritic stainless steel alloy cladding that may be used to contain metallic fuels in future nuclear reactors.

3.3.1 Thermal Conductivity

The thermal conductivity model in MatLib for HT-9 cladding is a function of one parameter:

1. Temperature

The thermal conductivity of the cladding can also be a function of residual stress levels, crystal orientation, and minor composition differences. These effects are typically secondary and not addressed in the current MatLib model of thermal conductivity. An accurate prediction of the cladding thermal conductivity is required to accurately predict the temperature profile of the fuel, including the centerline fuel temperature.

3.3.1.1 Model Description

The thermal conductivity model is given by [Akiyama, 1991]:

$$k = A_0 + A_1 T \quad (3-39)$$

Where,

k = Cladding thermal conductivity, W/m-K

T = Temperature, K

$A_0 = 22.47$ W/m-K

$A_1 = 4.397 \times 10^{-3}$ W/m-K²

3.3.1.2 Comparison to Data

Due to limited experimental thermal conductivity data for HT-9, no comparison to experimental data is made but a model-to-model comparison is. Two thermal conductivity models are compared in Figure 3-24: [Akiyama, 1991] (used in MatLib) and [Leibowitz and Blomquist, 1988]. Both models are empirical correlations based on experimental measurements. As more data becomes available, data will be plotted against the correlations.

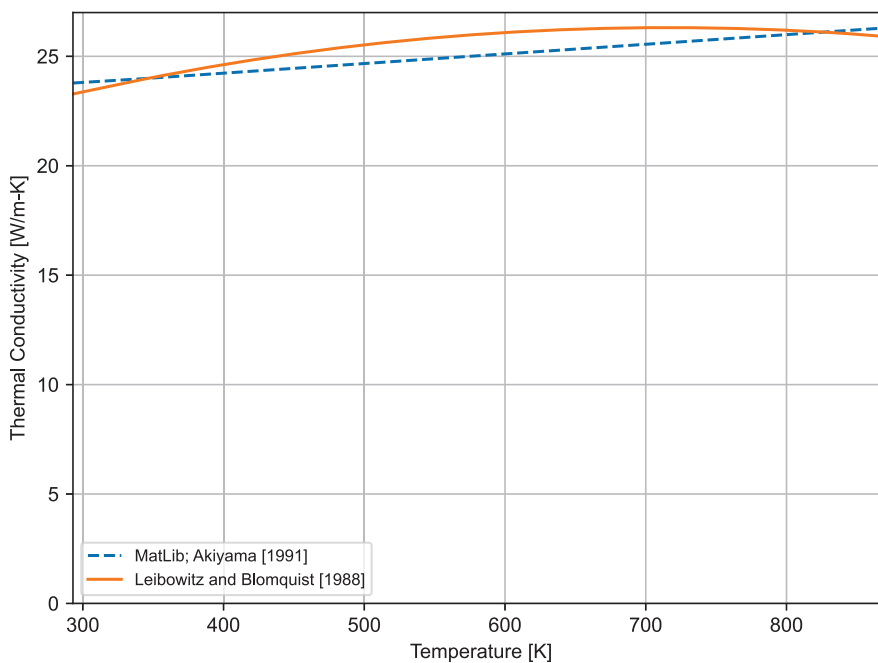


Figure 3-24. Model-to-Model Comparison for HT-9 Alloy Thermal Conductivity Correlations

Several differences between the two correlations are seen. MatLib utilizes a linear correlation [Akiyama, 1991] for the prediction of the thermal conductivity, whereas the Leibowitz model [Leibowitz and Blomquist, 1988] is developed from a second order polynomial. Comparison between the applicable temperature range is only made as the Leibowitz model provides an expression for above 1050 K.

3.3.1.3 Applicability and Uncertainty

The HT-9 thermal conductivity model is applicable for the following conditions:

- Cladding types: HT-9
- Temperature: 293 to 873 K

No uncertainty is given.

3.3.2 Specific Heat Capacity

The specific heat capacity at constant pressure for HT-9 cladding is modeled in MatLib as a function of one parameter:

1. Temperature

3.3.2.1 Model Description

The specific heat model is based on experimental data [Yamanouchi et al., 1992]:

$$C_p = A_0 + A_1T \quad (3-40)$$

Where,

C_p = Specific heat capacity at constant pressure, J/kg-K

T = Temperature, K

A_x = Fitting constants (see Table 3-11)

Table 3-11 provides the values of the fitting constants.

Table 3-11. Constants Used in the HT-9 Specific Heat Capacity Correlation

Alloy	Valid Temperature Range (K)	A_0 (J/kg-K)	A_1 (J/kg-K ²)
HT-9	$T < 800.15$ K	416.642	0.167
HT-9	$T \geq 800.15$ K	69.910	0.600

3.3.2.2 Comparison to Data

The MatLib specific heat capacity correlation for HT-9 cladding [Yamanouchi et al., 1992] is presented in Figure 3-25. The two regions are clearly observed. Above 800.15 K, there is a slight decrease in the rate the specific heat increases as a function of temperature. As more experimental data becomes available, comparisons against the implemented MatLib model will be made and Figure 3-25 will be updated.

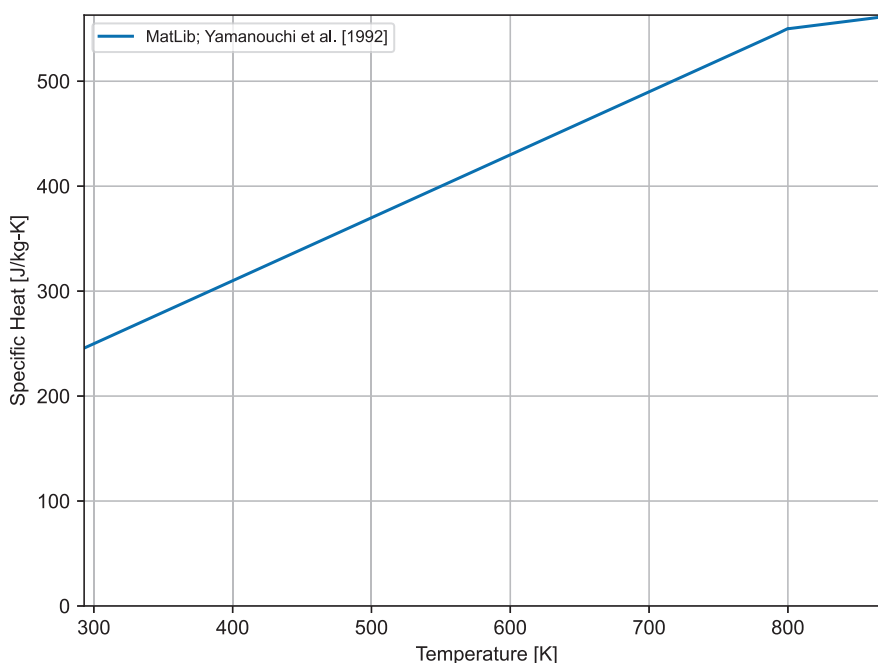


Figure 3-25. HT-9 Alloy Specific Heat Capacity Correlation

3.3.2.3 Applicability and Uncertainty

The specific heat capacity correlation is applicable over the following range of conditions:

- Cladding types: HT-9
- Temperature: 298 to 873 K
- Burnup: unirradiated

No uncertainty for the specific heat capacity is reported.

3.3.3 Melting Temperature

The melting temperature for HT-9 cladding is modeled in MatLib using the eutectic temperature between HT-9 and metallic fuel as opposed to the melting temperature of pure HT-9 cladding as a eutectic forms between the cladding and fuel at a temperature lower than pure HT-9.

It is assumed constant [Baker and Wilson, 1992].

$$T_{melt} = T_{eutectic} = 973 \text{ K} \quad (3-41)$$

3.3.4 Thermal Expansion

The MatLib model for the thermal expansion of HT-9 is a function of one parameter:

1. Temperature

The thermal expansion is assumed isotropic.

3.3.4.1 Model Description

The thermal expansion model is based on a second order polynomial [Yamanouchi et al., 1992]:

$$\alpha = A_1 + A_2T + A_3T^2 \quad (3-42)$$

Where,

α = Thermal expansion coefficient, K^{-1}

T = Temperature, K

A_x = Fitting constants (see Table 3-12)

Table 3-12. Constants Used in the HT-9 Thermal Expansion Correlation

x	A_x
1	-2.882×10^{-3}
2	9.226×10^{-6}
3	1.842×10^{-9}

3.3.4.2 Comparison to Data

Due to limited experimental data measuring thermal expansion, no comparison to experimental data is made but a model-to-model comparison is. Two thermal expansion models are compared in Figure 3-26: [Yamanouchi et al., 1992] (used in MatLib) and [Leibowitz and Blomquist, 1988]. Both models are empirical correlations based on experimental data. As more data becomes available, data will plotted against the correlations.

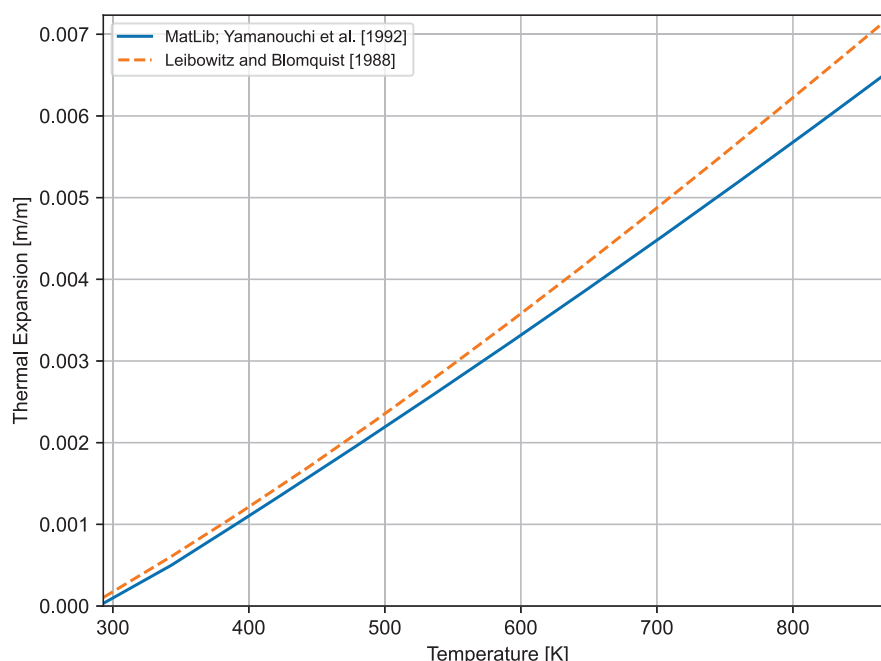


Figure 3-26. Model-to-Model Comparison for HT-9 Alloy Thermal Expansion Correlations

Minor differences between the models are seen. Both models follow the same trend but differ slightly in magnitude. Both models similarly predict the thermal expansion of HT-9 at lower temperature but as temperatures increase, the models begin to predict different thermal expansion strains. Comparison between the temperature range of 298 to 873 K is made as only the Leibowitz model provides an applicable expression for higher temperature.

3.3.4.3 Applicability and Uncertainty

The thermal expansion correlation is applicable over the following range of conditions:

- Cladding types: HT-9
- Temperature: 298.15 to 1073.15 K

No uncertainty is given.

3.3.5 Emissivity

The emissivity of HT-9 cladding is modeled in MatLib as a constant value [Dutt and Baker, 1974]:

$$\epsilon = 0.9 \quad (3-43)$$

Where,

ϵ = Emissivity, unitless

3.3.5.1 Applicability and Uncertainty

The emissivity model is applicable over the following range of conditions:

- Cladding types: HT-9
- Temperature: No temperature dependence observed
- Burnup: No burnup dependence observed

No uncertainty is given.

3.3.6 Density

3.3.6.1 Model Description

The density of HT-9 cladding is modeled in MatLib as a constant value [[Akiyama, 1991](#)]:

$$\rho = 7750 \text{ kg/m}^3 \quad (3-44)$$

Where,

$$\rho = \text{Density, kg/m}^3$$

3.3.6.2 Applicability and Uncertainty

The density model is applicable over the following range of conditions:

- Cladding types: HT-9
- Temperature: No temperature dependence observed
- Burnup: No burnup dependence observed

No uncertainty is given.

3.3.7 Young's Modulus

Young's modulus (or elastic modulus) for HT-9 cladding is modeled as a function of one parameter:

1. Temperature

3.3.7.1 Model Description

The Young's modulus model in MatLib is a linear function with fitting constants based on experimental measurements [Akiyama, 1991]:

$$E = A_0 + A_1T \quad (3-45)$$

Where,

E = Young's modulus, Pa

T = Temperature, °C

A_0 = Fitting constant = 2.137×10^{11} Pa

A_1 = Fitting constant = -1.0274×10^8 Pa/°C

3.3.7.2 Applicability and Uncertainty

The Young's modulus model is applicable over the following range of conditions:

- Cladding types: HT-9
- Temperature: 298.15 to 873.15 K
- Burnup: No burnup dependence observed

No uncertainty is given.

3.3.8 Shear Modulus

The shear modulus of HT-9 cladding is modeled as a function of one parameter:

1. Temperature

3.3.8.1 Model Description

The shear modulus of HT-9 cladding is given by:

$$G = A_0 + A_1T \quad (3-46)$$

Where,

G = Shear modulus, Pa

T = Temperature, °C

A_0 = Fitting constant = 8.964×10^{10} Pa

A_1 = Fitting constant = -5.378×10^7 Pa/°C

The shear modulus decreases with increasing temperature.

3.3.8.2 Applicability and Uncertainty

The shear modulus model is applicable over the following range of conditions:

- Cladding types: HT-9
- Temperature: 298.15 to 873.15 K
- Burnup: No burnup dependence observed

No uncertainty is given.

3.3.9 Meyer's Hardness

The Meyer's hardness model for HT-9 cladding utilizes the same Meyer's hardness model for zirconium-based cladding (see Section 3.1.8).

3.3.10 Strain (Creep) Rate

The strain rate of HT-9 cladding is modeled in MatLib as a function of four parameters:

1. Time
2. Effective stress
3. Temperature
4. Fast neutron flux

3.3.10.1 Model Description

The thermal strain rate model is based on the proposed model by [Akiyama, 1991]. The thermal creep rate is a summation of the primary, secondary, and tertiary thermal creep rates:

$$\dot{\epsilon}_{th} = \dot{\epsilon}_1 + \dot{\epsilon}_2 + \dot{\epsilon}_3 \quad (3-47)$$

Where,

$\dot{\epsilon}_{th}$ = Total thermal strain rate, s^{-1}

$\dot{\epsilon}_1$ = Primary thermal strain rate, s^{-1}

$\dot{\epsilon}_2$ = Secondary thermal strain rate, s^{-1}

$\dot{\epsilon}_3$ = Tertiary thermal strain rate, s^{-1}

and,

$$\dot{\epsilon}_1 = \left[C_1 \sigma \exp \left(\frac{-Q_1}{RT} \right) + C_2 \sigma^4 \exp \left(\frac{-Q_2}{RT} \right) + C_3 \sqrt{\sigma} \exp \left(\frac{-Q_3}{RT} \right) \right] C_4 \exp (-C_4 t) \quad (3-48a)$$

$$\dot{\epsilon}_2 = C_5 \sigma^2 \exp \left(\frac{-Q_4}{RT} \right) + C_6 \sigma^5 \exp \left(\frac{-Q_5}{RT} \right) \quad (3-48b)$$

$$\dot{\epsilon}_3 = 4\sigma^{10} \left(C_7 \exp \left(\frac{-Q_6}{RT} \right) t \right)^3 \quad (3-48c)$$

Where,

C_x, Q_x = Fitting constants (Table 3-13)

t = Time s

σ = Effective stress at time t MPa

R = Universal gas constant = 1.987 cal/mol-K

T = Temperature K

Table 3-13 shows the fitting constants used to determine the thermal strain rate for HT-9 alloy. The fitting constants are taken from [Akiyama, 1991].

Table 3-13. Constants Used in the HT-9 Thermal Strain Rate Correlation

x	C_x	Q_x
1	13.4	15027.0
2	8.43×10^{-3}	26451.0
3	4.08×10^{18}	89167.0
4	1.6×10^{-6}	83142.0
5	1.17×10^9	108276.0
6	8.33×10^9	94233.3
7	2.12×10^7	—

The irradiation strain rate correlation is also an empirical-based model:

$$\varepsilon_{irr} = \left[\left(B_0 + A_1 \exp \left(\frac{-Q_{irr}}{RT} \right) \right) \phi \sigma^{1.3} \right] \times 10^{-22} \quad (3-49)$$

Where,

$\dot{\varepsilon}_i$ = Irradiated creep rate, s^{-1}

B_0 = Fitting constant = 1.83×10^{-4}

A_1 = Fitting constant = 2.59×10^{14}

Q_{irr} = Fitting constant = 73000.0

ϕ = Fast neutron flux ($E > 1$ MeV), n/cm^2-s

σ = Effective stress at time t , MPa

R = Universal gas constant = 1.987 cal/mol-K

T = Temperature, K

The total strain rate is the sum of the thermal and irradiation strain rates:

$$\dot{\varepsilon}_s = \dot{\varepsilon}_{th} + \dot{\varepsilon}_{irr} \quad (3-50)$$

3.3.10.2 Applicability and Uncertainty

The strain rate model is applicable for the following conditions:

- Cladding types: HT-9
- Temperature: 298.15 to 873.15 K
- Burnup: No burnup dependence found

No uncertainty is given.

3.3.11 Yield Stress

The MatLib model for the yield stress of HT-9 cladding is a function of one parameter:

1. Temperature

The ultimate tensile stress for HT-9 cladding is assumed to be equal to the yield stress.

3.3.11.1 Model Description

The yield stress model is given by [Akiyama, 1991]:

$$\sigma_y = A_1 + A_2T + A_3T^2 + A_4T^3 \quad (3-51)$$

Where,

σ_y = Yield stress, Pa

A_x = Fitting constants (see Table 3-14)

T = Temperature, K

Table 3-14. Constants Used in the HT-9 Yield Stress Correlation

x	A_x
1	1.290×10^9
2	-3.561×10^6
3	6.371×10^3
4	-3.959

3.3.11.2 Applicability and Uncertainty

The yield stress model is applicable over the following range of conditions:

- Cladding types: HT-9
- Temperature: 298.15 to 873.15 K
- Burnup: No burnup dependence found

No uncertainty is given.

This page intentionally blank.

4.0 Gas Material Properties

This section describes material property correlations for gap gases. The modeled gases include:

- Helium
- Argon
- Krypton
- Xenon
- Hydrogen
- Nitrogen
- Air
- Water Vapor

4.1 Thermal Conductivity

For gases other than water vapor, the thermal conductivity is modeled in MatLib as a function of one parameter:

1. Temperature

For water vapor, the thermal conductivity is modeled in MatLib as a function of two parameters:

1. Temperature
2. Pressure

4.1.1 Model Description

For gases other than water vapor, the thermal conductivity is given by:

$$k = AT^B \quad (4-1)$$

Where,

k = Gas thermal conductivity, W/m-K

T = Temperature, K

A, B = Constants (see Table 4-1)

The parameters A and B used for each gas are given in the table below.

Table 4-1. Constants Used in the Gas Thermal Conductivity Correlation

Gas	A	B
He	2.531×10^{-3}	0.7146
Ar	4.092×10^{-4}	0.6748
Kr	1.966×10^{-4}	0.7006
Xe	9.825×10^{-5}	0.7334
H ₂	1.349×10^{-3}	0.8408
N ₂	2.984×10^{-4}	0.7799
Air	1.945×10^{-4}	0.8586

Water Vapor

The thermal conductivity of water vapor is given by:

For $T \leq 973.15$ K

$$\begin{aligned}
 k = \frac{P}{T} & \left(-2.8516 \times 10^{-8} + 9.424 \times 10^{-10}T - 6.005 \times 10^{-14}T^2 \right) \\
 & + 1.009 \frac{P^2}{T^2(T - 273.15)^{4.2}} + 1.76 \times 10^{-3} + 5.87 \times 10^{-5}(T - 273.15) \\
 & + 1.08 \times 10^{-7}(T - 273.15)^2 - 4.51 \times 10^{-11}(T - 273.15)^3
 \end{aligned} \quad (4-2)$$

For $T > 973.15$ K

$$k = 4.44 \times 10^{-6}T^{1.45} + 9.45 \times 10^{-5} \left(2.1668 \times 10^{-9} \frac{P}{T} \right)^{1.3} \quad (4-3)$$

Where,

k = Gas thermal conductivity, W/m-K

P = Gas pressure, Pa

T = Temperature, K

The thermal conductivity of gas mixtures is calculated by [Hagman et al., 1981]:

$$k_{mix} = \sum_i^n \left(\frac{k_i x_i}{x_i + \sum_{j=1}^n (1 - \delta_{ij})_{ij} x_j} \right) \quad (4-4)$$

Where,

$$_{ij} = \varphi_{ij} \left(1 + 2.41 \frac{(M_i - M_j)(M_i - 0.142M_j)}{(M_i + M_j)^2} \right) \quad (4-5)$$

$$\varphi_{ij} = \frac{\left[1 + \left(\frac{k_i}{k_j} \right)^{1/2} \left(\frac{M_i}{M_j} \right)^{1/4} \right]^2}{2^{3/2} \left(1 + \frac{M_i}{M_j} \right)^{1/2}} \quad (4-6)$$

and,

δ_{ij} = Kronecker delta = 1 for $i = j$, 0 otherwise, unitless

n = Number of components in mixture, unitless

M_i = Molecular weight of component i , kg

x_i = Mole fraction of component i , unitless

k_i = Thermal conductivity of component i , W/m-K

4.1.2 Comparisons to Data

Thermal conductivity data have been collected for helium at various temperatures [Johnston and Grilly, 1946], [Saxena and Saxena, 1968], [Timrott and Totskii, 1965], [Timrot and Umanskii, 1966], [Zaitseva, 1959], [Cheung et al., 1962], [Kannuluik and Carman, 1952], [Gambhir et al., 1967], [von Ubisch, 1959], [Faubert and Springer, 1973], [Jain and Saxena, 1975], and [Jody et al., 1977]. A comparison between these data for helium is presented in Figure 4-5. This comparison demonstrates good agreement between the correlation and the database between 273 and 2500 K.

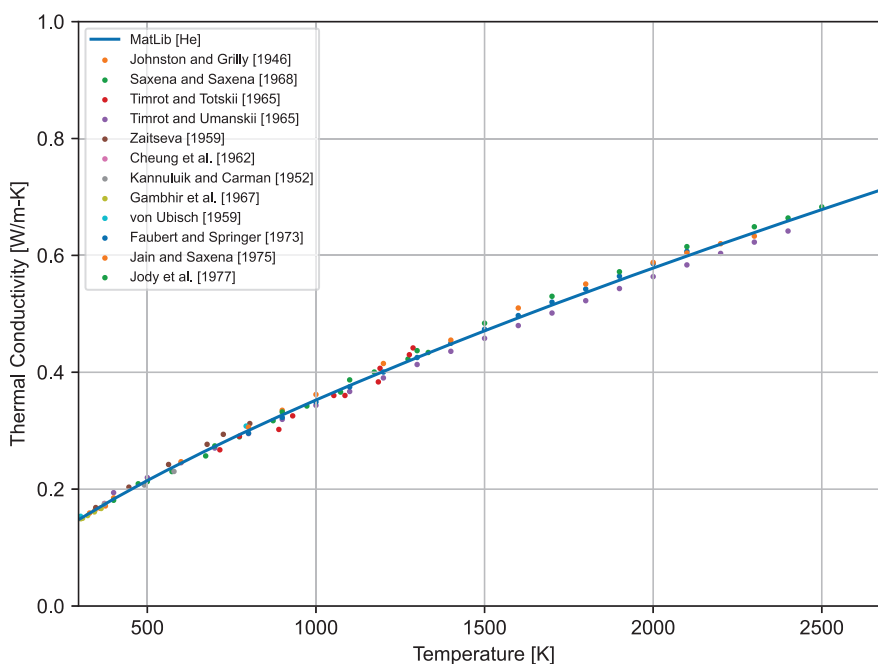


Figure 4-1. Model-to-Data Comparison for Helium Thermal Conductivity Correlation

Thermal conductivity data have been collected for argon at various temperatures [Brokaw, 1969], [Zaitseva, 1959], [Cheung et al., 1962], [Kannuluik and Carman, 1952], [Gambhir et al., 1967], [von Ubisch, 1959], [Timrot and Umanskii, 1966], [Saxena and Saxena, 1968], [Faubert and Springer, 1972], [Springer and Wingeier, 1973], and [Stefanov et al., 1976]. A comparison between these data for argon is presented in Figure 4-2. This comparison demonstrates good agreement between the correlation and the database between 273 and 2500 K.

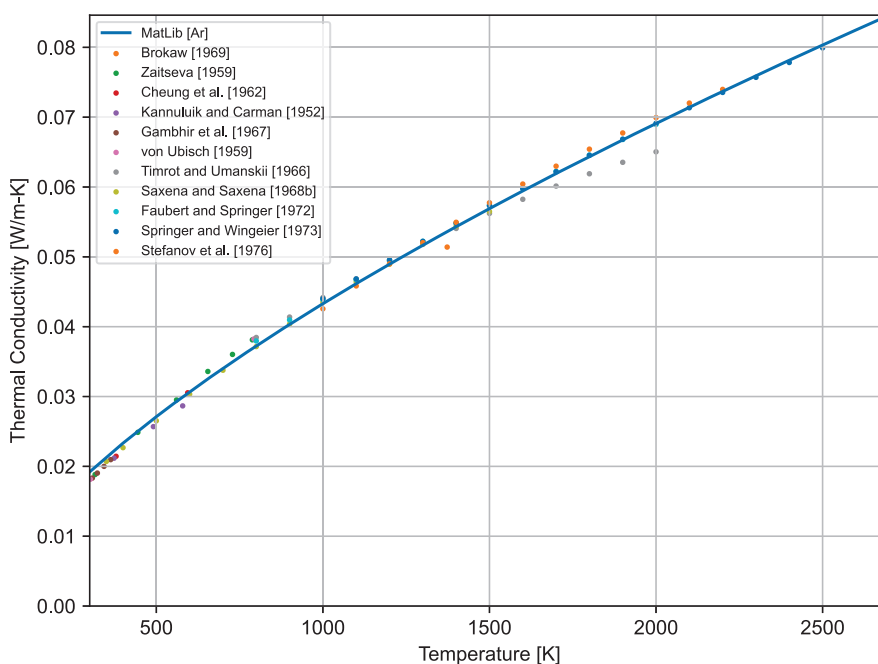


Figure 4-2. Model-to-Data Comparison for Argon Thermal Conductivity Correlation

Thermal conductivity data have been collected for krypton at various temperatures [Kannuluik and Carman, 1952], [Gambhir et al., 1967], [von Ubisch, 1959], [Saxena and Saxena, 1969], [Stefanov et al., 1976], [Vargaftik and Yakush, 1971], [Zaitseva, 1959]. A comparison between these data for krypton presented in Figure 4-3 . This comparison demonstrates good agreement between the correlation and the database between 273 and 2300 K.

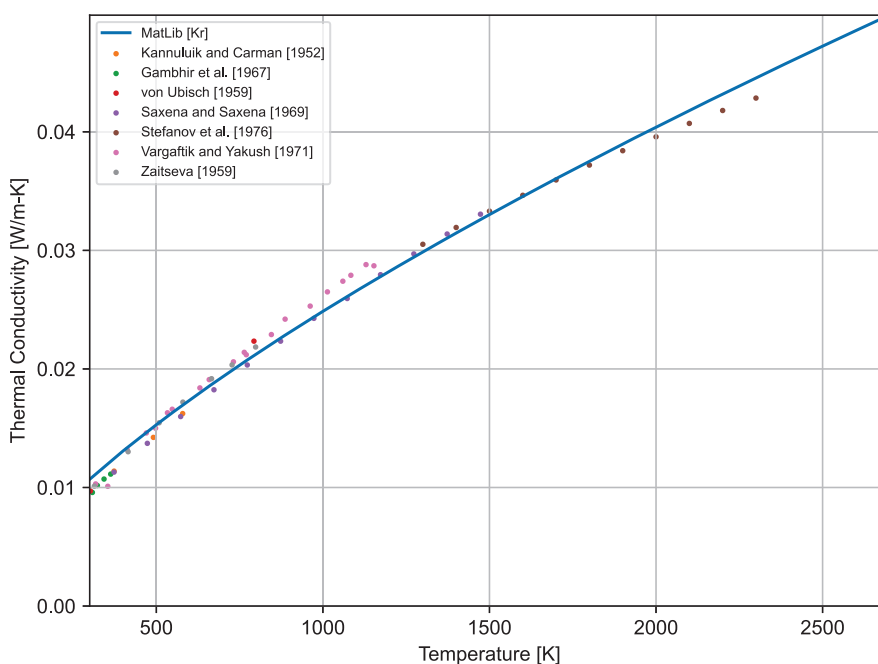


Figure 4-3. Model-to-Data Comparison for Krypton Thermal Conductivity Correlation

Thermal conductivity data have been collected for xenon at various temperatures [Zaitseva, 1959], [Kannuluik and Carman, 1952], [Gambhir et al., 1967], [von Ubisch, 1959], [Stefanov et al., 1976], [Springer and Wingeier, 1973], [Saxena and Saxena, 1969], [Vargaftik and Yakush, 1971]. A comparison between these data for xenon is presented in Figure 4-4. This comparison demonstrates good agreement between the correlation and the database between 273 and 2200 K.

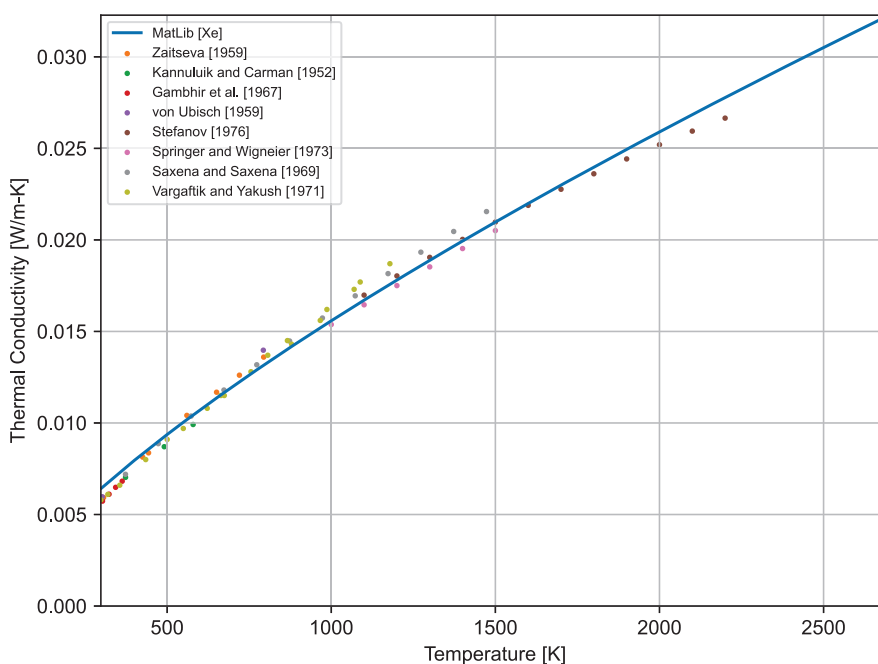


Figure 4-4. Model-to-Data Comparison for Xenon Thermal Conductivity Correlation

Thermal conductivity data have been collected for hydrogen at various temperatures [Johnston and Grilly, 1946], [Timrot and Umanskii, 1966], [Saxena and Saxena, 1970]. A comparison between these data for hydrogen is presented in Figure 4-5. This comparison demonstrates good agreement between the correlation and the database between 273 and 2000 K.

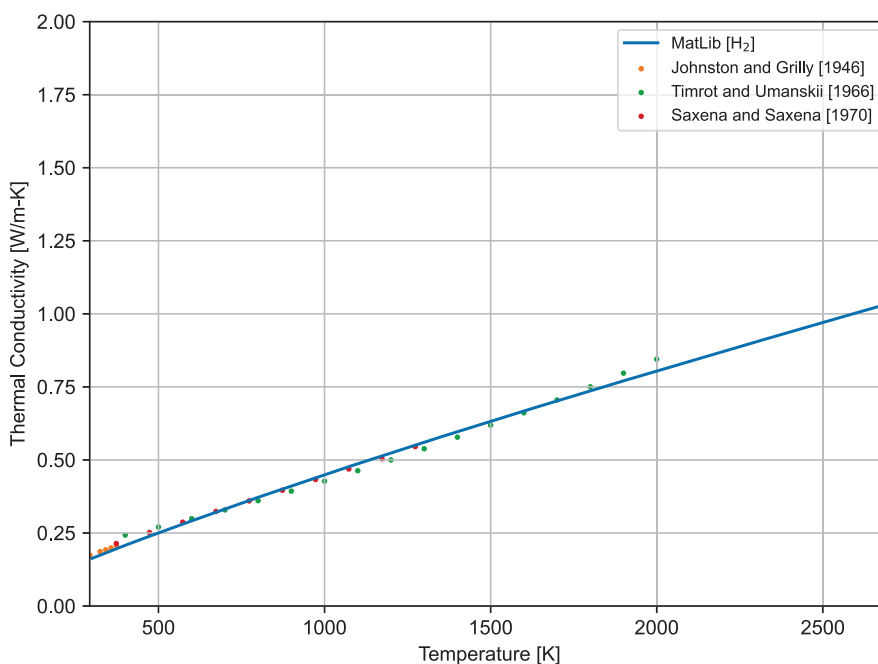


Figure 4-5. Model-to-Data Comparison for Hydrogen Thermal Conductivity Correlation

Thermal conductivity data have been collected for nitrogen at various temperatures [Cheung et al., 1962], [Brokaw, 1969], [Vargaftik and Zimina, 1964], [Faubert and Springer, 1972], [Chen and Saxena, 1973]. A comparison between these data for nitrogen is presented in Figure 4-6. This comparison demonstrates good agreement between the correlation and the database between 273 and 2500 K.

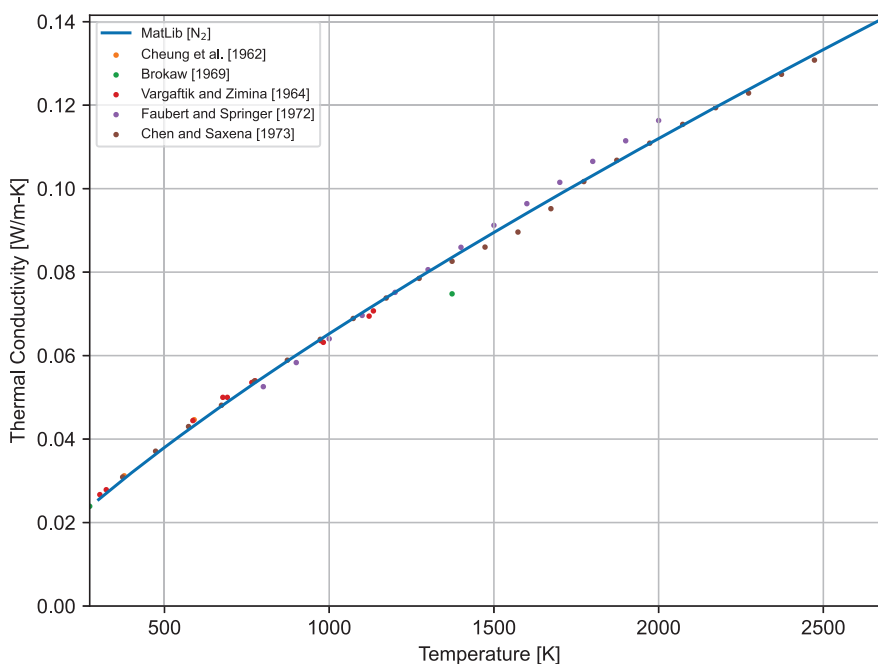


Figure 4-6. Model-to-Data Comparison for Nitrogen Thermal Conductivity Correlation

Thermal conductivity data have been collected for steam at various temperatures and 1×10^7 Pa [Hagman et al., 1981]. A comparison between these data for steam is presented in Figure 4-7. This comparison demonstrates reasonable agreement between the correlation and the database between 600 and 973 K.

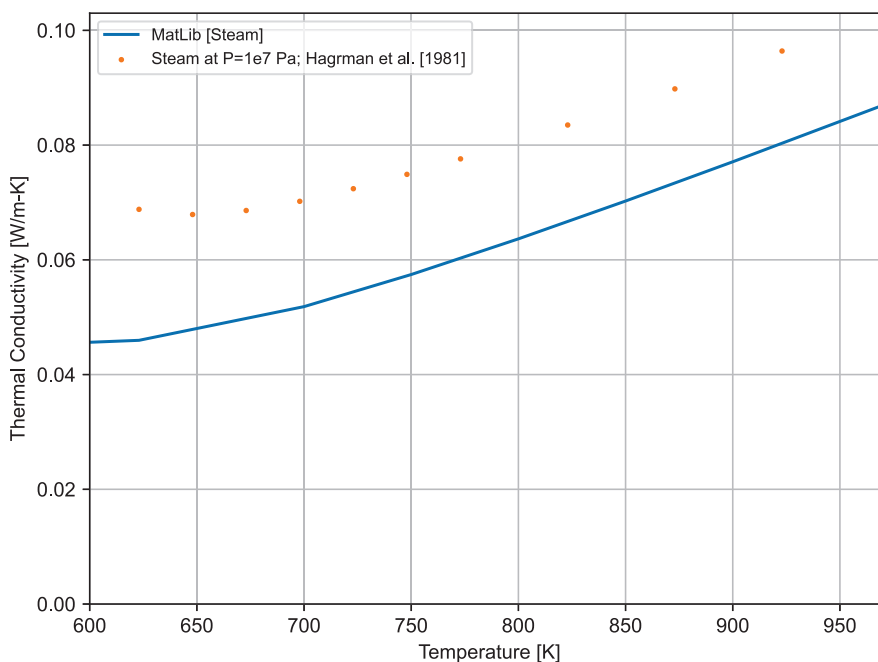


Figure 4-7. Model-to-Data Comparison for Steam Thermal Conductivity Correlation

Thermal conductivity data have been collected for various gas mixtures at various temperatures [Andrew and Calvert, 1966]. A comparison between these data is presented in Figure 4-8. This comparison demonstrates reasonable agreement between the correlation and the database between 273 and 800 K.

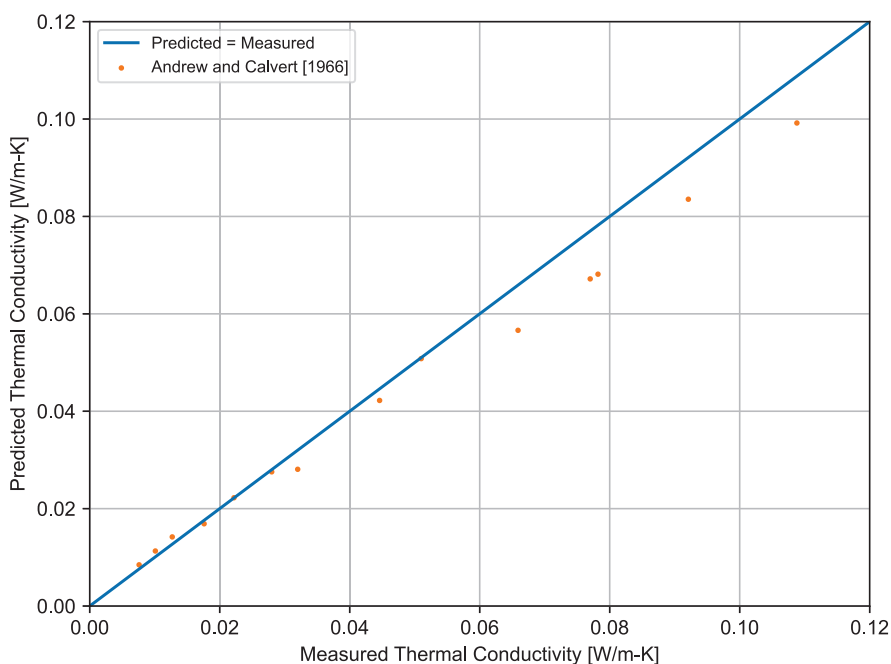


Figure 4-8. Model-to-Data Comparison for Gas Mixture Thermal Conductivity Correlation

4.1.3 Applicability and Uncertainty

The thermal conductivity is applicable for the following range of conditions:

- Temperature:
 - Helium, argon, nitrogen: 273 to 2500 K
 - Krypton: 273 to 2300 K
 - Xenon: 273 to 2200 K
 - Hydrogen: 273 to 2000 K
 - Steam: 600 to 973 K
 - Gas mixtures: 273 to 800 K

The uncertainty of the correlation is given below for all gases as an absolute standard error:

- Helium: 8.99×10^{-3} W/m-K
- Argon: 9.66×10^{-4} W/m-K
- Krypton: 8.86×10^{-4} W/m-K
- Xenon: 5.34×10^{-4} W/m-K
- Hydrogen: 1.67×10^{-2} W/m-K

- Nitrogen: $1.99 \times 10^{-3} \text{ W/m-K}$
- Steam: $1.75 \times 10^{-2} \text{ W/m-K}$

5.0 Oxide/CRUD Material Properties

5.1 Zirconium Dioxide (ZrO₂)

5.1.1 Thermal Conductivity

The thermal conductivity of zirconium dioxide (ZrO₂) that forms in-reactor on zirconium-based alloy cladding tubes is modeled in MatLib as a function of one parameter:

1. Temperature

5.1.1.1 Model Description

The thermal conductivity of ZrO₂ is given by:

$$k = 1.9599 - 2.41 \times 10^{-4}T + 6.43 \times 10^{-7}T^2 - 1.946 \times 10^{-10}T^3 \quad (5-1)$$

Where,

k = ZrO₂ thermal conductivity, W/m-K

T = Temperature, K

5.1.1.2 Comparison to Data

Thermal conductivity data have been collected for ZrO₂ that is prototypic to that found on zirconium alloy cladding [Kingery et al., 1954] [Adams, 1954]. A comparison between these data is presented in Figure 5-1. This comparison demonstrates a good agreement between the correlation and the database within a range of 285 to 1770 K.

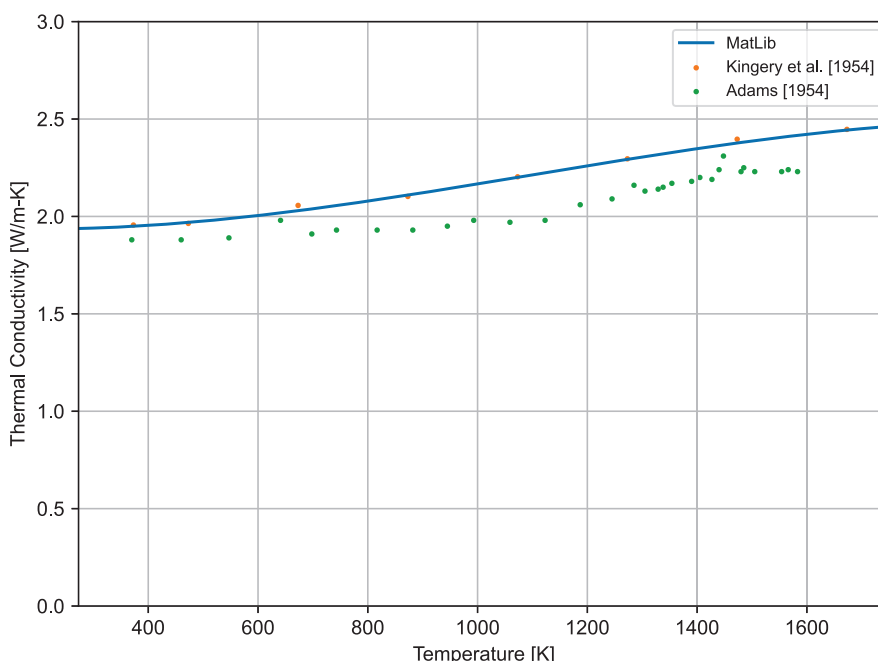


Figure 5-1. Model-to-Data Comparison for ZrO₂ Thermal Conductivity Correlation

5.1.1.3 Applicability and Uncertainty

The thermal conductivity model is applicable to the range of available data:

- Oxide layer on cladding types: Zircaloy-4, Zircaloy-2, M5, ZIRLO, and Optimized ZIRLO
- Temperature: 285 to 1770 K
- Rod-average burnup: No burnup dependence observed

Engineering judgment should be used if analysis outside of these ranges is needed.

The uncertainty of the correlation is given below. No variation in thermal conductivity uncertainty is observed with increasing temperature, so an absolute uncertainty is used.

- ZrO₂: $\sigma = 0.14$ W/m-K

5.1.2 Specific Heat Capacity

The specific heat capacity of ZrO₂ is modeled in MatLib as a constant value. A range of values were found [AZO Materials, 2015]; however, their applicability to ZrO₂ formed in-reactor is unknown. The values found ranged from 420 to 540 J/kg-K. For conservatism, the upper bound value is used.

$$C_p = 540 \text{ J/kg-K} \quad (5-2)$$

Where,

C_p = Specific heat capacity of ZrO_2 , J/kg-K

5.1.2.1 Applicability and Uncertainty

An upper and lower bound of 540 J/kg-K and 420 J/kg-K have been observed. No uncertainty is given.

5.1.3 Melting Temperature

5.1.3.1 Model Description

The melting temperature of ZrO_2 is modeled in MatLib as a constant value. A range of values were found [AZO Materials, 2015]; however, their applicability to ZrO_2 formed in-reactor is unknown. The values found ranged from 2823 to 2973 K. For conservatism, the lower bound value is used.

$$T_{melt} = 2823 \text{ K} \quad (5-3)$$

Where,

T_{melt} = Melting temperature of ZrO_2 , K

5.1.3.2 Applicability and Uncertainty

An upper and lower bound of 2973 K and 2823 K have been observed. No uncertainty is given.

5.1.4 Density

The density of ZrO_2 is modeled in MatLib as a constant value:

$$\rho = 5680 \text{ kg/m}^3 \quad (5-4)$$

Where,

ρ = density of ZrO_2 , kg/m³

5.2 CRUD

Modeling CRUD in a fuel performance code is challenging for a number of reasons. The presence or absence of CRUD is highly dependent on small changes in coolant chemistry and other operational parameters. Additionally, there are several types of CRUD that are observed. Tenacious

CRUD is hard and does not easily brush off. This type of CRUD is often included in the measurement of oxide thickness but can be modeled separately from oxide. Fluffy CRUD is sometimes observed and can easily be brushed off. The effective thermal conductivity of this layer is large and is typically not modeled in the modeling of nuclear fuel rods. For BWR applications, the effect of CRUD is not typically modeled as it is assumed that the water can boil through the CRUD layer that is typically observed.

For application in FAST, the following properties are assumed for modeling the thermal effects of the tenacious CRUD layer in PWR applications. Due to the scarcity of data, no attempt has been made to quantify uncertainties or perform data comparisons to any of these quantities.

5.2.1 Thermal Conductivity

The thermal conductivity of CRUD is modeled in MatLib as a constant value:

$$k = 0.8648 \text{ W/m-K} \quad (5-5)$$

Where,

$$k = \text{Thermal conductivity of CRUD, W/m-K}$$

5.2.2 Specific Heat Capacity

The specific heat of CRUD is modeled in MatLib as a constant value:

$$C_p = 800 \text{ J/kg-K} \quad (5-6)$$

Where,

$$C_p = \text{Specific heat capacity of CRUD, J/kg-K}$$

5.2.3 Density

The density of CRUD is modeled in MatLib as a constant value [Wilson and Comstock, 1999]:

$$\rho = 1200 \text{ kg/m}^3 \quad (5-7)$$

Where,

$$\rho = \text{Density of CRUD, kg/m}^3$$

6.0 Fluid Material Properties

This section describes material property correlations for the following fluids:

- Water
- Sodium

6.1 Water

The thermodynamic water properties contained in MatLib are based off of the 1967 ASME Steam Tables [[Meyer et al., 1967](#)].

The water properties package used in MatLib is based on the STH2X Water Properties Subroutines [[Wagner, 1977](#)]. The subroutines derived from the STH2X package include the following:

`sth2x0` = Calculates the saturation pressure as a function of temperature

`sth2x2` = Calculates saturation properties as a function of pressure and quality

`sth2x3` = Calculates single phase thermodynamic properties as a function of temperature and pressure

`sth2x5` = Calculates single phase thermodynamic properties as a function of pressure and enthalpy

The properties modeled by the package include the following:

1. Enthalpy
2. Specific heat
3. Specific volume
4. Density
5. Entropy
6. Thermal expansion
7. Isothermal compressibility
8. Temperature
9. Saturation pressure and temperature
10. Quality

For more information regarding the water properties, see the references listed above.

6.2 Sodium

6.2.1 Thermal Conductivity

The thermal conductivity of liquid sodium is modeled in MatLib as a function of one parameter:

1. Temperature

6.2.1.1 Model Description

The thermal conductivity of liquid sodium is given by [Fink and Leibowitz, 1995]:

$$k = 124.67 - 0.11381T + 5.5226 \times 10^{-5}T^2 - 1.1842 \times 10^{-8}T^3 \quad (6-1)$$

Where,

k = Thermal conductivity of sodium, W/m-K

T = Temperature, K

6.2.1.2 Applicability and Uncertainty

The thermal conductivity model for liquid sodium is applicable over the following ranges of conditions:

- Material: Sodium
- Temperature: T_{melt} (371.944 K) to 1500 K

No uncertainty is given.

6.2.2 Viscosity

The viscosity of liquid sodium is modeled in MatLib as a function of one parameter:

1. Temperature

6.2.2.1 Model Description

The viscosity of liquid sodium is given by [Fink and Leibowitz, 1995]:

$$\eta = \exp \left(-6.4406 - 0.3958 \ln(T) + \frac{556.835}{T} \right) \quad (6-2)$$

Where,

η = Viscosity of liquid sodium, Pa-s

T = Temperature, K

6.2.2.2 Applicability and Uncertainty

The viscosity model for liquid sodium is applicable over the following ranges of conditions:

- Material: Sodium
- Temperature: T_{melt} (371.944 K) to 2500 K

The following relative uncertainties should be applied to the viscosity model:

$$\sigma \% = \begin{cases} 2.3 + 0.0018T & \text{for } T_{melt} (371.944 \text{ K}) < T \leq 1500 \text{ K} \\ -10 + 0.01T & \text{for } 1500 \text{ K} < T \leq 2500 \text{ K} \end{cases}$$

Where,

T = Temperature, K

6.2.3 Density

The density of liquid sodium is modeled in MatLib as a function of one parameter:

1. Temperature

6.2.3.1 Model Description

The density of liquid sodium is given by [Fink and Leibowitz, 1995]:

$$\rho = \rho_c + f \left(1 - \frac{T}{T_c} \right) + g \left(1 - \frac{T}{T_c} \right)^h \quad (6-3)$$

Where,

ρ = Density, kg/m³

ρ_c = Density at the critical temperature of sodium = 219.0 kg/m³

f = Constant = 275.32 kg/m³

T = Temperature, K

T_c = Critical temperature of sodium = 2503.7 K

g = Constant = 511.58 kg/m³

h = Constant = 0.5

6.2.3.2 Applicability and Uncertainty

The density model for liquid sodium is applicable over the following ranges of conditions:

- Material: Sodium
- Temperature: T_{melt} (371.944 K) to T_c (2503.7 K)

No uncertainty is given.

6.2.4 Specific Heat Capacity

The specific heat capacity of liquid sodium is modeled in MatLib as a function of one parameter:

1. Temperature

6.2.4.1 Model Description

The specific heat capacity of liquid sodium is given by [Fink and Leibowitz, 1995]:

$$C_p = 1658.2 - 0.8479T + 4.4541 \times 10^{-4}T^2 - \frac{2.9926 \times 10^6}{T^2} \quad (6-4)$$

Where,

C_p = Specific heat capacity of liquid sodium, J/kg-K

T = Temperature, K

6.2.4.2 Applicability and Uncertainty

The specific heat capacity model for liquid sodium is applicable over the following ranges of conditions:

- Material: Sodium
- Temperature: T_{melt} (371.944 K) to T_c (2503.7 K)

No uncertainty is given.

6.2.5 Enthalpy

The enthalpy of liquid sodium is modeled in MatLib as a function of one parameter:

1. Temperature

6.2.5.1 Model Description

The enthalpy of liquid sodium is given by [Fink and Leibowitz, 1995]:

$$H = \begin{cases} -3.6577 \times 10^5 + 1658.2T - 0.42395T^2 \\ \quad + 1.4847 \times 10^{-4}T^3 + \frac{2.9926 \times 10^6}{T}, & \text{for } 371.944 \text{ K} \leq T \leq 2000 \text{ K} \\ E + FT - 0.5H_{vap}, & \text{for } 2000 \text{ K} < T \leq 2503.7 \text{ K} \end{cases} \quad (6-5a)$$

Where,

$$H_{vap} = 393.37 \left(1 - \frac{T}{T_c}\right) + 4398.6 \left(1 - \frac{T}{T_c}\right)^{0.29302} \quad (6-5b)$$

and

H = Enthalpy of liquid sodium, J/kg

T = Temperature, K

H_{vap} = Enthalpy of vaporization, J/kg

E = Constant = 2.1284×10^6 J/kg

F = Constant = 8.6496×10^2 J/kg-K

T_c = Critical temperature of sodium = 2503.7 K

6.2.5.2 Applicability and Uncertainty

The enthalpy model for liquid sodium is applicable over the following ranges of conditions:

- Material: Sodium
- Temperature: T_{melt} (371.944 K) to T_c (2503.7 K)

The following relative uncertainties should be applied [Fink and Leibowitz, 1995]:

$$\sigma \% = \begin{cases} 1, & \text{for } 371.944 \text{ K} < T \leq 1000 \text{ K} \\ 0.17 + 8.3 \times 10^{-4}T, & \text{for } 1000 \text{ K} < T \leq 1600 \text{ K} \\ -0.5 + 1.25 \times 10^{-3}T, & \text{for } 1600 \text{ K} < T \leq 2000 \text{ K} \\ 10, & \text{for } 2000 \text{ K} < T \leq 2400 \text{ K} \\ -38 + 0.02T, & \text{for } 2400 \text{ K} < T \leq 2500 \text{ K} \end{cases}$$

Where,

T = Temperature, K

6.2.6 Melting Temperature

The melting temperature of sodium is modeled in MatLib as a constant value [Fink and Leibowitz, 1995]:

$$T_{melt} = 371.944 \text{ K} \quad (6-6)$$

Where,

T_{melt} = Melting temperature of sodium, K

6.2.6.1 Comparison to Data

No comparisons to data are provided as this is a theoretical quantity.

6.2.6.2 Applicability and Uncertainty

The melting temperature of sodium is applicable over the following ranges of conditions:

- Material: Sodium

No uncertainty is given.

6.2.7 Vapor Pressure

The vapor pressure of sodium is modeled in MatLib as a function of one parameter:

1. Temperature

6.2.7.1 Model Description

The specific heat capacity of liquid sodium is given by [Fink and Leibowitz, 1995]:

$$P = \exp \left(11.9463 - \frac{12633.73}{T} - 0.4672 \ln(T) \right) \quad (6-7)$$

Where,

P = Vapor pressure of liquid sodium, MPa

T = Temperature, K

6.2.7.2 Applicability and Uncertainty

The vapor pressure model for sodium is applicable over the following ranges of conditions:

- Material: Sodium
- Temperature: T_{melt} (371.944 K) to T_c (2503.7 K)

No uncertainty is given.

This page intentionally blank.

7.0 References

- [Adams, 1954] Adams M. 1954. "Thermal Conductivity: III, Prolate Spheroidal Envelope Method." *Journal of the American Ceramic Society* 37(2):74–79.
- [Affortit and Marcon, 1970] Affortit C and J Marcon. 1970. "Chaleur spécifique à haute température des oxydes d'uranium et de plutonium." *Revue Internationale des Hautes Températures et des Réfractaires* 7:236–241.
- [Akiyama, 1991] Akiyama M. 1991. *Design Technology of Fusion Reactors*. World Scientific.
- [Amaya and Hirai, 1997] Amaya M and M Hirai. 1997. "The effects of oxidation on the thermal conductivity of (U,M)O₂ pellets (M = Gd and/or simulated soluble FPs)." *Journal of Nuclear Materials* 246(2–3):158–164.
- [Anderson et al., 1962] Anderson W, C Beck, A Kephart, and J Theilacker. 1962. "Zirconium Alloys." *Reactor Structural Materials: Engineering Properties as Affected by Nuclear Reactor Service*, number ASTM-STP-314, pp. 62–93. American Society for Testing and Materials, Philadelphia, PA.
- [Andrew and Calvert, 1966] Andrew A and C Calvert. 1966. *Thermal Conductivity and Viscosity of Neon, Helium, Argon, Xenon, and their Binary Mixtures*. GE-TM-66-7-9, General Electric Co., Nuclear Materials and Propulsion Operation, Cincinnati, OH.
- [Armstrong and Brown, 1964] Armstrong P and H Brown. 1964. "Dynamic Young's Modulus Measurement above 1000 °C on Some Pure Polycrystalline Metals and Commercial Graphites." *Metallurgical Society of AIME* 230:962–966.
- [AZO Materials, 2015] AZO Materials. 2015. Zirconia - ZrO₂, Zirconium Dioxide. <https://www.azom.com/properties.aspx?ArticleID=133>.
- [Baker and Wilson, 1992] Baker R and D Wilson. 1992. *SIEX4 - A Correlated Computer Code for Prediction of Fast Reactor Fuel and Blanket Pin Performance*. WHC-SP-0865, Westinghouse Hanford Company, Richland, WA.
- [Baldock et al., 1966] Baldock P, W Spindler, and T Baker. 1966. "The X-ray thermal expansion of near-stoichiometric UO₂." *Journal of Nuclear Materials* 18(3):305–313.
- [Banks, 1974] Banks D. 1974. "Some observations of density and porosity changes in UO₂ fuel irradiated in water-cooled reactors." *Journal of Nuclear Materials* 54(1):97–107.
- [Bates et al., 1967] Bates J, C Hinman, and T Kawada. 1967. "Electrical conductivity of uranium dioxide." *Journal of the American Ceramic Society* 50(12):652–656.
- [Bolmaro and Povolo, 1988] Bolmaro R and F Povolo. 1988. "Anelastic behaviour of materials under multiaxial strains." *Journal of Materials Science* 23(1):371–379.
- [Brett and Russel, 1960] Brett N and L Russel. 1960. "The thermal expansion of PuO₂ and some other actinide oxides between room temperature and 1000 °C." In *Second International Conference on Plutonium Metallurgy*, pp. 397–410.

- [Brokaw, 1969] Brokaw RS. 1969. "Predicting Transport Properties of Dilute Gases." I&EC Process Design and Development 8(2):240–253.
- [Brooks and Stansbury, 1966] Brooks C and E Stansbury. 1966. "The specific heat of Zircaloy-2 from 50 to 700 °C." Journal of Nuclear Materials 18:223.
- [Bunnell et al., 1983] Bunnell L, J Bates, and G Mellinger. 1983. "Some high-temperature properties of Zircaloy-Oxygen alloys." Journal of Nuclear Materials 116(2–3):219–232.
- [Bunnell et al., 1977] Bunnell L, G Mellinger, C Bates, and C Hann. 1977. High temperature properties of Zircaloy-Oxygen alloys. EPRI NP-524, Battelle Pacific Northwest Laboratory, Richland, WA.
- [Burdick and Parker, 1956] Burdick M and H Parker. 1956. "Effect of Particle Size on Bulk Density and Strength Properties of Uranium Dioxide Specimens." Journal of the American Ceramic Society 39(5):181–187.
- [Burgoyne and Garlick, 1976] Burgoyne T and A Garlick. 1976. "The Effect of Oxidation and Crud Deposition on the Emissivity of Zircaloy-2 Cladding." In OECD-CSNI Meeting on the Behavior of Water Reactor Fuel Elements under Accident Conditions. Spatid, Norway.
- [Busby, 1966] Busby C. 1966. Properties of Zircaloy-4 Tubing. WAPD-TM-585, Bettis Atomic Power Laboratory, Pittsburgh, PA.
- [Cabannes et al., 1967] Cabannes M, J Stora, and J Tsakiris. 1967. "Facteurs de réflexion et d'émission de UO₂ à haute température." C.R. Acad. SC. 264B:45–48.
- [Carrol et al., 1994] Carrol J, R Gomme, and N Leech. 1994. "Thermal Diffusivity Measurements on Unirradiated Archive Fuel, and Fuel Irradiated in the Halden IFA-558 Experiment." In Enlarged HPG Meeting on High Burnup Fuel Performance, Safety and Reliability and Degradation of In-Core Materials and Water Chemistry Effects and Man-Machine Systems Research. HWR-345/13.
- [Chen and Saxena, 1973] Chen S and S Saxena. 1973. "Experimental determination of thermal conductivity of nitrogen in the temperature range 100-2200 °C." High Temperature Science 5(3):206–233.
- [Cheung et al., 1962] Cheung H, L Bromley, and C Wilke. 1962. "Thermal conductivity of gas mixtures." AIChE Journal 8(2):221–228.
- [Chirigos et al., 1961] Chirigos J, S Kass, W Kirk, and S G.J.. 1961. "Development of Zircaloy-4." In Fuel Element Fabrication with Special Emphasis on Cladding Materials, pp. 19–55.
- [Christensen et al., 1964] Christensen J, A Bush, H Ferrari, and R Allio. 1964. "Uranium Dioxide Thermal Conductivity." Transactions of the American Nuclear Society 7:391–392.
- [Colombier et al., 2010] Colombier V, M Horvath, T Tverberg, and H Jenssen. 2010. Comparative Study of the Gadolinia Experiments IFA-515.10, IFA-636, IFA-681.1, and IFA-676.1. HWR-924, OECD Halden Reactor Project, Halden, Norway.

- [Deem and Eldridge, 1967] Deem H and E Eldridge. 1967. Specific Heats of Transformation of Zircaloy-2 and Low Nickel Zircaloy-2. USAEC BM1-1803, Battelle Memorial Institute, Columbus, OH.
- [Dideon and Bain, 1983] Dideon C and G Bain. 1983. Fuel Performance under Extended Burnup for the B&W 15x15 Design. DOE/ET-34212-38, U.S. Department of Energy.
- [Duriez et al., 2000] Duriez C, J Allesandri, T Gervais, and Y Philipponneau. 2000. "Thermal conductivity of hypostoichiometric low Pu content (U,Pu)O_{2-x} mixed oxide." *Journal of Nuclear Materials* 277(2–3):143–158.
- [Dutt and Baker, 1974] Dutt D and R Baker. 1974. SIEX: a correlated code for the prediction of Liquid Metal Fast Breeder Reactor (LMFBR) fuel thermal performance. HEDL-TC-250, Hanford Engineering Development Lab, Richland, WA.
- [Faubert and Springer, 1972] Faubert F and G Springer. 1972. "Measurement of the Thermal Conductivity of Argon, Krypton, and Nitrogen in the Range 800-2000 K." *The Journal of Chemical Physics* 57(6):2333–2340.
- [Faubert and Springer, 1973] Faubert F and G Springer. 1973. "Measurement of the thermal conductivity of helium up to 2100 K by the column method." *The Journal of Chemical Physics* 58(10):4080–4083.
- [Feith, 1966] Feith A. 1966. Thermal Conductivity and Electrical Resistivity of Zircaloy-4. GEMP-669, General Electric Company, Missile and Space Division, Nuclear Systems Programs, Cincinnati, OH.
- [Field, 2018] Field K. 2018. Handbook on the Material Properties of FeCrAl Alloys for Nuclear Power Production Applications (FY18 Version: Revision 1.1). ORNL/SPR-2018/905, U.S. Department of Energy Nuclear Technology Research and Development Advanced Fuels Campaign.
- [Field et al., 2015] Field K, M Gussev, X Hu, and Y Yamamoto. 2015. Preliminary Results on FeCrAl Alloys in the As-received and Welded State Designed to Have Enhanced Weldability and Radiation Tolerance. ORNL/TM-2015/579, Oak Ridge National Laboratory, Oak Ridge, TN.
- [Fink and Leibowitz, 1995] Fink J and L Leibowitz. 1995. Thermodynamic and Transport Properties of Sodium Liquid and Vapor. ANL/RE-95/2, Argonne National Laboratory, Argonne, IL.
- [Franklin et al., 1983] Franklin D, G Lucas, and A Bement. 1983. Creep of Zirconium Alloys in Nuclear Reactors. Number ASTM-STP-815. American Society for Testing and Materials, Philadelphia, PA.
- [Freshley et al., 1976] Freshley M, D Brite, J Daniel, and P Hart. 1976. "Irradiation-induced densification of UO₂ pellet fuel." *Journal of Nuclear Materials* 62:138–166.
- [Freshley et al., 1979] Freshley M, D Brite, J Daniel, and P Hart. 1979. "Irradiation-induced densification and PuO₂ particle behavior in mixed-oxide pellet fuel." *Journal of Nuclear Materials* 81:63–92.

- [Gambhir et al., 1967] Gambhir R, J Gandhi, and S Saxena. 1967. "Thermal conductivity of rare gases deuterium and air." *Indian Journal of Pure & Applied Physics* 5(10):457.
- [Garde, 1986] Garde AM. 1986. Hot Cell Examination of Extended Burnup Fuel from Fort Calhoun. DOE/ET-34030-11, U.S. Department of Energy.
- [Geelhood et al., 2023a] Geelhood K, D Colameco, W Luscher, L Kyriazidis, C Goodson, J Corson, and J Whitman. 2023a. FAST-1.2: A Computer Code for Thermal-Mechanical Nuclear Fuel Analysis under Steady-state and Transients. PNNL-33994, Pacific Northwest National Laboratory, Richland, WA.
- [Geelhood et al., 2023b] Geelhood K, D Colameco, W Luscher, L Kyriazidis, C Goodson, J Corson, and J Whitman. 2023b. FAST-1.2: Integral Assessment. PNNL-33995, Pacific Northwest National Laboratory, Richland, WA.
- [Geelhood et al., 2015a] Geelhood K, W Luscher, and J Cuta. 2015a. FRAPTRAN-2.0: A Computer Code for the Transient Analysis of Oxide Fuel Rods. PNNL-19400, Vol. 1, Rev. 2, Pacific Northwest National Laboratory, Richland, WA.
- [Geelhood et al., 2023c] Geelhood K, W Luscher, L Kyriazidis, C Goodson, J Corson, and J Whitman. 2023c. MatLib-1.2: Nuclear Material Properties Library. PNNL-33996, Pacific Northwest National Laboratory, Richland, WA.
- [Geelhood et al., 2015b] Geelhood K, W Luscher, P Raynaud, and I Porter. 2015b. FRAPCON-4.0: A Computer Code for the Calculation of Steady-State, Thermal-Mechanical Behavior of Oxide Fuel Rods for High Burnup. PNNL-19418, Vol. 1, Rev. 2, Pacific Northwest National Laboratory, Richland, WA.
- [Gibby, 1971] Gibby R. 1971. "The Effect of Plutonium Content on the Thermal Conductivity of (U,Pu)O₂ Solid Solutions." *Journal of Nuclear Materials* 38(2):163–177.
- [Gibby et al., 1974] Gibby R, L Leibowitz, J Kerrisk, and D Clifton. 1974. "Analytical expressions for enthalpy and heat capacity for uranium-plutonium oxide." *Journal of Nuclear Materials* 50(2):155–161.
- [Gilbon et al., 2000] Gilbon D, A Soniak, and aMJ Doriot S.. 2000. "Irradiation creep and growth behavior, and microstructural evolution of advanced Zr-base alloys." In *Zirconium in the Nuclear Industry: Twelfth International Symposium*, number ASTM-STP-1354, pp. 51–73. American Society of Testing and Materials.
- [Gilchrist, 1976] Gilchrist K. 1976. "Thermal property measurements on Zircaloy-2 and associated oxide layers up to 1200 °C." *Journal of Nuclear Materials* 62(2–3):257–264.
- [Godfrey et al., 1964] Godfrey T, W Fulkerson, T Kollie, J Moore, and D McElroy. 1964. Thermal Conductivity of Uranium Dioxide and Armco Iron by an Improved Radial Heat Flow Technique. ORNL-3556, Oak Ridge National Laboratory, Oak Ridge, TN.
- [Goldsmith and Douglas, 1973] Goldsmith L and J Douglas. 1973. "Measurements of the Thermal Conductivity of Uranium Dioxide at 670-1270 K." *Journal of Nuclear Materials* 47(1):31–42.

- [Grønvold, 1955] Grønvold F. 1955. "High temperature X-ray study of uranium oxides in the $\text{UO}_2\text{-U}_3\text{O}_8$ region." *Journal of Inorganic and Nuclear Chemistry* 1(6):357–370.
- [Grønvold et al., 1970] Grønvold F, N Kveseth, A Sveen, and J Tichý. 1970. "Thermodynamics of the UO_{2+x} phase I. Heat capacities of $\text{UO}_{2.017}$ and $\text{UO}_{2.254}$ from 300 to 1000 K and electronic contributions." *Journal of Chemical Thermodynamics* 2(5):665–679.
- [Hagrman et al., 1981] Hagrman D, G Reymann, and G Mason. 1981. MATPRO-Version 11: A Handbook of Materials Properties for Use in the Analysis of Light Water Reactor Fuel Rod Behavior. NUREG/CR-0479 (TREE-1280), Rev. 2, EG&G Idaho, Inc., Idaho Falls, ID.
- [Harbottle, 1970] Harbottle J. 1970. "The Temperature and Neutron Dose Dependence of Irradiation Growth in Zircaloy-2. Irradiation Effect on Structural Alloys for Nuclear Reactor Applications." *Irradiation Effects on Structural Alloys for Nuclear Reactor Applications*, number ASTM-STP-485, pp. 287–299. American Society of Testing and Materials, West Conshohocken, PA.
- [Hein et al., 1968] Hein R, L Sjodahl, and R Swarc. 1968. "Heat content of uranium dioxide from 1200 to 3100 K." *Journal of Nuclear Materials* 25(1):99–102.
- [Held and Wilder, 1969] Held P and D Wilder. 1969. "High Temperature Hemispherical Spectral Emittance of Uranium Oxides at 0.65 and 0.70 μm ." *Journal of the American Ceramic Society* 52(4):182–185.
- [Hirai and Ishimoto, 1991] Hirai M and S Ishimoto. 1991. "Thermal Diffusivities and Thermal Conductivities of $\text{UO}_2\text{-Gd}_2\text{O}_3$." *Journal of Nuclear Science and Technology* 28(11):995–1000.
- [Hobson et al., 1974] Hobson I, R Taylor, and J Ainscough. 1974. "Effect of porosity and stoichiometry on the thermal conductivity of uranium dioxide." *Journal of Physics D: Applied Physics* 7(7):1003–1015.
- [Irisa and Alonso, 2000] Irisa MKGKSSSR Y. and J Alonso. 2000. "Segmented Fuel Rod Irradiation Programme on Advanced Materials for High Burnup." In *International Topical Meeting on Light Water Reactor Fuel Performance*. Park City, UT. American Nuclear Society.
- [Jain and Saxena, 1975] Jain P and S Saxena. 1975. "Transport properties of helium in the temperature range 400-2300 K." *Chemical Physics Letters* 36(4):489–491.
- [Jody et al., 1977] Jody B, S Saxena, V Nain, and R Aziz. 1977. "Thermal conductivity of helium: a probe for the repulsive wall of the interatomic potential." *Chemical Physics* 22(1):53–58.
- [Johnston and Grilly, 1946] Johnston HL and ER Grilly. 1946. "The Thermal Conductivities of Eight Common Gases between 80 and 380 K." *The Journal of Chemical Physics* 14(4):233–.
- [Juenke and Sjodahl, 1968] Juenke E and L Sjodahl. 1968. "Physical and Mechanical Properties: Emittance Measurements." *Advanced Pressure Vessel Materials*, number GEMP-1008, pp. 239–242. General Electric Co., Missile and Space Division, Cincinnati, OH.
- [Kannuliuk and Carman, 1952] Kannuliuk W and E Carman. 1952. "The Thermal Conductivity of Rare Gases." *Proceedings of the Physical Society, Section B* 65(9):701.

- [Kanthal, 2018] Kanthal. 2018. Kanthal APMT Tube. Sandvik AB, Hallstahammar, Sweden. <https://www.kanthal.com/products/material-datasheets/tube/kanthal-apmt/>.
- [Kearns, 1965] Kearns J. 1965. Thermal Expansion and Preferred Orientation in Zircaloy. WAPD-TM-472, Bettis Atomic Power Laboratory, Pittsburgh, PA.
- [Kerrisk and Clifton, 1972] Kerrisk J and D Clifton. 1972. Smoothed values for the enthalpy and heat capacity of UO₂. Volume 16, Pages 531-535.
- [Kingery et al., 1954] Kingery W, J Franci, R Coble, and T Vasilos. 1954. "Thermal Conductivity: X, Data for Several Pure Oxide Materials Corrected to Zero Porosity." Journal of the American Ceramic Society 37(2):107–109.
- [Knuutila, 2006] Knuutila A. 2006. Improvements on FRAPCON-3/FRAPTRAN Mechanical Modeling. VTT-R-11337-06, VTT Technical Research Centre of Finland, Espoo, Finland.
- [Krett and Cleveland, 1997] Krett V and J Cleveland. 1997. Thermophysical Properties of Materials for Water Cooled Reactors. IAEA-TECDOC-949, International Atomic Energy Agency, Vienna, Austria.
- [Kruger and Savage, 1968] Kruger O and H Savage. 1968. Heat capacity and thermodynamic properties of plutonium dioxide. Volume 45, Pages 4540-4544.
- [Lanning et al., 2005] Lanning D, C Beyer, and K Geelhood. 2005. FRAPCON-3 Updates, Including Mixed-Oxide Fuel Properties. Pacific Northwest National Laboratory, Richland, WA. NUREG/CR-6534, Vol. 4, PNNL-11513.
- [Leibowitz and Blomquist, 1988] Leibowitz L and R Blomquist. 1988. "Thermal conductivity and thermal expansion of stainless steels D9 and HT9." International Journal of Thermophysics 9(5):873–883.
- [Leibowitz et al., 1971] Leibowitz L, M Chasanov, L Mishler, and D Fischer. 1971. "Enthalpy of liquid uranium dioxide to 3500 K." Journal of Nuclear Materials 39(1):115–116.
- [Leibowitz et al., 1972] Leibowitz L, D Fischer, and M Chasanov. 1972. "Enthalpy of uranium-plutonium oxides (U_{0.8},Pu_{0.2})O_{1.07} from 2350 to 3000 K." Journal of Nuclear Materials 42(1):113–116.
- [Leibowitz et al., 1969] Leibowitz L, L Mishler, and M Chasanov. 1969. "Enthalpy of solid uranium dioxide from 2500 K to its melting point." Journal of Nuclear Materials 29(3):356–358.
- [Limbäck and Andersson, 1996] Limbäck M and T Andersson. 1996. "A model for analysis of the effect of final annealing on the in- and out-of-reactor creep behavior of zircaloy cladding." In Zirconium in the Nuclear Industry: Eleventh International Symposium, number ASTM-STP-1295, pp. 448–468. American Society for Testing and Materials.
- [Lucks and Deem, 1958] Lucks C and H Deem. 1958. Thermal Conductivity of Uranium and UO₂, pp. 7–9. Number BMI-1273. Battelle Memorial Institute, Columbus, OH.

- [Lucuta et al., 1996] Lucuta P, H Matzke, and I Hastings. 1996. "A pragmatic approach to modelling thermal conductivity of irradiated UO₂ fuel: review and recommendations." *Journal of Nuclear Materials* 232(2–3):166–180.
- [Luscher et al., 2015] Luscher W, K Geelhood, and I Porter. 2015. *Material Property Correlations: Comparisons between FRAPCON-3.5, FRAPTRAN-1.5, and MATPRO*. PNNL-19417, Rev. 2, Pacific Northwest National Laboratory, Richland, WA.
- [Maglić et al., 1994] Maglić K, N Perović, and A Stanimirović. 1994. "Calorimetric and Transport Properties of Zircalloy 2, Zircalloy 4, and Inconel 625." *International Journal of Thermophysics* 15(4):741–755.
- [Martin, 1988] Martin D. 1988. "The Thermal Expansion of Solid UO₂ and (U,Pu) Mixed Oxides – A Review and Recommendations." *Journal of Nuclear Materials* 152(2–3):94–101.
- [Matsson and Turnbull, 1998] Matsson I and J Turnbull. 1998. *The integral fuel rod behaviour test IFA-597.3: Analysis of the measurements*. HWR-543, OECD Halden Reactor Project, Halden, Norway.
- [Mehan, 1958] Mehan R. 1958. *Modulus of Elasticity of Zircaloy-2 Between Room Temperature and 1,000 °F*. KAPL-M-RLM-16, General Electric Company, Knolls Atomic Power Laboratory, Schenectady, NY.
- [Mehan and Wiesinger, 1961] Mehan R and F Wiesinger. 1961. *Mechanical Properties of Zircaloy-2*. KAPL-2110, Knolls Atomic Power Laboratory, Schenectady, NY.
- [Meyer et al., 1967] Meyer C, R McClintock, G Silvestri, and R Spencer. 1967. *1967 ASME Steam Tables-Thermodynamic and Transport Properties of Steam*. The American Society of Mechanical Engineers, New York, NY.
- [Minato et al., 2001] Minato K, T Shiratori, H Serizawa, K Hayashi, K Une, K Nogita, M Hirai, and M Amaya. 2001. "Thermal conductivities of irradiated UO₂ and (U,Gd)O₂." *Journal of Nuclear Materials* 288(1):57–65.
- [Murabayashi et al., 1975] Murabayashi M, S Tanaka, and Y Takahashi. 1975. "Thermal Conductivity and Heat Capacity of Zircaloy-2, -4 and Unalloyed Zirconium." *Journal of Nuclear Science and Technology* 12(10):661–662.
- [Murphy and Havelock, 1976] Murphy E and F Havelock. 1976. "Emissivity of Zirconium Alloys in Air in the Temperature Range 100-400 °C." *Journal of Nuclear Materials* 60(2):167–176.
- [Newman, 1982] Newman L. 1982. *Development and Demonstration of an Advanced Extended-Burnup Fuel-Assembly Design Incorporating Urania-Gadolinia*. DOE/ET/34212-36, Babcock & Wilcox, Lynchburg, VA.
- [Newman, 1986] Newman L. 1986. *The Hot Cell Examination of Oconee 1 Fuel Rods After Five Cycles of Irradiation*. DOE/ET/34212-50, Babcock and Wilcox Company, Lynchburg, VA.
- [Northwood et al., 1975] Northwood D, I London, and L Bähnen. 1975. "Elastic constants of zirconium alloys." *Journal of Nuclear Materials* 55(3):299–310.

- [NRC, 1978] NRC. 1978. An Acceptable Model and Related Statistical Methods for the Analysis of Fuel Densification. Regulatory Guide 1.126, Rev. 1, U.S. Nuclear Regulatory Commission, Washington, D.C.
- [Ohira and Itagaki, 1997] Ohira K and N Itagaki. 1997. "Thermal conductivity measurements of high burnup UO₂ pellet and a benchmark calculation of fuel center temperature." In Proceedings of the American Nuclear Society International Topical Meeting on LWR Fuel Performance, pp. 541–549. Portland, OR. American Nuclear Society.
- [Padel and Groff, 1976] Padel A and A Groff. 1976. "Variation du module de Young du zirconium β en fonction de la température." Journal of Nuclear Materials 59(3):325–326.
- [Peggs and Godin, 1975] Peggs I and D Godin. 1975. "The yield strength-hot hardness relationship of Zircaloy-4." Journal of Nuclear Materials 57(2):246–248.
- [Peggs et al., 1976] Peggs I, A Stadnyk, and D Godin. 1976. "Thermophysical Properties of Zr-Alloy Fuel-Channel Components." High Temperatures-High Pressures 8(4):441–450.
- [Petiprez, 2002] Petiprez B. 2002. Ramp Tests with Two High Burnup MOX Fuel Rods in IFA-629.3. HWR-714, OECD Halden Reactor Project, Halden, Norway.
- [Philipponneau, 1992] Philipponneau Y. 1992. "Thermal conductivity of (U,Pu)O_{2-x} mixed oxide fuel." Journal of Nuclear Materials 188:194–197.
- [Popov et al., 2000] Popov S, J Carbajo, V Ivanov, and G Yoder. 2000. Thermophysical Properties of MOX and UO₂ Fuels Including the Effects of Irradiation. ORNL/TM-2000/351, Oak Ridge National Laboratory, Oak Ridge, TN.
- [Powers, 1961] Powers A. 1961. Application of the Ewing Equation for Calculating Thermal Conductivity from Electrical Conductivity from Electrical Conductivity. KAPL-2146, Knolls Atomic Power Laboratory, Schenectady, NY.
- [Rolstad et al., 1974] Rolstad E, A Hanevik, and K Knudsen. 1974. "Measurements of the Length Changes of UO₂ Fuel Pellets During Irradiation." In Enlarged HPG Meeting on Computer Control and Fuel Research.
- [Ronchi et al., 1999] Ronchi C, M Sheindlin, M Musella, and G Hyland. 1999. "Thermal conductivity of uranium dioxide up to 2900 K from simultaneous measurements of the heat capacity and thermal diffusivity." Journal of Applied Physics 85(2):776–789.
- [Ronchi et al., 2004] Ronchi C, M Sheindlin, D Staicu, and M Kinoshita. 2004. "Effect of burn-up on the thermal conductivity of uranium dioxide up to 100000 MWdt⁻¹." Journal of Nuclear Materials 327(1):58–76.
- [Sabol et al., 1994] Sabol G, R Comstock, R Weiner, P Larouere, and R Stanutz. 1994. "In-Reactor Corrosion Performance of ZIRLO™ and Zircaloy-4." In Zirconium in the Nuclear Industry: Tenth International Symposium, number STP-1425, pp. 724–744. American Society for Testing and Materials.

- [Savage, 1968] Savage H. 1968. "The heat content and specific heat of some metallic fast-reactor fuels containing plutonium." *Journal of Nuclear Materials* 25(3):249–259.
- [Saxena and Saxena, 1970] Saxena S and V Saxena. 1970. "Thermal conductivity data for hydrogen and deuterium in the range 100-1100 °C." *Journal of Physics A: General Physics* 3(3):309–320.
- [Saxena and Saxena, 1968] Saxena V and S Saxena. 1968. "Measurement of the thermal conductivity of argon using hot-wire type thermal diffusion columns." *Chemical Physics Letters* 2(1):44–46.
- [Saxena and Saxena, 1969] Saxena V and S Saxena. 1969. "Thermal Conductivity of Krypton and Xenon in the Temperature Range 350-1500 K." *Journal of Chemical Physics* 51(8):3361–3368.
- [Scott, 1965] Scott D. 1965. *Physical and Mechanical Properties of Zircaloy 2 and 4*. WCAP-3269-41, Westinghouse Electric Corporation, Pittsburgh, PA.
- [Shestopalov et al., 1999] Shestopalov A, K Lioutov, L Yegorova, G Abyshov, and K Mikitiouk. 1999. Modification of USNRC's FRAP-T6 Fuel Rod Transient Code for High Burnup VVER Fuel. NUREG/IA-0164, U.S. Nuclear Regulatory Commission, Washington, D.C.
- [Siefken et al., 2001] Siefken L, E Coryell, E Harvego, and J Hohorst. 2001. *SCDAP/RELAP5/MOD 3.3 Code Manual MATPRO-A Library of Materials Properties for Light-Water-Reactor-Accident Analysis*. NUREG/CR-6150, Vol. 4, Rev. 2, INEL-96/0422, Idaho National Engineering and Environmental Laboratory, Idaho Falls, ID.
- [Smith et al., 1994] Smith G, R Pirek, H Freeburn, and D Schrire. 1994. *The Evaluation and Demonstration of Methods for Improved Nuclear Fuel Utilization*. DOE/ET-34-013-15, Combustion Engineering, Windsor, CT.
- [Soniak et al., 2002] Soniak A, N L'Hullier, J Mardon, V Rebeyrolle, P Boffioux, and C Bernaudat. 2002. "Irradiation Creep Behavior of Zr-Base Alloys." In *Zirconium in the Nuclear Industry: Thirteenth International Symposium*, number ASTM-STP-1423, pp. 837–862. West Conshohocken, PA. ASTM International.
- [Sontheimer and Nissen, 1994] Sontheimer F and K Nissen. 1994. "Evaluation of the Stress Reversal Creep Experiment IFA-585 in the HBWR and the Lift-Off Experiment ROPE-1 in the R2 Studsvik using the Siemens/KWU Clad Creep Model." In *Enlarged HPG Meeting on High Burnup Fuel Performance, Safety and Reliability and Degradation of In-Core Materials and Water Chemistry Effect and Man-Machine Systems Research*, number HPR-345/28.
- [Spasic et al., 1968] Spasic Z, M Pavlovic, and G Simic. 1968. "Variation du Module D'Elasticité du Zircaloy-2 en Fonction de la Température." In *Conference on the Use of Zirconium Alloys in Nuclear Reactors*, number USAEC CONF-681086, pp. 277–284. Mariánské Lázně, Czechoslovakia.
- [Springer and Wingeier, 1973] Springer G and E Wingeier. 1973. "Thermal conductivity of neon, argon, and xenon at high temperatures." *The Journal of Chemical Physics* 59(5):2747–2750.

- [Stefanov et al., 1976] Stefanov B, L Zarkova, and D Oliver. 1976. "Measurement of the thermal-conductivity coefficient of gases and vapors up to 2500 K." *High Temperature* 14(1):48–57.
- [Timrot and Umanskii, 1966] Timrot D and A Umanskii. 1966. "Thermal conductivity of hydrogen and argon." *High Temperature* 3(2):285–287.
- [Timrott and Totskii, 1965] Timrott D and E Totskii. 1965. "Dilatometric Method for Experimental Determination of Thermal Conductivity of Corrosive Gases and Vapors at High Temperatures." *High Temperature* 3(5):685.
- [Tokar and Nutt, 1972] Tokar M and A Nutt. 1972. "Thermal expansion of PuO_2 from 25 to 1420 °C." *Transactions of the American Nuclear Society* 10(1):210–211.
- [Turnbull, 2001] Turnbull J. 2001. "Concluding Report on Three PWR Rods Irradiated to 90 MWd/kg UO_2 in IFA-519.9: Analysis of Measurements Obtained In-pile and by PIE." In EHPG-Meeting, number HWR-668. Lillehammer, Norway.
- [Vargaftik and Yakush, 1971] Vargaftik N and L Yakush. 1971. "Measurement of the thermal conductivities of neon, krypton, and xenon over a wide range of temperatures." *Journal of Engineering Physics* 21(3):1156–1161.
- [Vargaftik and Zimina, 1964] Vargaftik N and N Zimina. 1964. "Thermal conductivity of nitrogen at high temperatures." *High Temperature* 2(6):782–790.
- [von Ubisch, 1959] von Ubisch. 1959. "The Thermal Conductivities of Mixtures of Rare Gases at 29 °C and at 520 °C." *Arkiv Fysik* 16:93–100.
- [Wagner, 1977] Wagner R. 1977. *STH2X Water Property Subroutines. NRTS Environmental Subroutine Manual.*
- [Weilbacher, 1972] Weilbacher J. 1972. "Diffusivité thermique de l'oxyde d'uranium et de l'oxyde de thorium à haute température." *High Temperatures-High Pressures* 4(4):431–438.
- [Wilson and Comstock, 1999] Wilson W and R Comstock. 1999. *Potential Impacts of Crud Deposits on Fuel Rod Behavior on High Powered PWR Fuel Rods. IAEA-TECDOC-1128, Westinghouse Electric Company.*
- [Yamada et al., 1999] Yamada T, H Matsuda, and M Yoshimura. 1999. "Melting and measurements of solidification point of $\text{UO}_2\text{-Gd}_2\text{O}_3$ solid solutions under solar furnace." *Journal of High Temperature Study* 25(2):71–79.
- [Yamanouchi et al., 1992] Yamanouchi N, M Tamura, H Hayakawa, A Hishinuma, and T Kondo. 1992. "Accumulation of engineering data for practical use of reduced activation ferritic steel: 8%Cr-2%W-0.2%V-0.04%Ta-Fe." *Journal of Nuclear Materials* 191–194:822–826.
- [Zaitseva, 1959] Zaitseva L. 1959. "An experimental investigation of the heat conductivity of monatomic gases over wide temperature intervals." *Soviet Physics-Technical Physics* 4(4):444–450.

This page intentionally blank.

Pacific Northwest National Laboratory

902 Battelle Boulevard
P.O. Box 999
Richland, WA 99352
1-888-375-PNNL (7675)

www.pnnl.gov